University of Naples Federico II

SCHOOL OF POLYTECHNIC AND BASIC SCIENCES
Department of Chemical, Materials and Production Engineering

Report PhD "Industrial product and process engineering" XXXIII cycle

"Developing of an organ on chip device as novel in vitro platform to study organ mechanobiology: Peristalsis on a chip."

Coordinator:
Andrea D'anna

Supervisor:
Paolo Antonio Netti

Candidate PhD:
Sara Sibilio

Correlator:
Vincenza De Gregorio
Giorgia Imparato
Francesco Urciuolo

Academic year 2020/2021

Developing of an organ on chip device as novel in vitro platform to study organ mechanobiology: Peristalsis on a chip.

Knowing the mechanical properties of the gastrointestinal (GI) tract appears to be important for understanding the molecular and cellular responses to mechanical stimuli on physiological processes such as foods, xenobiotic or drugs digestion/absorption. These processes are mediated by various intestinal cells such as epithelial cells, interstitial cells, smooth muscle cells, and neurocytes. The loss or dysfunction of specific cells or mechanical strength of cell bowel wall directly results in GI tract disease. Reversing the abnormal status of pathogenic cells has been considered crucial to treatment of gut diseases. Gut bioengineered models have been developing for the purpose to replace the damaged tissues and to provide three-dimensional platforms that mimic the in vivo environment to study drug development, absorption and toxicity. Nevertheless, the need to develop more complex models in vitro to study mechanical stress is growing. In this perspective, this project will allow us to get an automatized microfluidic gut platform to evaluate the pathophysiology of the small intestine through the study of the shear stress of the bolus on the epithelial cells layer at the lumen side of the healthy or diseased 3D intestine models. To this aim, the major goals of this project are the the design and fabrication of complex and innovative microfluidic device provided with an integrated PDMS membrane designed to mimic the crypt-villus axis in order to promote the differentiation of the intestinal epithelium and the establishment of peristaltic motion by means of an automatized and controlled elettrovalve system. The platform was used to estimate the intestinal transport properties of the bolus and the physiological condition of the shear stress under peristaltic motion. An important feature of the device, is the possibility to induce a fluid flow both at the basolateral and the lumen side of the intestinal epithelium, therefore the possibility to introduce integrated electrodes in the apical side and basoteral side in order to be enable continuous monitoring of cells behaviour and differentiation through TransEpithelial Electrical Resistance measurements. The effect of PDMS membrane morphology, peristaltic motion and shear stress on intestinal epithelial cell differentiation, mucus production and molecules adsorption process has been evaluated. The development of the Peristalsis on chip device could be reduce the poorly predictive preclinical evaluation generated by the phylogenetic distance between laboratory animals and humans, the discrepancy between current in vitro systems and the human body, and the restrictions of in silico modelling.

Index

Index of figures

1. In vitro models of intestinal epithelium: State of art.

Tissue engineering offers a new approach for treating diseases by fabricating tissue replacements. The conventional tissue engineering strategies follow a "top-down" mechanism, wherein cells are seeded onto pre-fabricated scaffolds and expected to re-populate the scaffolds by extracellular matrix (ECM) deposition and remodelling, often with medium perfusion, growth factors addition, and/or mechanical stimulation [1]. Innovative technologies for producing three-dimensional constructs with complex shapes would be highly useful in tissue engineering [2]. Currently, the widely used animal models often fail to predict human physiological responses to orally delivered drugs and poorly mimic thedrug interactions. For this reason, there is great interest in developing models that recapitulate the complex functions of human intestine *in vitro* [3]. In particular, to recapitulate the complex microenvironment of human organs, living cells were continuously perfused into microfluidic devices with micrometric sized chambers, to model physiological functions of tissues and organs. These systems can incorporate physical forces, including physiologically relevant levels of fluid shear stress, cyclic strain and mechanical compression, and allow to make analysis of organ-specific responses including recruitment of circulating immune cells, drug toxicity evaluation or other environmental perturbations [4].

1.1 The importance of the Gastro-Intestinal tract: The small intestine

As it well knows, the absorption evaluation plays an important role at the early stage of drug discovery due its robust potential that removes molecules with poor absorption, distribution, metabolism, excretion and toxicity (ADMET). The absorption of the drug can occur in all the segments of the gastro intestinal (GI) tract in particular in the stomach, small intestine and colon. The GI tract is an organ system which digests food, absorb energy and nutrients, and expels the waste products as feci and urine. It can be divided into different segments: mouth cavity, oesophagus, stomach, small intestine and large intestine [5,6]. The gastrointestinal lumen houses more than 400 species of microorganisms. The composition of this microbial community varies along the length of the gastrointestinal tract as a function of regional epithelial secretory activity. Like the skin, the gastrointestinal tract creates a barrier between external and internal environments [7]. It has been well demonstrated that small intestine is the organ where the vast majority of digestion takes place. The essential nutrients are made

accessible to the body by the absorption through the mucous layer into the blood or lymphatic circulation. Concurrently, the intestinal lining epithelial layer works as an effective barrier against the systemic access of substances and, therefore, has crucial influence on the bioavailability of orally administered drugs. Hence, the knowledge of the absorption and metabolism of active ingredients at the intestinal mucosa is of particular significance, since the oral bioavailability of a drug is defined as the fraction of an oral dose that reaches the systemic circulation [8]. One major factor that is missing in conventional *in vitro* culture models is the lack of the natural mechanical microenvironment of the normal gut that experiences trickling fluid flow as well as cyclic peristaltic motions [7]. The small intestine is a specialized tubular structure within the abdominal cavity in continuity with the stomach proximally and the colon distally. The small bowel increases 20 times in length with aging, from 200 cm in the new born to almost 6 m in the adult, and its length is approximated by three times the length of the infant, or height of the child or adult [9]. The small intestine structurally includes the duodenum, jejunum, and ileum. It is so called because its lumen diameter is smaller than that of the large intestine, although it is longer in length than the large intestine [10]. The first section is the duodenum, which is approximately 1 foot in length (25 cm) and extends from the pylorus to the duodenal jejunal flexure; this point is marked by the ligament of Treitz. The duodenum is anatomically divided into four parts and curves in the shape of the letter C around the head of the pancreas.
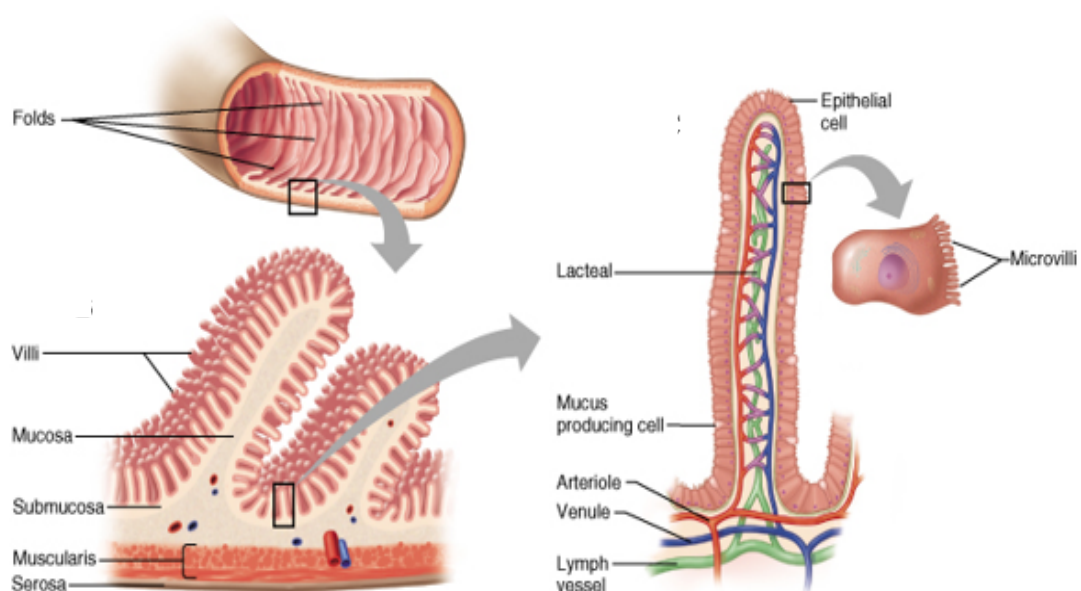
Figure 1. Small intestine anatomy and physiology. Focus on Lumen of small intestine. Focus on 4 layers of small intestine: Serosa, Muscularis, Submucosa, Mucosa and epithelial layer formed by villi. Focus on Villo-Crypts axis and its components.

At its origin the duodenum is covered with peritoneum for about 2.5 cm after which it becomes a retroperitoneal organ. The upper half of the small intestine is termed the jejunum and the remainder is the ileum. The character of the small intestine does change as it is followed distally towards the caecum. The jejunum has a thicker wall as the circular folds of mucosa (valvulae conniventes) are large and thick. The proximal small bowel is of greater diameter than the distal small bowel. In addition, the jejunum tends to lie towards the umbilical region of the abdomen and the ileum to the hypogastrium and pelvis. Mesenteric vessels tend to form fewer arcades in the jejunum with long and relatively infrequent terminal branches passing to the intestinal wall. However, the ileum tends to be supplied by shorter and more numerous vessels which arise from a number of complete arcades [11]. The wall of the small intestine is composed of four layers: mucosa (or mucous membrane), submucosa, muscularis (or muscularis propria), and adventitia (or serosa) [12]. The mucosa and submucosa are specialized to increase surface area and maximize the absorptive capabilities of the mucosa layer [7].
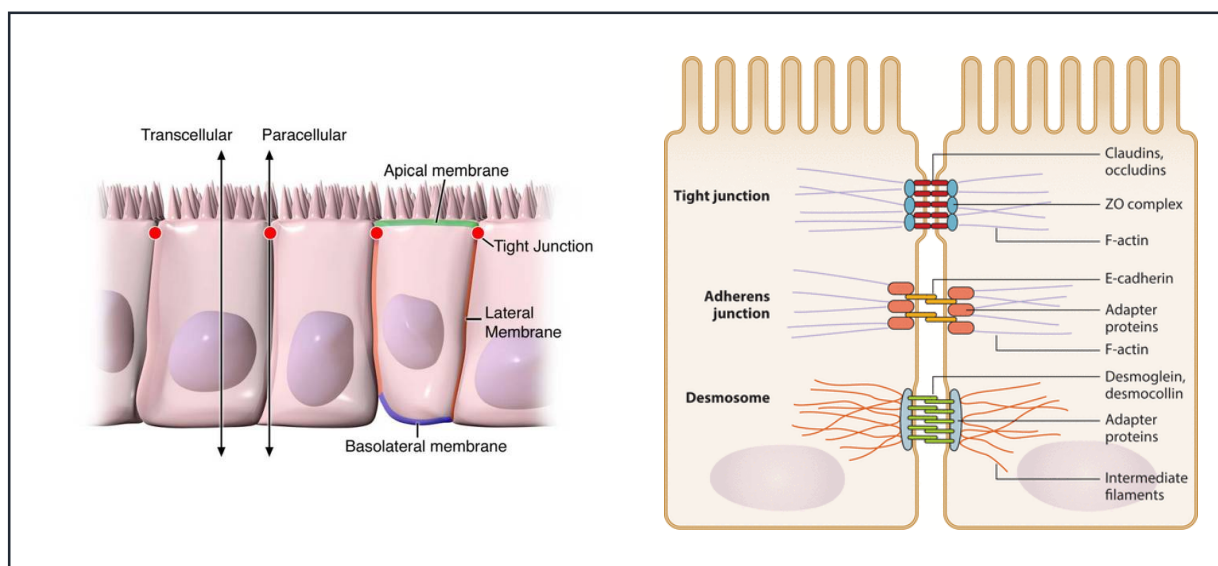
Figure 2. Epithelial layer and its function as a barrier. Focus on single cells of small intestine epithelial layer and different pathway of cross trough the intestinal epithelial layer. Focus of different biding intestinal epithelial cells.

1.2 Intestinal peristalsis

Peristalsis is a reflex response that is started when the gut wall is stretched by the contents of the lumen, and it occurs in all parts of the GI tract from the oesophagus to the rectum. The stretch initiates a circular contraction behind the stimulus and an area of relaxation in front of

it (Figure 4). The wave of contraction then moves in an oral-to-caudal direction, propelling the contents of the lumen forward at rates that vary from 2 to 25 cm/s. Peristaltic activity can be increased or decreased by the autonomic input to the gut, but its occurrence is independent of the extrinsic innervation. Peristalsis is an excellent example of the integrated activity of the enteric nervous system.

When the meal is present, the enteric nervous system promotes a motility pattern that is related to peristalsis, but is designed to retard the movement of the intestinal contents along the length of the GI tract to provide time for digestion and absorption [13].

This motility pattern is known as segmentation, and it provides for ample mixing of the intestinal contents (known as chyme) with the digestive juices. A segment of bowel contracts at both ends, and then a second contraction occurs in the center of the segment to force the chyme both backward and forward. Unlike peristalsis, therefore, retrograde movement of the chyme occurs routinely in the setting of segmentation. This mixing pattern persists for as long as nutrients remain in the lumen to be absorbed. It presumably reflects programmed activity of the bowel dictated by the enteric nervous system, and can occur independent of central input, although the latter can modulate it.
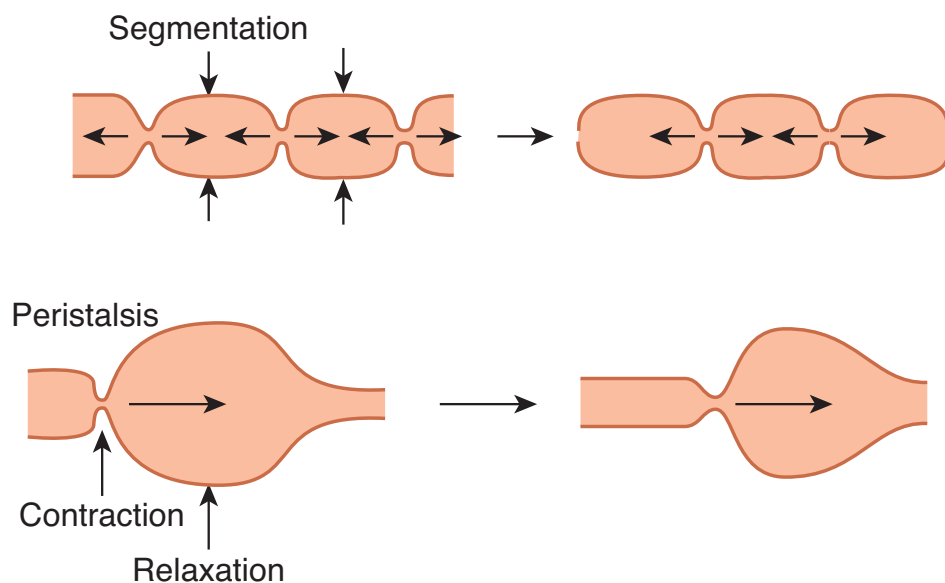
Figure 3. Different type of GI Movement. Focus on Segmentation, movement that break up and mix the bolus. Focus on Peristalsis, movement that move on inside intestine lumen the content of food.

Except in the esophagus and the proximal portion of the stomach, the smooth muscle of the GI tract has spontaneous rhythmic fluctuations in membrane potential between about –65 and –45 mV. This basic electrical rhythm (BER) is initiated by the interstitial cells of Cajal, stellate mesenchymal pacemaker cells with smooth muscle-like features that send long multiply branched processes into the intestinal smooth muscle. In the stomach and the small intestine, these cells are located in the outer circular muscle layer near the myenteric plexus. In the stomach and small intestine, there is a descending gradient in pacemaker frequency, and as in the heart, the pace-maker with the highest frequency usually dominates.

The BER itself rarely causes muscle contraction, but spike potentials superimposed on the most depolarizing portions of the BER waves cause increase muscle tension. The depolarizing portion of each spike is due to Ca^{2+} influx, and the repolarizing portion is due to K^+ efflux. Many polypeptides and neurotransmitters affect the BER. The rate of the BER is about 12/min in the duodenum and falls to about 8/min in the distal ileum. The function of the BER is to coordinate peristaltic and other motor activity; contractions occur only during the depolarizing part of the waves.
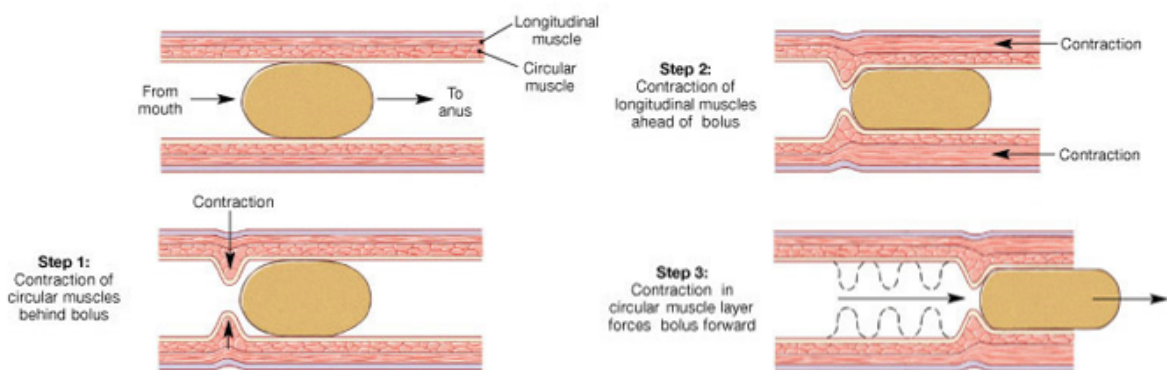
Figure 4. Intestinal Peristalsis from Mouth to intestinal small intestine lumen and its steps. Small Intetine Mucosa formed by Longitudinal and Circular Muscle. Step of contraction by longitudinal and circular muscle and blosu forced by contraction forward trough the lumen.

1.3 Mechanical Properties of Healthy Gastrointestinal Tissue

The mechanical properties of the GI tract are important for its function as a digestive organ. Hence, in the last decade it has become increasingly popular to acquire distensibility data in motility research by luminal balloon distension or bolus injection [14]. The tensile properties of the human esophagus, stomach, small and large bowel were examined on an Instron 1221 tensiometer. The values of maximal stress and destructive strain were the following: for

esophagus-1.2 MPa and 140%, respectively, for stomach axial specimens-0.7 MPa and 190%, for stomach transversal specimens-0.5 MPa and 190%, for small bowel transversal specimens-0.9 MPa and 140% and for large bowel transversal specimens-0.9 MPa and 180%. Tests conducted on small and large bowel axial specimens permitted examination of the intestinal wall as a multi-layered structure. The mechanical properties of tested bowels in axial and transversal directions were qualitatively different. The submucosa and muscular layers affect the mechanical strength of bowel wall, while the serosa and mucosa showed no significant strength. Reproducible results were generated for cadaveric and surgically removed stomach and small intestine, which showed their mechanical properties similar under certain storage conditions. The data received could be used for monitoring of the mechanical properties of bowel wall layers under different conditions and for checking of bowel distension sequences [15].

Term	Definition
Stress	Force per unit surface area that the part lying on the positive side of a surface element (the side on the positive side of the outer normal) exerts on the part lying on the negative side. Stress is a tensor quantity with six independent components (τ_{11}, τ_{22}, τ_{33}, $\tau_{12} = \tau_{21}$, $\tau_{13} = \tau_{31}$, and $\tau_{23} = \tau_{32}$). The components τ_{11}, τ_{22}, and τ_{33} are called normal stresses, and the remaining components are called shear stresses. A normal stress is perpendicular to the surface while a shear stress is parallel to the surface.
Strain	Forces applied to solids cause deformation or strain. Consider a string with initial length L_0 and stretched length L. It is useful to describe the change in length by dimensionless ratios such as L/L_0 or $(L - L_0)/L_0$ as this eliminates the absolute length from consideration. Elongation causes tensile (positive) strain while shortening causes compressive (negative) strain.
Elastic modulus	The proportionality constant between stress and strain. Hooke's law applies for a homogenous, isotropic, linearly elastic material implying that a single elastic modulus describes the stiffness. As the mechanical behaviour in biological tissues is non-linear, an incremental approach must be used.
Isotropy	Materials whose mechanical properties do not depend on directions are said to be isotropic. Biological tissues are usually anisotropic, mainly owing to their heterogeneous, layered structure.
Viscoelasticity	Time dependence of the response to stress or strain. Stress relaxation, creep and hysteresis are features of viscoelasticity.
Preconditioning	In mechanical testing of living tissues in vitro, the loading and unloading processes are repeated for a number of cycles until the stress–strain relation becomes stabilised and repeatable results are obtained.
Constitutive equation	A constitutive equation describes the material properties of a material, e.g. the stress–strain relation.
Zero-stress state	The tissue configuration where no stress is present. For a tubular organ, the zero-stress state is obtained by making radial cuts in a ring of tissue so that it springs open into a sector. The difference in strain between the zero-stress state and the no-load state where all external forces are absent is called residual strain.
Plastic deformation	Deformation that does not return to its initial state when the stress is removed.

Figure 5. Table with reference guide to some common mechanims terms in GI tract

1.4 Engineered intestinal tissues in vitro

Over the last several years the pre-clinical screening was carried out with *in vitro* 2D culture model as well as animal models. *In vitro* methods are widely used to investigate the ADMET (Absorption, Distribution, Metabolism, Excretion, Toxicity) of drug. Conventional *in vitro* gut model are characterized by the culture of intestinal epithelial monolayer under static condition. The cell line commonly used are immortalized or cancerous intestine-like cells, [16] such as Caco-2, HT-29, T84, TC-7, and SW620. Among these cell types, Caco-2 and HT-29 cells are used extensively as substitutes for enterocytes and goblet cells, respectively [17]. Caco-2 cells are derived from human colon carcinoma and have been shown to form a polarized enterocyte-like monolayer after 21 days in culture on Transwell inserts where they become fully differentiated. Polarized Caco-2 monolayers are characterized by the presence of villi, brush border enzymes, and drug transporters. Caco-2 cells can be cultured on a variety of biomaterials including alginate, collagen, polycarbonate, polystyrene, and Biocoat. This cell line was very versatile and it was extremely appealing for use in engineered *in vitro* models. Unfortunately, in terms of xenobiotic transport modelling, such culture models have low permeability because 2D Caco-2 monolayer is eight-times smaller than that of human small intestine epithelium, which is considered as one of the reasons for poor drug paracellular permeability correlation between conventional *in vitro* models and human small intestine [16]. 2D culture have a lot of limitation, in fact they cannot support the tissue-specific, differentiated functions of many cell types or accurately predict *in vivo* tissue functions and drug activities. These limitations have led to increased interest in more complex 2D models, such as those that incorporate multiple cell types or involve cell patterning [4]. The 3D models were the system that better represented the spatial and chemical complexity of living tissues. 3D cell cultures, developed over 50 years ago, usually rely on hydrogels, composed of either natural extracellular matrix (ECM) molecules or synthetic polymers, which induce cells to polarize and to interact with neighboring cells. They can take many forms, including cells randomly interspersed in ECM or clustered in cellular self-assembling microstructures known as organoids. 3D intestinal model obtained by microfabrication techniques was a human small intestine crypt-like topography fabricated using photolithography and transferred to poly(dimethylsiloxane) (PDMS) and collagen membrane substrates [16]. Human small intestine villus structures had also been fabricated by combining different microfabrication techniques. 3D printing (3DP) was used to construct porous poly(lactic-coglycolic acid) (PLGA) villous scaffolds [17]. Recently, by combining laser techniques, a collagen villous scaffold was fabricated with 0.5 mm villous

height and 25 villi per mm^2 density, with striking similarity to the human jejunal villi [18]. By using a custom-made cell culture insert kit, the collagen villous scaffold was integrated with a six-well cell culture plate to study drug absorption [19]. When cultured on collagen villous scaffold, Caco-2 exhibited differentiation gradients along the villous axis, on the top of the villous cells were more columnar and polarized than cells near the bottom of the villus, according to the *in vivo* observation that enterocytes become more differentiated when migrating from the crypt to the top of the villus [19].
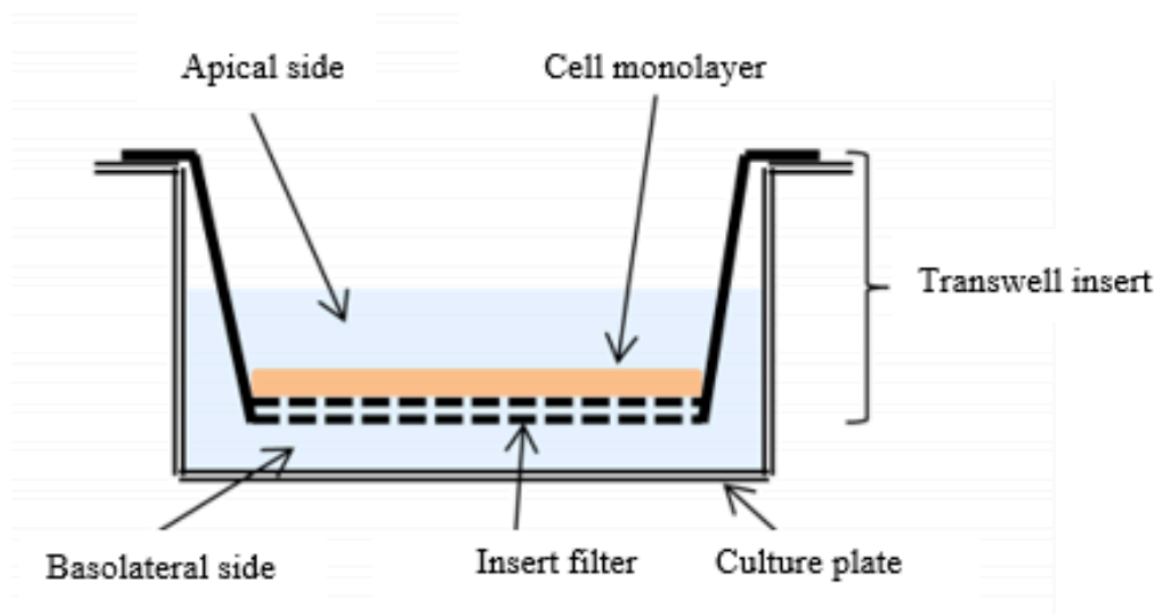
Figure 6. Schematic representation of Cell culture on a Transwell insert.

Another 3D human dynamic *in vitro* tissue model was a co-culture of human Caco-2 with primary-isolated human microvascular endothelial cells (hEMCs) on decellularized porcine jejunal segments. Under 14 days of dynamic condition, the Caco-2 cells showed a high-prismatic morphology, resembling normal primary enterocytes within their native environment [20]. Caco-2 cells was also co-cultured with HT29-methotraxate cells and seeded on a Transwell filter insert with collagen gel and stromal cells (fibroblasts and immunocytes) incorporation. The 3D model displayed, then 2D model, more physiologically relevant characteristics evidenced by its decreased TEER value and mucus-like layer formation [8]. 3D models have been very useful for studying the molecular basis of tissue function and better

capture signaling pathways and drug responsiveness in some disease states compared with 2D models. But they also have some limitations, in particular cells was usually not exposed to normal mechanical cues on the apical side (luminal), including fluid shear stress, tension and compression, which influence organ development and function in health and disease. The absence of serosal fluid flow also precludes the study of how cultured cells interact with circulating blood and immune cells [4]. Recent studies aim to replicate the microenvironment into micrometric chamber that allowed to model physiological functions of tissues and organs.

2. Mechanomedicine: Microfluidics for mechanobiology of organ model

Mechanical stimuli play a critical role in organ development, tissue homeostasis, and disease. Understanding how mechanical signals are processed in multicellular model systems is critical for connecting cellular processes to tissue- and organism-level responses. However, progress in the field that studies these phenomena, mechanobiology, has been limited by lack of appropriate experimental techniques for applying repeatable mechanical stimuli to intact organs and model organisms. Microfluidic platforms, a subgroup of microsystems that use liquid flow for manipulation of objects, are a promising tool for studying mechanobiology of small model organisms due to their size scale and ease of customization.

2.1 Organ on chip: An Overview

In the last decade, an emerging bioengineering field has been developed that promises to transform medical science and radically overhaul the arduous process of bringing new products to market. More physiologically relevant in vitro human models are highly requested by pharmaceutical, chemical and food industries to test drugs, foods, cosmetics and dietary supplements for evaluating their efficacy and/or toxicity, with the goal to replace the traditional cell culture and to reduce the use of animal-based models.

Besides being costly, labour-intensive and ethically contentious, animal models often fail in reproducing human physiological responses, as evinced by the small percentage (12%) of drugs that demonstrate the maximum clinical success and obtain approval from the Food and Drug Administration (FDA) [21]. This lack of predictive value can be partly attributed to poorly conducted animal experiments, but also to the differences in physiology between humans and animals. For example, species-to-species variations occur in the expression profiles of several genes and the transporter proteins. To overcome these species-specific problems, the use of human tissues in a realistic in vitro environment is of great interest. However, the conventional two-dimensional cell cultures was the most commonly used in vitro models, that are characterized by cell seeding on flat and hard plastic or glass substrates. These models are too simplified and not faithfully replicate the tissue-specific, differentiated structure and functions of many cell types. As a result, these 2D culture system do not accurately predict in vivo tissue functions and drug activities [22] with the lack of the predictive value. These limitations have led to develop more complex models, including multiple cell types or integrating cell patterning in a three-dimensional (3D) configuration, which better represent the spatial and chemical

complexity of living tissues. Among 3D cell cultures, organoids have been of great interest: they consist in cell aggregates derived from primary tissue or stem cells that are capable of self-renewal, self-organization and exhibit organ functionality.
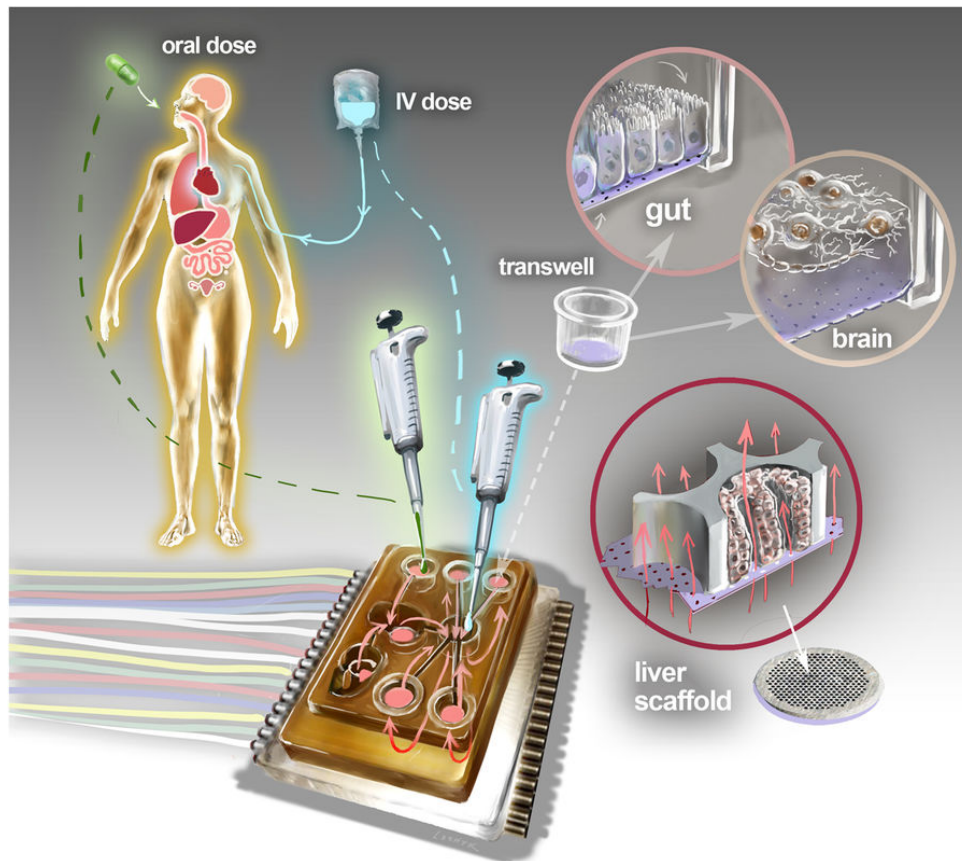
Figure 7. Schematic overview of "Physiome-on-a-chip" approach, using bioengineered devices that nurture many interconnected 3D "microphysiological systems" (MPSs), aka "organs-on-chips." MPSs are in vitro (lab) models that capture facets of in vivo (live) organ function. They represent specified functional behaviors of each organ of interest, such as gut, brain, and liver, as shown here. MPSs are designed to capture essential features of in vivo physiology that is based on quantitative systems models tailored for individual applications, such as drug fate or disease modeling. (illustration credit: Victor O. Leshyk)

Organoids address the limitations of existing model systems by providing similar composition and architecture to primary tissue: this occurs thanks to the presence of cells that can differentiate into cells of all major cell lineages, with similar frequency as in physiological condition. In addition, they are more biologically relevant to other model systems and are amenable to manipulate niche components and to analyse the gene expression. Finally, organoids provide stable system for extended cultivation: they can be cryopreserved as

biobanks and expanded indefinitely by leveraging self-renewal, differentiation capability of stem cell and intrinsic ability to self-organize [23]. However, these 3D models are highly variable in size and shape, and it is difficult to maintain cells in consistent positions in these structures for extended analysis. Moreover, functional analysis to quantify transport, absorption or secretion is often prevented by the difficulty of sampling luminal contents. Another drawback is that some of these systems lack of multiscale architecture and tissue-tissue interfaces, such as the interface between vascular endothelium and surrounding connective tissue and parenchymal cells, where critical transport of fluids, nutrients, immune cells, and other regulatory factors occurs. In addition, Organoids models do not permit the application of dynamic mechanical forces (e.g., breathing movements in lung, shear in blood vessels, peristalsis in gut, tension in skin) that are critical for the development and function of living organs in health and disease. In order to overcome these limitations, the need of in vitro cell culture models, in which the cells can reside in an environment with chemical and physical cues that enhance their functionality, are strongly required. Over the last decade, new platforms have been developed and are known as Organs-on-Chips (OoC), a potentially game-changing technology born from the convergence of microfluidics and tissue engineering research. The word 'chip' in organ-on-chip stems from the original fabrication method, a modified form of photolithographic etching used to manufacture computer microchips, which allows the control of the surface feature such as shapes and sizes on the same scale (nm to μm) that living cells sense and respond to in their natural tissue milieu. The word 'organ', instead, is related to the engineered microenvironmental stimuli applied to replicate organ-level functions, such as breathing-derived mechanical stretch for lung cells, fluid shear stress for vascular cells or cyclic physical loading for cardiomyocytes.

In other words, OoCs are microfluidic devices for culturing living cells in continuously perfused, micrometer-sized chambers in order to model physiological functions of specific tissues and organs. The goal is not to build a whole living organ but rather to synthesize minimal functional units that recapitulate tissue- and organ-level functions.

OoC technology allows reconstitution of the microarchitecture of the organ supported by the design of a dedicated mechanical context matching the shape, surface pattern and stiffness of organ-specific microenvironments. Microfluidic technologies provide control over many system parameters that are not easily controlled in 3D static cultures or bioreactors, simplifying the study of a plethora of physiological phenomena. Fluid shear stresses can be controlled by altering flow rates or channel dimensions, and by separating cells from the flow path using a microporous membrane. Moreover, the precise control over the microfluidic flow rate enables

the optimal oxygenation and nutrition supply. It affords not only long-term viability of healthy tissues but also an efficient circulation of immune cells, antibodies, biochemical signaling molecules and metabolites, and the ability to collect small volumes of fluid containing secreted cell products for analyses. Continuous perfusion and mechanical stress help to build dynamic tissue models, which are physiologically more relevant than conventional static cell cultures and enable spatiotemporal control of chemical gradients and mechanical cues to study the influence of the microenvironment on the cells. Finally, because these devices are totally microengineered, they can be integrated with micro-sensors to provide information about the cultured cells or microenvironmental conditions. Micro-sensors incorporated in chips are used, for example, for analysis of tissue barrier integrity, cell migration, fluid pressure, pH, Temperature and also to measure some chemicals delivery, such as glucose, lactate and oxygen [24].
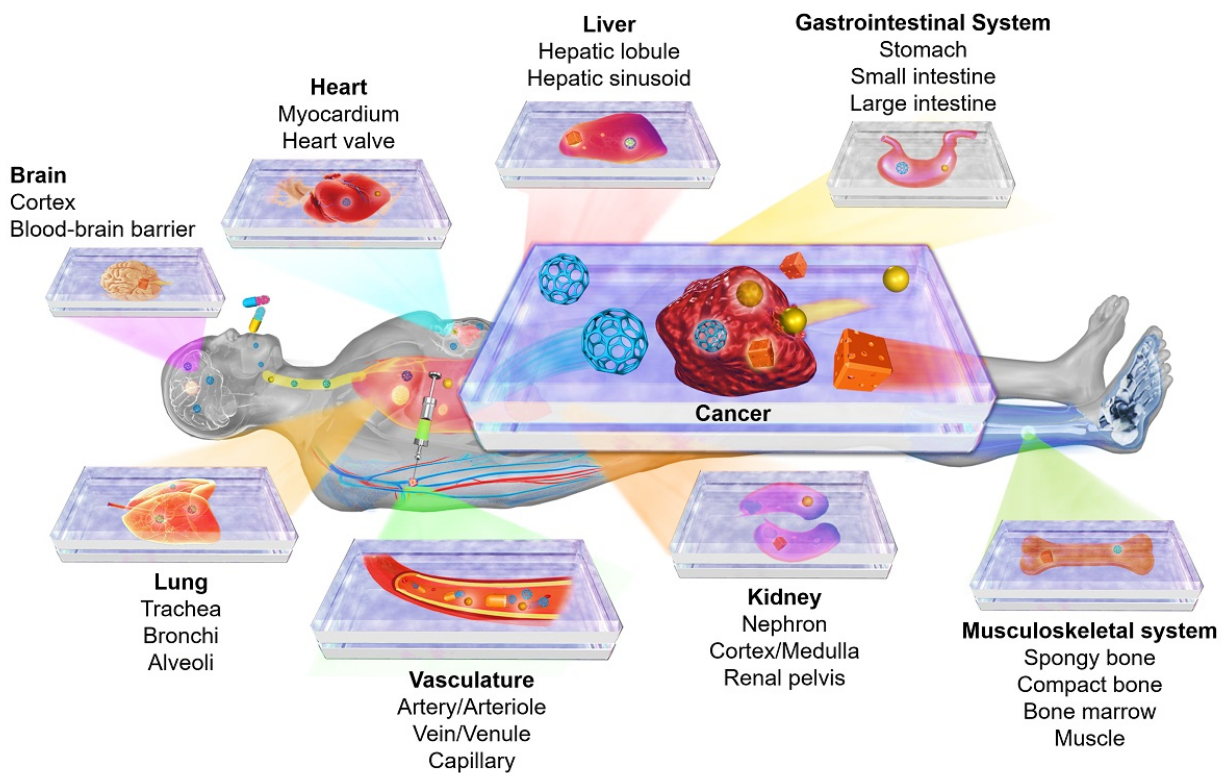
Fig 8. Overview of "Organ on chip". All typical chip that is reproduced and interconnected each other. Focus on Cancer on chip, new frontier of recent studies.

The small size of these new models, the ability to control the microenvironment, the optical access at high spatial resolution, the real-time imaging, and the possibility of interfacing with

both targeted and untargeted mass spectrometry provide OoCs with important advantages compared to other models. The great diversity and range of complexity achievable in OoCs offer the opportunity to optimize or even customize the design for targeted studies, paving the way to personalized medicine. In light of these potential benefits, the main applications of OoCs start from toxicity testing to human disease model building and drug discovery. Users are increasingly from a wider spectrum of fields and include not only biomedical researchers attempting to understand disease mechanisms and etiology but also industrials with different profiles – pharmaceutics, biotechnology, cosmetics, chemistry and environment – all interested in predicting efficacy and safety of compounds for humans. This approach has made it possible to microfabricate models such as blood vessels, muscles, bones, airways, liver, brain, gut and kidney (Figure 7).

2.2 Organ on chip: Intestine on chip

Organs-on-chips are microfluidic devices for culturing living cells in continuously perfused, micrometre sized chambers in order to model physiological functions of tissues and organs. These systems can incorporate physical forces, including physiologically relevant levels of fluid shear stress, cyclic strain and mechanical compression, and permit analysis of organ-specific responses including recruitment of circulating immune cells, in reaction to drugs, toxins or other environmental perturbations [4].
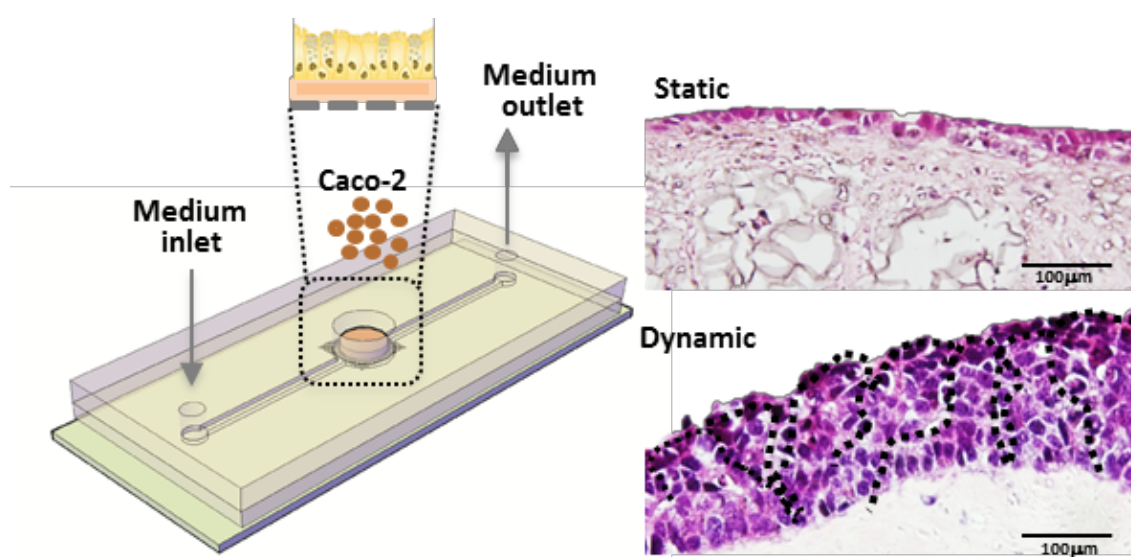
Figure 9. Intestine-on-chip device increases ECM remodeling inducing faster epithelial cell differentiation. Gut on chip device and histology in static and dynamic condition

Recently, microporous SU-8 membranes were fabricated with 3D villus-like features, with the goal of incorporating a more relevant 3D intestinal microenvironment into the microscale cell culture analogues (mCCA) system [25]. Long-term perfusion culture of Caco-2 cells on track etched membranes was demonstrated in a micro-fluidic device with integrated micro pumps and on-chip optical fibre sensors [26]. Kim *et al.* reported a human gut-on-a-chip device that include peristalsis, fluid flow, and microbial flora [27]. Compared to static culture, cells cultured on the device exhibited accelerated intestinal epithelial cell differentiation, formation of villi-like structures and increased intestinal barrier functions. Integration of 3D tissues in a microfluidic device could be better reproduce the *in vivo* interaction with ECM under dynamic condition. Ingber *et al.* recently developed a human 'Gut-on-a-Chip' in which Caco-2 intestinal epithelial cells are cultured within micro-fluidic channels of a clear, flexible, polydimethylsiloxane (PDMS) device created with microchip manufacturing that permits application of fluid flow as well as cyclic mechanical strain at levels similar to those experienced by epithelial cells in living intestine. Using this device, they showed that Caco-2 cells immediately polarize, differentiate into a columnar epithelium, and spontaneously form undulating structures that were reminiscent of intestinal villi [28-29-30]. Furthermore, Shuler's group create a microfluidic device containing several fluidically linked chambers representing different organs that could be used to test drugs, chemicals or toxins. This group creates many types of microscale devices that contain a multiple culture chambers, each holding a single cell type and which are linked by microfluidic channels. This suitable chip mimics basic organ-organ coupling and permitted analysis of drug ADMET characteristics that are usually determined *in vivo* [4]. Many groups have explored the use of organs-on-chips to study drug ADMET properties. More recently, GI tract μCCAs have been developed that include digestion, a mucus layer, and physiologically realistic cell populations to determine oral bioavailability of drugs. Sant *at al.* showed that acetaminophen was absorbed and metabolized by GI cells, then circulated to the liver cell compartment. Combination of microfabrication with microfluidics has allowed precise control over microscale structures. In addition, the ability to pattern physiologically relevant cell types, as well as to manipulate geometry of the substrate in 3D and flow patterns/hydrodynamic shear stress in the physiological range upon the cells takes us one step closer to creating whole-body-on-a-chip for efficient screening of drug efficacy and toxicity [32].

1. Top Channel
2. Intestine Epithelial Cells
3. Vacuum Channel
4. Porous Membrane
5. Endothelial Cells
6. Bottom Channel
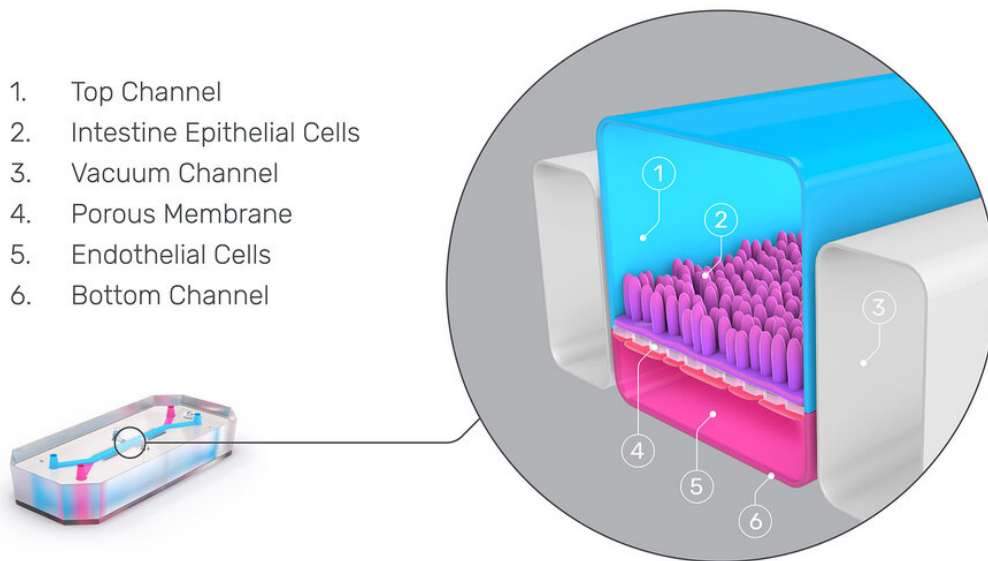
Fig 10. Human gut-on-a-chip. (A) A schematic representation of the gut-on-a-chip device showing the flexible porous ECM-coated membrane lined by gut epithelial cells cross horizontally through the middle of the central microchannel, and the full height vacuum chambers on both sides. (B) Schematic image of intestinal monolayer cultured within the gut-on-a-chip in the absence (left) or presence (right) of mechanical strain.

While the mechanical stimuli reproduced by Ingber et al. were of small amplitudes, mainly designed to stretch and stimulate epithelial cells, other researcher try to emulate intestinal wall contraction that enable mixing for bacterial growth. The minigut differs from the in vitro gut-like devices discussed above by emulating wall contractions with an array of flexible membrane valves evenly spread along the length of the channel [28].

Precisely, the ceiling of the channel is made of a silicone elastomer and has a regular array of eight individually addressable, pressure-actuated membrane valves. The application of pressure to a valve leads to its contraction and partial channel occlusion (from a minor reduction of the channel height all of the way to the ceiling touching the floor), emulating local contraction of intestinal walls. The standard pattern of actuation of the valves is a peristaltic wave propagating from the mini-gut channel inlet to its outlet. As expected, the flow in the channel resulting from contraction of the valves that led to obtain the efficient mixing along the channel, especially, when the ceiling touched the floor, resulting in major occlusion.
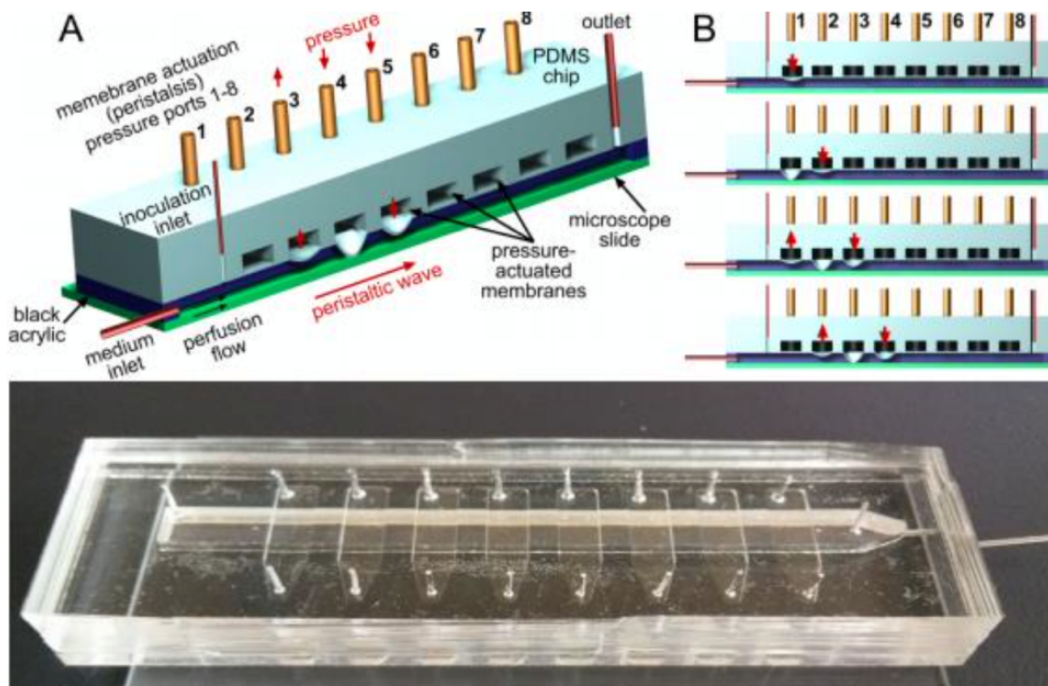
Fig 11. Mini-gut device. (A) Schematic of the mini-gut device showing a cross-section during peristaltic wave. (B) Cross-sections of the device at three consecutive stages of a peristaltic wave. (C) Photo of the device.

2.3 The effects of mechanical forces on intestinal physiology and pathology

Study of the GI tract requires understanding of the interactions between cells, tissues and gastrointestinal organs in health and disease. Data on the biomechanical properties are crucial for the understanding of the normal function of the GI tract and dysfunction due to disease. In fact, peristaltic motion that propels the food through the GI tract is a result of interaction of the passive and active tissue forces and the hydrodynamic forces in the food bolus and the remodelling of the mechanical properties reflects the changes in the tissue structure that determine a specific sensory-motor dysfunction.
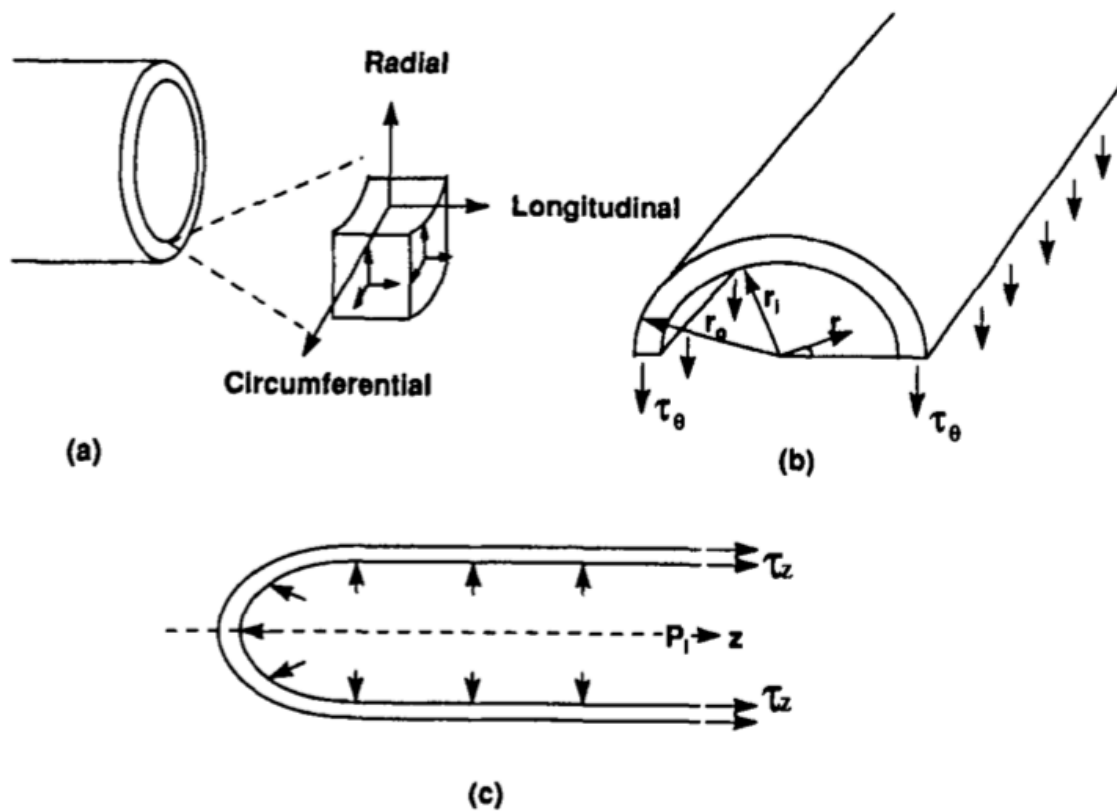
Figure 12. GI tract mechanics, in particular A pressurized cylindrical tube. An infinitesimal element of the cylindrical tube showing the radial, longitudinal and circumferential directions.

With reference to the zero-stress state, combining the morphometry data and pressure data, is possible to compute the stress-strain relationship of the GI wall. The stress-strain distribution mainly reflects the elastic properties of the GI tract. Changes in the elastic properties reflect structural remodelling of the GI wall in different diseases. The opening angle of the zero-stress state, residual strain and stress-strain relationship as the most relevant biomechanical parameters to describe diseases causing GI remodelling. However, the effect of different factors on the opening angle and residual strain of GI tract depend on the changes of layered structure. It is well known that mechanosensation have a crucial role in GI function. The biomechanical remodelling by the disease, such as alterations of residual strain, stress distribution and wall stiffness, can alter the tension and stress distribution of the mechanosensitive afferents. As demonstrated [32], the perception and motility of the GI tract can also change. Therefore, the morphological changes and biomechanical remodelling of the GI tract are likely to affect the

function of mechanosensitive afferents in the GI wall and further affect the motor and sensory functions.

2.4 Permeability

As previously described, the Caco-2 monolayer contains an apical brush border, forms tight junctions and contains many of the enzymes and transport proteins that mediate the active uptake or efflux of drugs and chemicals in the intestine. For these reasons, the Caco-2 permeability assay has become the gold standard for in vitro prediction of intestinal food and drug permeability and absorption.
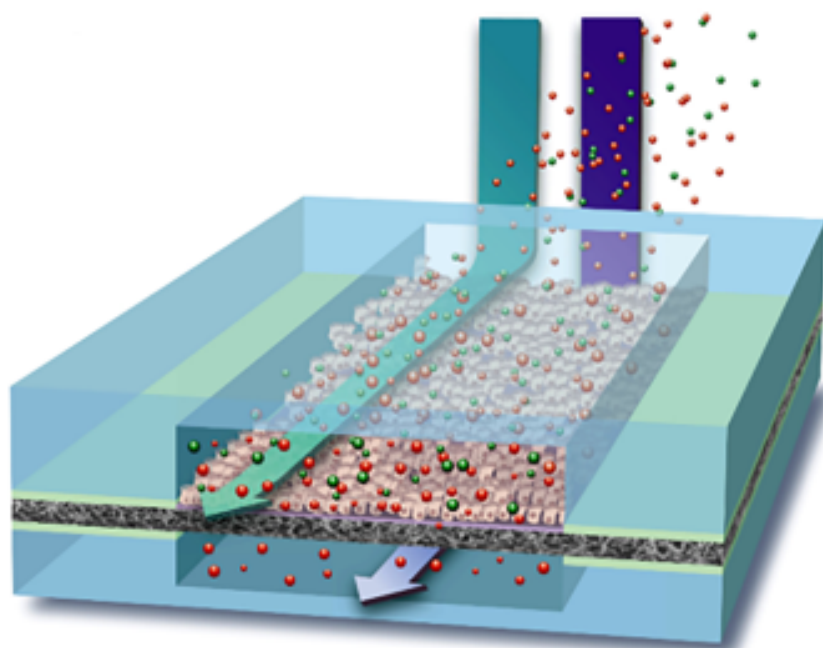
Figure 13. Permeability assay inside organ on chip, diffusive transport of molecule across a confluent cell monolayer can be quantified.

Cell monolayer permeability is typically measured using tracer-based assay in which the diffusive transport of a fluorescent molecule across a confluent cell monolayer is quantified. Increased diffusive transport corresponds to increased monolayer permeability and therefore decreased barrier function. Conventional methods for permeability studies are usually performed in a Transwell system where the donor and acceptor chambers are vertically separated by the cell monolayer cultured on the insert membrane. The compounds to be evaluated are loaded to either the apical or the basolateral side of each cell monolayer to simulate the influx (oral administration) or efflux (systemic administration) of compounds

across the intestinal epithelium. At various time points, the appearance of the compounds in the receiving compartment is measured and the transport rate is typically expressed as the apparent permeability coefficient (Papp), which is calculated using the equation:

$Papp = dQ/\mathrm{dt} \times 1/\ A*C_0$

where:

- dQ is the amount of model compound transported over the time interval [g s^{-1}]

- dt time during model compound transported [s]

- A culture surface area [cm^2]

- C_0 initial concentration [mg mL^{-1}]

Additional assessments of the tested compound can be made as well. These include the efflux ratio, measured by assessing the basal to apical Papp as well as the standard apical to basal Papp. It provides an indicator as to whether the compound undergoes active transport (e.g. by P-glycoprotein). However, Transwell static conditions are distinctly different from the dynamic in vivo microenvironment where the intestine is constantly exposed to mechanical stresses due to fluid flow. The unstirred thick fluid layer in the static Transwell culture might limit diffusion, which could lead to lower permeability values than those observed in human intestine in vivo. Some researchers have found that the fluid under dynamic conditions could decrease the thickness of the unstirred diffusion layer and hence increase the permeability [29]. Also in this field, microfluidic systems have significant potential to overcome several problems thanks to their native advantages including small reagent and sample consumption, high integration, rapid analysis, the potential for parallelization and being well suited for shear stress applications. Above all, the epithelial monolayer formed in these devices could be probed from both the apical and basal sides of the epithelium, and this enabled quantification of tight junction barrier function and absorption of nutrients and drugs reproducing more faithfully the in vivo context. Furthermore, microfluidic systems have been adapted to handle fluid precisely and flexibly, giving also the possibility to apply more physiological mechanical stimulation. The successful application of a system to predict drug or nutrient absorption depends on how closely the in vitro model can mimic the characteristics of the in vivo barrier integrity. Ingber's group have demonstrated that the application of low levels of fluid flow and shear stress together with cyclic mechanical strain in the gut on chip could largely increase the paracellular permeability [20]. They measured the Papp of the intestinal epithelium using fluorescent isothiocyanate (FITC)-labeled dextran (FD20; 20 kDa), which characterizes the paracellular barrier function of the intestinal epithelium due to pores associated with tight junctions. The FD20 solution (1mg mL-1) was perfused through the upper channel and sample aliquots (30 μl) are collected

every hour from the outlet of the lower channel in order to analyze the fluorescence intensity and quantitate the amount of FD20 that was transported across the Caco-2 paracellular barrier. As opposed to what expected, the fluid flow alone did not alter the paracellular permeability in Ingber groups system, but when coupled with mechanical stimulation increased Papp values, suggesting that mechanical distortion might alter directly the paracellular mechanisms of transport.

Recently, some researchers (Sun et al., 2020) have shown in an intestine- on-chip model a decrease in transport of the high permeability compounds like antipyrine, ketoprofen and digoxin (i.e. 4.2-, 2.7- and 1.9-fold respectively) compared to the transport in the static Transwell model. They used a glass two-chamber microfluidic chips separated by a PET membrane on which they cultured epithelial cells (Caco2) under dynamic conditions. At day 21 post-seeding, a non-toxic concentration of 100 μM antipyrine, 100 μM ketoprofen, 125 μM digoxin, and 250 μM amoxicillin was prepared in a transport medium (HBSS). Each compound solution was perfused through the upper channel with a flow rate of 100 μL/h, whereas 4% BSA in HBSS was pumped through the basolateral channel. An aliquot (100 μL) was collected from the apical and basolateral outlet every hour for six hours. They concluded that differences in apparent permeability coefficient can be explained by laminar flow related effects and by the influence of the design of the chip and/or the material of the membrane on the diffusion of these compounds. The laminar flow (with Re ~0.007, viscous forces dominate) implies a low migration (or diffusion) of the dissolved chemicals across the layers resulting in less contact of the compounds with the cell surface. The use of different membranes and the influence of different designs (i.e. apical and basolateral volumes) in the gut-on-chip and Transwell models could have contributed to these observed differences. The consequences of these design characteristics, and thus accompanying shear forces, on cell morphology, cell physiology, and cell differentiation and on how this affects compound transport still needs to be assessed [30].

Gut-on-chip device developed by Ingber et al., as the most of the microfluidic systems for permeability assays, requires to collect the samples manually and analyze off-line, which slows experimental progress. Time required is dependent on the analytical method used and an automated process normally performs analysis. The quantification of the samples will be dependent on the test compound used: for example, scintillation counting could be appropriate for radioactive-labeled compounds or, for other compounds, analysis by HPLC with either UV, fluorescence or MS detection or analysis using a UV or fluorescence-plate reader/spectrophotometer [31]. One recent study reported a membrane-based microfluidic chip that was able to measure the permeation coefficients directly with online laser-induced

fluorescence detection. However, the analytes should be tagged with a fluorescent reagent prior to use, which might vary the permeability property of the analytes.

2.5 TransEpitehlial Electrical Resistance (TEER)

To perform reliable in vitro experiments, qualitative and quantitative techniques have been developed to first confirm and quantify the barrier integrity before starting the molecular permeability test. Electrical measurements have been introduced to enable non-invasive, label-free and real-time measurements of the barrier function. Meza et al. in 1980 (kidney epithelium) [33] and Rutten et al. in 1987 (brain endothelium) [34] were among the first researchers to carry out such electrical characterizations of barrier function in vitro. At that time, it was already recognized that the low ionic conductance (i.e. high electrical resistance) across a cellular barrier is mainly controlled by tight junctions between the cells and thus reflects the transport via the paracellular pathway. This "transendothelial / transepithelial electrical resistance" (TEER) is a useful and functional measure of barrier integrity. The TEER measurements have become a widely accepted method for non-invasive and real-time monitoring of barrier tightness. TEER provides a strong indicator of the integrity of the tight junctions and of the cell monolayer. Generally, the electrical resistance of a cellular barrier is measured by introducing two electrodes, one on either side of the cellular barrier. In theory, the ohmic resistance of the path between the electrodes can be determined by applying a direct current (DC) voltage and measuring the resulting current. The ohmic resistance is calculated based on Ohm's law as the ratio of the voltage and current. However, DC currents can damage both the cells and the electrodes. To overcome this issue, an alternating current (AC) voltage signal with a square waveform is applied. The measurement procedure includes measuring the blank resistance (RBLANK) of the semipermeable membrane (without cells) and measuring the resistance across the cell layer on the semipermeable membrane (RTOTAL). The cell specific resistance (RTISSUE) in units of Ω can be obtained as:

$$RTISSUE(\Omega) = RTOT - RBLANK$$

TEER values are typically reported in units of $\Omega\ cm^2$, so the found resistance is multiplied with the culture area A (cm^2) that was sampled. Thus, the normalized TEER value is independent of the porous membrane that was used and the culture area and can be compared across platforms. In the widely used and commercially available TEER measurement system, known as Epithelial Voltmeter (EVOM), an AC square wave at a frequency of 12.5 Hz is used to avoid any charging effects on the electrodes and the cell layer. The EVOM system has a measurement range of 1-

9999 Ω with a 1Ω resolution and uses a pair of electrodes popularly known as a STX2/"chopstick"-electrode pair. Each stick of the electrode pair (4 mm wide and 1 mm thick) contains a silver/silver chloride pellet for measuring voltage and a silver electrode for passing current. Due to concerns about the positioning stability and the membrane area that is actually sampled by chopstick-type electrodes due to their orientation in the insert and well, the EndOhm chamber with plate electrodes has been introduced [35]. This chamber contains two round silver/silver chloride readout electrodes surrounded by two annular silver excitation electrodes positioned parallel to the membrane. This parallel and concentric orientation ensures a fixed electrode position with respect to the cellular barrier as well as a more uniform current distribution through the insert, resulting in more accurate TEER measurements and less variation.
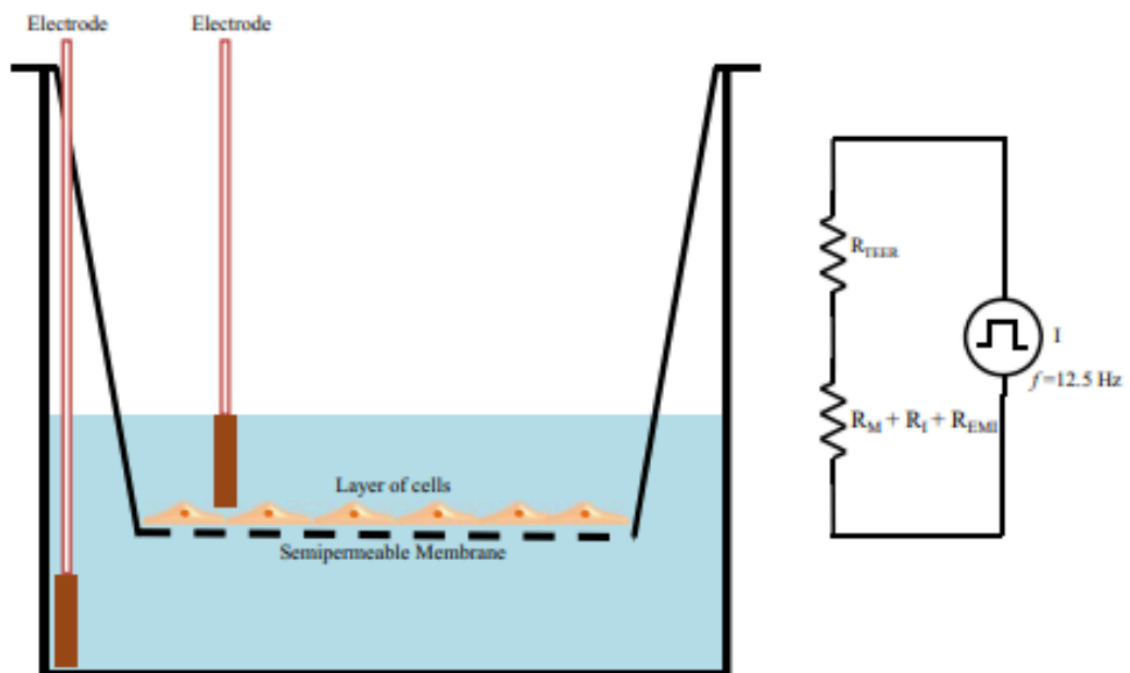
Figure 14. Transepithelial electrical resistance (TEER) measurement with chopstick electrodes. The total electrical resistance includes the ohmic resistance of the cell layer RTEER, the cell culture medium RM, the semipermeable membrane insert RI, and the electrode medium interface REMI.

The DC methods rely on the assumption that the change in measured resistance can be exclusively contributed to biological changes in the barrier, i.e. tight junction formation, rather than changes of non-biological origin, such as differences in medium resistance. In order to overcome this assumption, impedance spectroscopy can be performed by using an alternating

current (AC) signal at various frequencies. The equivalent circuit corresponding to AC measurements is displayed in Figure 14, next to the equivalent DC circuit. The difference is here that the capacitive behaviour of the cellular membrane is included. The barrier function is now characterized by the impedance, which is a complex quantity comprising both resistive and capacitive contributions. Capacitors act as frequency- dependent resistors, with a decreasing impedance at increasing frequency, and generally comprise two conducting parts separated by an electrically insulating material. In these measurements, the capacitive behaviour of the cellular membrane arises from the lipid bilayer, acting as an insulator between the electrically conducting culture medium and cytoplasm. Figure 15 shows a typical equivalent circuit diagram that can be applied to analyse the impedance spectrum of cellular systems. In this circuit, the current can flow through the junctions between cells (paracellular route) or through the cell membrane of the cells (transcellular route). The tight junction proteins in the paracellular route contribute to an ohmic resistance (RTISSUE) in the equivalent circuit. Each lipid bilayer in the transcellular route contributes to a parallel circuit consisting of ohmic resistance (RMEMBRANE) and an electrical capacitance (CC).
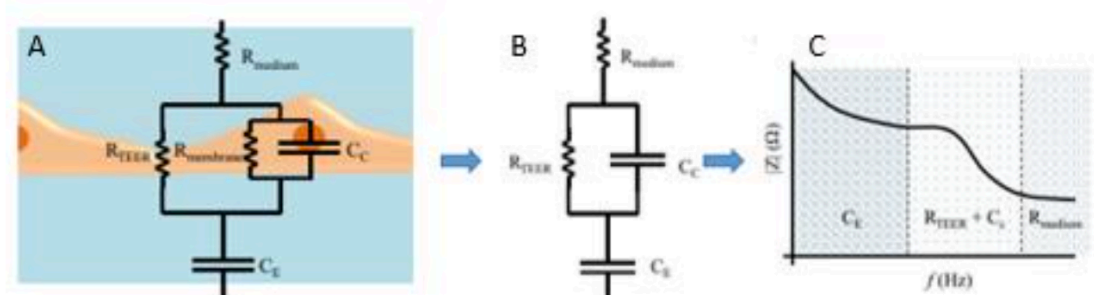
Figure 15. TEER circuits. (A) A typical equivalent circuit diagram that can be applied to analyze the impedance spectrum of cellular systems. (B) Simplified equivalent circuit. (C) A typical impedance spectrum with distinct frequency-dependent regions. Adapted from Benson et al.26.

In addition to these elements, the resistance of the cell culture medium (RMEDIUM) and the capacitance of the measurement electrodes (CE) also have to be considered. The high values of RMEMBRANE cause the current to mostly flow across the capacitor and allows an approximation where RMEMBRANE can be ignored, while the lipid bilayers can be represented with just CC. The impedance spectrum observed will have a nonlinear frequency dependency. Typically, there are three distinct frequency regions in the impedance spectrum

where the impedance is dominated by certain equivalent circuit elements. In the low frequency range, the impedance signal is dominated by CE. In the mid frequency range, the impedance signal is dominated by circuit elements related to the cells, namely RTEER and CC. In the high frequency range, CC and CE provide a more conductive path and the impedance signal is dominated by RMEDIUM. In this way, with a single impedance spectroscopy measurement and suitable parameter fitting the TEER can be calculated.

Two commercial systems used to perform this kind of TEER measurement are the cellZscope (nanoAnalytics GmbH, Münster, Germany) [36] and the ECIS TransFilter system (Applied BioPhysics, Troy, New York, USA) [30]. In these systems, gold or stainless steel electrodes are inserted on both sides of the membrane. An AC signal at a range of frequencies roughly between 1 Hz to 1 MHz is applied between the electrodes and the resulting impedance is measured. From the thus obtained impedance versus frequency data, the equivalent circuit parameters can be estimated by fitting the experimental impedance spectrum data to the equivalent circuit model using non-linear least squares fitting techniques to obtain the best-fit parameters.

As in Transwell systems, in organs-on-chips two electrodes can be introduced on either side of the cellular barrier. This is done either by inserting electrodes in the chip inlets or by integrating electrodes into the chip during the fabrication process. An integration of immobilized TEER electrodes directly within the chip model and in close proximity to the cellular monolayer can reduce not only the contribution of electrical resistance from the cell culture medium but also the signal noise generated by any electrode motion. The size of the electrodes can be scaled relative to the microchannel dimensions within the system and also their material can be tuned. Most commonly used electrodes are Ag/AgCl-ones and platinum-ones, but also gold-plated electrodes covered with a conducting polymer have been applied in order to reduce the influence of the double layer capacitance. Ingber's group also performed TEER measurements in its gut on chip model: they used a voltage-ohm multimeter (87V Industrial Multimeter, Fluke Corporation, Everett, WA, USA) coupled to Ag/AgCl electrodes (0.008" in diameter; A-M Systems, Inc., Sequim, WA, USA). The electrodes were inserted in the tubing of the inlet of the top channel of the microdevice and the outlet of the bottom channel of the microdevice. The baseline resistance value measured in the absence of cells was subtracted from values of devices with a cell monolayer. Analysis of the same human intestinal epithelial Caco-2 cells grown in both the gut-on-a-chip and Transwell inserts revealed that the absolute TEER values measured in the gut-on-a-chip are consistently higher than those measured in the Transwell cultures. The TEER measurements initially follow a similar trend in both systems; however, after approximately 70 hours TEER values in the gut-on-a-chip measurements keep increasing and

become significantly higher than the TEER values measured in Transwell. This is likely because Caco-2 cells spontaneously undergo 3D villus morphogenesis from a 2D monolayer when the cells experience flow and peristalsis-like motions in the gut-on-a-chip, beginning about 3 days of culture.

2.6 Introduction of Microbioma

Oral ingested compound (e.g. nutrients, drugs or toxicants) is subjected to the digestive process that may have different effects on the amount absorbed by the intestinal epithelium, affecting the dose that reaches the bloodstream. Understanding the route and the absorption rate of the compounds during the entire digestive process through the GI tract is of great importance, especially for drugs and toxicants, as this strongly influences their bioavailability [37]. In particular, at the intestinal level, the mutually beneficial relationship between commensal microorganisms that populate the luminal microenvironment and the intestinal epithelial cells plays a critical role in the metabolism of the endogenous or exogenous compounds. The intestinal microbiota greatly enriches human's food processing capabilities, providing the host with a metabolic arsenal that enables the digestion of compounds which otherwise could not be processed by the human enzymatic machinery. Furthermore, the bacteria along the GI tract fulfill several beneficial functions for health - including vitamin production, ions absorption (Ca, Mg, and Fe), competitive exclusion against pathogens, and establishment of immune tolerance. For this reason, investigation of the intestine-microbiota crosstalk may provide more information on digestion processes in health and disease conditions of the small intestine.

As introduced in the Section 1.3, the human microbiome has an emerging role as a key player that leads to human health or disease. It is well-known that the aerobic and anaerobic gut microorganisms and their eventual imbalances in the intestine can contribute to the development of a broad range of pathological disorders within and beyond the GI system, including inflammatory bowel disease, colorectal cancer, enteropathy, diabetes, hepatic steatosis, obesity and rheumatoid arthritis. Thus, there is a great need for in vitro models that are able to sustain the complex populations of the human aerobic and anaerobic microbiota in direct contact with living human tissues in order to analyze the dynamic and physiologically relevant human host-microbiome interactions [38]. In previous decades, the analysis of gut-microbiome crosstalk almost exclusively relied on the genomic or metagenomic analysis of samples collected in vivo. The in vitro models such as Transwell inserts or organoid cultures - although previously employed - could not be co-cultured with living microorganisms for more

than few hours, or days. Furthermore, they could not provide the correct vascular interface, nor they could hardly sustain the luminal oxygen levels below 0.5%, required for the co-culture of certain obligate anaerobes. Recent advances in multi-layer microfluidics have led to the development of the first complex human-microbiota interaction on a chip, which allowed the analysis of aerobic and anaerobic microorganisms co-cultured with human Caco2 intestinal epithelial cells under an oxygen gradient; however, microorganisms were separated from the human cells by a nanoporous membrane with an artificial mucus layer and, even under these conditions, the co-culture were maintained for only 48h. Ingber et al. instead, described a two-channels microfluidic device - lined with human Caco2 intestinal epithelial cells and cultured under dynamic fluid flow and peristalsis-like mechanical deformations - which enabled the establishment of in vitro co-cultures with eight different strains of human commensal gut microorganisms, that remained stable for weeks under aerobic conditions [39].
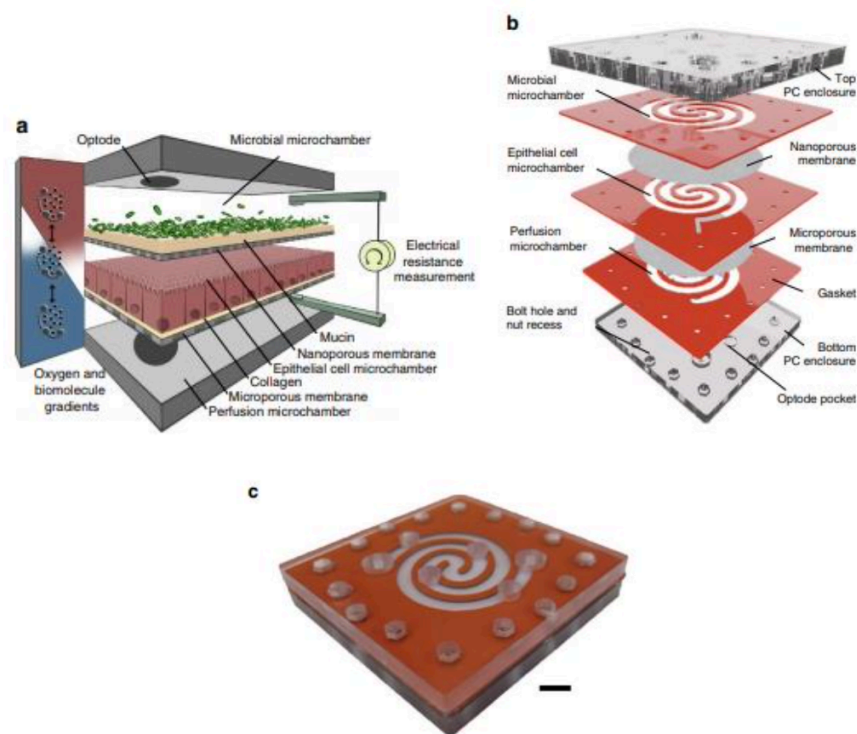
Figure 16 – a: Conceptual diagram of the HuMiX model; b: Exploded view of the HuMiX device with chamber's notation; c: Photograph of the assembled HuMiX device (scale bar, 1 cm).

However, this environment would not favor the growth of the hundreds of human gut bacteria which are obligate anaerobes. Thus, the necessity of a method able to sustain complex microbial

communities in direct contact with living human intestinal cells and their overlying mucus layer in vitro for multiple days. To meet this challenge, two relevant works have been made in this direction. Shah et al. developed a modular microfluidics-based device, which allowed the establishment of a model of the gastrointestinal human–microbe interface, named HuMiX (human-microbial crosstalk) (Figure 16 a, c). The device consisted of three co-laminar microchannels: a medium perfusion microchamber, a human epithelial cell culture microchamber and a microbial culture microchamber (Figure 16 b).
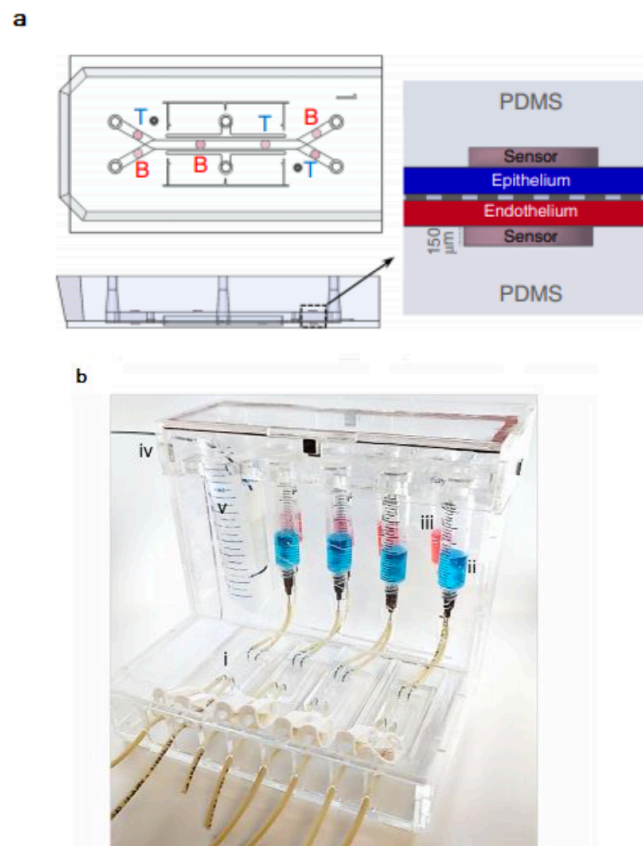
Figure 17 – a: A schematic representation of the Intestine Chip with six oxygen-quenched fluorescent particles embedded in the inlets, middles, and outlets of the top (T) and bottom (B) channels; b: Photograph of an anaerobic chamber while in use: Chips (i) are placed in the hypoxic region of the chamber and medium is flowed through epithelial cells (ii). The medium reservoirs for the vascular channels are placed outside the anaerobic chamber (iii), exposed to room air. The chamber is purged with N2 flow (iv) through a bubbler (v).

Each microchamber had a dedicated inlet for the inoculation of cells as well as for the precise control of physicochemical parameters through the perfusion of laminar streams of dedicated culture media. Dedicated outlets instead provided the means to collect eluates from the individual chambers for downstream characterization. Furthermore, the model integrated

oxygen sensors for the real-time monitoring of the dissolved oxygen concentrations within the device. By juxtaposing the human and microbial cell contingents at a distance of 0.5-1 mm across a separatory nanoporous membrane, the HuMiX model demonstrated to be representative of a healthy intact epithelial barrier which – specifically – was tested for the co-culture of differentiated human epithelial cells (Caco-2) with the facultative anaerobe Lactobacillus rhamnosus GG (LGG) - grown solely under aerobic or anaerobic conditions, or grown in combination with an obligate anaerobe, Bacteroides caccae, under anaerobic conditions [40].
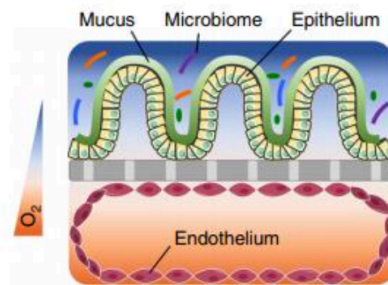
Figure 18. Schematic representation of the two-channel microfluidic Organ Chip device with an oxygen gradient (color scale).

Ingber groups' developed the extended co-culture of living human intestinal epithelium with stable communities of aerobic and anaerobic human gut microbiota, using a microfluidic intestine-on-a-chip that permitted the control and real-time assessment of physiologically relevant oxygen gradients [38]. Device fabrication started from human Caco2 Intestine Chips provided with two parallel channels separated by a porous matrix-coated membrane to mimic both the luminal and vascular part of the intestinal epithelium. These chips were then modified by integrating – in both channels - six microscale oxygen sensors containing oxygen-quenched fluorescent particles for the real-time, non-invasive monitoring of oxygen concentration in both chambers. The chips were then placed in an engineered anaerobic chamber (Figure 17 a). To simultaneously provide adequate oxygen to maintain human cells and an anaerobic microenvironment suitable for culturing complex human microbiota, the custom anaerobic chamber was continuously flushed with humidified 5% CO_2 in nitrogen gas. Simultaneously, the medium reservoirs for the vascular channels were placed outside the anaerobic chamber, exposed to room air and thereby, maintained under normoxia conditions. In this way, this set-

up enabled to maintain low oxygen levels within the lumen of the upper chamber while the epithelium was sustained via oxygen diffusion through the permeable PDMS membrane from the well-oxygenated medium flowing through the lower endothelium-lined vascular channel (Figure 17b). Establishing a hypoxia gradient across the engineered tissue−tissue (endothelium−epithelium) interface of the Intestine Chip effectively allowed for the stable co-culture of highly complex communities of anaerobic and aerobic human commensal gut bacteria in the same channel as mucus-producing human villus intestinal epithelium for at least 5 days in vitro (Figure 18) [38].

3. In-Crypts device

Abstract

Organs-on-chips are technological microfluidic device that are meant to mimic human physiological conditions within a microchip. The need of reliable human tissue models, particularly for the development of pharmaceutical drugs and study of nutrient absorption, has drawn increased attention as the current widespread models; static cell cultures and animal tests have proven poor predictability, are costly and are increasingly ethically problematic. By providing physiologically relevant bio-chemical, mechanical and other relevant cues to the cells cultured, these in vitro 'organs' develop similar characteristics to those observed in their in vivo counterparts.

Among several requests, a functional human intestine model able to recreate the in vivo dynamic nature as well as the native tissue morphology is of great interest. In this perspective, the goal of this next two chapter is the realization of an in vitro model of intestinal epithelium suitable for real-time tissue investigations and for studying absorption and permeability of food, drugs and chemicals. Precisely, a microfluidic device will be designed and fabricated to allow human epithelial colorectal adenocarcinoma (Caco-2) cells culture in both static and dynamic conditions. Particular attention will be paid to the effects of fluid flow on cell differentiation as well as on the support on which the cells were cultured. In particular, a new "custom made" porous PDMS membrane will be fabricated and successfully integrated in the microfluidic device: this custom-made membrane and a commercial PDMS membrane will be compare in terms on epithelial differentiation to select a suitable substrate. The In-Crypts device will be designed to mimic and impart the key aspects of the in vivo microenvironment of the human small intestine, including Villus-Crypts axis topography, in order to be integrated on chip. At the same time, the integration of electrodes inside the In-Crypts device will enable continuous monitoring of cells behaviour and differentiation through TransEpithelial Electrical Resistance measurements.

Methods and Materials

3.1 Fabrication of an integrated In-Crypts Device.

The In-Crypts device was fabricated from a flexible polydimethylsiloxane (Sylgard 184, Dow Corning) polymer. The PMMA master inverse mold was designed by AutoCAD and carved with micromilling machine (Minithech CNC Mini-Mill Figure 19) making a relief positive

geometry [36]. Device architecture consisted of two different layers obtained by aligning the central micro-channels. The design of the lower PMMA mold layer design consisted of a central micro-channel (600 μm x 1000 μm), with custom made conical pillars (height 360 μm). In detail, the "custom-made" aligned conical pillars were obtained by varying their diameters along the height: in the first layer that had the height of 40 μm, the pores diameter was 20 um, second 80 μm height and 40 μm pores, third 120 heights and 60 μm pores, last one 120 heights and 80 μm pores, for all 200 μm spacing (centre to centre). Upper layer design consisted of a simple aligned central micro-channel (1000 μm x 1000 μm).
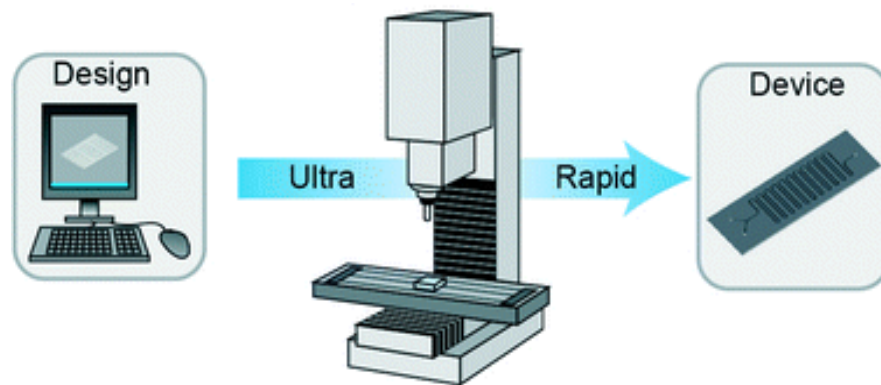
Figure 19. Minithech CNC Mini-Mill procedure, CAD design by software, mold in PMMA trough Milling and device production.

Once all layers were obtained, upper and lower layers were prepared by casting PDMS prepolymer (10:1 w/w; PDMS/Curing agent) on a PMMA fabricated inverse mold and, then, the polymer was curing at 65° C for 12 h. After peelings, the PDMS layers from PMMA support, the lower layer was re-treated to allow the closure of the lower micro-channel. A thin layer (100 μm) of pre polymer PDMS was curing at 90° C for 8 min. After, the lower layer was placed on thin layer and re-cured at 65° C for 12 h.

Figure 20. Replica molding, once obtained PMMA mold, PDMS layer adter curing on the PMMA mold.

Afterward, the upper layer exposed from open microchannel side and lower layers exposed from PDMS channel with membrane, were brushed by pre polymer PDMS and cured at 65° C for 12h for the final bonding. The PDMS device, tubes and connectors were sterilized by ethanol 70% for 40 min and washed twice with sterile PBS. 2-Stop Tygon sterilized tubes (Tygon 3350 silicone tubing, ID 1/3299, OD 3/3299, Beaverton, MI) were inserted into the upper and lower of the central channels at inlet and outlet of the PDMS device using custom connectors hub-free stainless steel blunt needles (18G; Kimble Chase, Vineland, NJ). The fabrication of PDMS Conventional device, was obtained with same protocol of In-Crypts Device, but the PDMS custom made membrane was inserted upside down, in order to show only the porosity of 20 microns to the cells. Furthermore, for dynamic culture, In-Crypts device was connected to a syringe pump (Syringe Pump Harvard Apparatus 11 Plus) to obtain a specific flow rate (2μL/min).

3.2 Integrated Electrodes In-Crypts Device

In order to measure TEER directly into the PDMS device, two Gold wires (200 μm diameter) was used. Breafly, two Gold wires were sterilized with ethanol for 20 minutes, rinsed with deionized water and allowed to dry for 10 minutes under biological hood. When the PDMS poured on the PMMA mold was halfway through the polymerization process, the copper electrodes were placed in correspondence with the specific patterns drawn on the mold by using tweezers. In particular, they were inserted in order to protrude into the culture channel along all its width. Then, the whole set-up was incubated at 80 °C to allow the complete polymerization. Once the device was assembled, the two electrodes resulted one in the upper channel, the other in the lower channel separated by the integrated PDMS membrane. Then, the device was sterilized as reported in the previous paragraph in order to culture the epithelial cells.
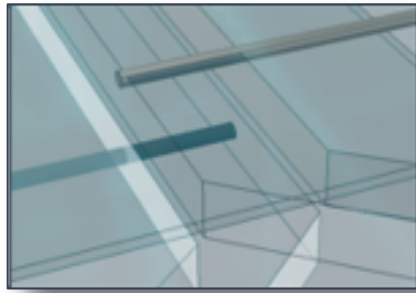
Figure 21. Integrated gold wire electrodes inside microchannels of device.

3.3 Mathematical model CFD simulation In-Crypts Device

The oxygen gradient and velocity of nutrient supply were measured by using commercial CFD COMSOL Multiphysics vers.55.3a. CFD analysis was performed dividing the entire In-Crypts device or PDMS conventional device, into three different domains: two fluid domains, which identified the region filled with culture medium, and a tissue domain, which identified the region covered by the Caco2 intestinal epithelium.
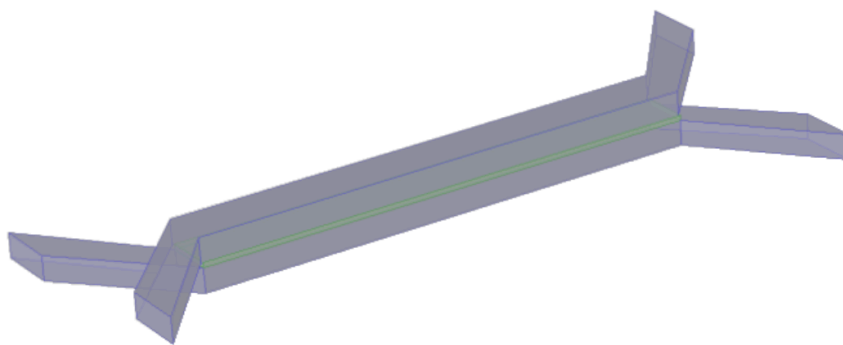
Figure 22. Domains inserted in Comsol simulation: in green the tissue domain and in blue the fluid domain.

The culture medium was considered to have the same physical characteristics of water, while

in the tissue domain, the properties of the Caco2 cells were introduced. To simulate culture conditions, and the distribution of oxygen throughout the epithelial layer, the velocity field and the fluid shear stress were coupled: 'Free and Porous Media Flow' and 'Transport of Diluted Species'. In particular, Simulations within the fluid domain were performed by using the steady state Navier- Stokes equation, with no slip boundary conditions set on the walls. Laminar flow with a flow rate of 0 µL/min for the static condition and 2 µL/min for resembling dynamic condition, was set at the inlet and reference pressure was set at the outlet (pref = 1 atm):

$$\rho(u \cdot \nabla)u = \nabla \cdot [-pI + \mu(\nabla u + (\nabla u)^T)] + F$$

$$\nabla u = 0$$

where µ is the dynamic viscosity, u is the fluid velocity, p is the hydrostatic pressure, and ρ is the fluid density. Brinkman equation was used to describe the flow through the porous medium (tissue domain):

$$\left(\frac{\mu}{\kappa} + Q\right)u = \nabla \cdot \left(-pI + \left(\frac{1}{\varepsilon}\right)\left(\mu(\nabla u + (\nabla u)^T) - \left(\frac{2\mu}{3} - \kappa_{dv}\right)(\nabla \cdot u)I\right)\right) + F$$

$$\nabla \cdot u = \frac{Q}{\rho}$$

The oxygen concentration within the system was calculated by means of the following mass balance equation:

$$\frac{\partial C}{\partial T} = D\nabla^2 C - \nabla(Cu) + R$$

where C is the oxygen concentration, u is the fluid velocity field, and D is the diffusion coefficient of the oxygen. R is the volumetric oxygen consumption rate expressed by the Michaelis–Menten law, according to the following equation:

$$R = \rho \frac{V_{max} \, C}{K_m + C}$$

where Vmax is the maximum oxygen consumption rate, Km is the concentration at which the oxygen consumption rate is half of Vmax and ρ is the cell density. The CFD simulation was repeated after changing the geometry and increasing the viscosity of the upper fluid domain at 10^{-2} Pa s that is the zero shear viscosity of intestinal lumen in vivo [36].

Property	Variable	Value	Unit
Porosity	epsilon	0.7	1
Permeability	kappa...	1E-11	m²
Density	rho	999.7	kg/m³
Dynamic viscosity	mu	0.001	Pa·s

Figure 23. Caco2 proprieties utilized in CFD comsol simulation

3.4 Cell line and splitting procedure

Human epithelial colorectal adenocarcinoma cells, Caco-2, were provided by American Type Culture Collection (ATCC, USA). They were maintained in T25 culture flasks in high glucose Dulbecco's Modified Eagle Medium (hg-DMEM) medium containing 10% Fetal Bovine Serum (FBS), 100 μg mL-1 L-glutamine and 1% penicillin-streptomycin, at 37 °C in a humidified atmosphere containing 5% CO_2. When the confluence conditions were reached (almost 70% of the flask surface was covered), a 1:3 split procedure was performed. Briefly, the medium was removed from the flask and cells were washed with 4 mL of Trypsin- Phosphate Buffer Saline (PBS) solution (1:1v/v). Then, T25-flask were supplemented with 1 mL of fresh trypsin– EDTA solution and left in the incubator 4-5 min to remove the cells from surface. After that, 2 mL of complete medium was added to block the Trypsin action and all the solution was thoroughly pipetted up and down to break the cell clumps. The cell suspension was transferred in a 15 mL tube and centrifuged 5 min at 1000 RPM. After removing supernatant, cell pellet was re-suspended in 2 ml of hg-DMEM. Finally, 1 mL of suspension was seeded in a T25 flask and incubated.
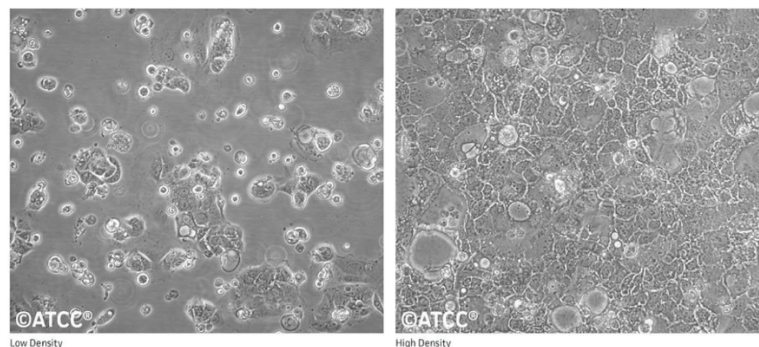
Figure 24. - Human epithelial colorectal adenocarcinoma cells, Caco-2, provided by American Type Culture Collection (ATCC, USA). Image shows cells at low (left) and high (right) density.

3.5 Caco2 cell seeding on PDMS membranes

In order to produce a polarized human intestine epithelium, the PDMS device was coated fibronectin (20/1; µl/ml; Sigma Aldrich) prior the Caco-2 cell seeding. The apical channel was washed with PBS and 500 µL of human Fibronectin solution was introduced into the upper micro-channel by using a disposable and sterile 1 mL syringe (BD). The whole setup was incubated in a 37 °C humidified 5% CO_2 incubator for 45 min (25 min at room temperature and 20 min into the CO_2 incubator at 37° C) Then, a suspension of 5 x 10^5 cells/500 µL of Caco2 cells was loaded on the top of the fibronectin-coated porous membrane by gently flowing the cell solution into the upper micro-channel using a sterile syringe avoiding the presence of air bubbles. The entire setup of the In-Crypts device and PDMS conventional device was placed in the incubator to allow the Caco2 cells adhesion on the surface of the porous membrane for 2-3 hours. When the cells were definitely attached to the membrane, the pre-warmed DMEM into the upper channel was replaced to remove the unbounded cells. Then, Caco-2 cells were cultured in standard culture conditions (5% CO_2, 37 °C) for up to 8 days. Simultaneously, a control sample was cultured in static conditions by refreshing manually every day the apical and basolateral channels by means of a 1 mm syringe. Control sample in a 2D petri dish was cultured to monitor Caco2 cell attachment and confluence in static conditions.

Caco2 cells in the In-Crypts device were cultured also in dynamic condition, the device was connected to a siringe pump (Syringe Pump Harvard Apparatus) to obtain a specific flow rate (2µL/min), and was cultured up to 8 days.

3.6 Epithelial characterization

To compare the epithelial differentiation on different home-made porous membrane with PDMS holes 20 µm up *vs* 100 µm up, the samples were confocal microscope analyses were performed. Briefly, the culture medium was removed and PBS was perfused through upper and lower channel of the In-Crypts device or PDMS conventional device. To allow morfological analysis, the samples were fixed by flowing Paraformaldehyde (PAF) solution 4% for 20 minutes. The micro-channels were washed 2-3 times by flowing 0.2% Triton in PBS solution for 15 minutes to increase cell permeability and allow dye penetration. The samples were rinsed with PBS and, then, a Phalloidin-PBS solution (1:200) was added and incubated for 40 minutes. After rewash, DRAQ5-PBS solution (1:1000) was inserted and incubated for 15 minutes. During staining procedures, the entire device was covered with aluminum foil to preserve fluorescence. The 'PDMS conventional vs In-Crypts device' were analyzed with Leica SP5 II

laser scanning confocal microscope (qua bisogna inserire le caratteristiche dei laser in eccitazione ed emission per verde e blu, li trovi in qualsiasi nostro articolo).

3.6.1 Quantitative analysis

Both In-Crypts Device and Conventional DPMS device images were acquired under confocal microscope and were analyzed by using ImageJ software. Specific ROIs with fixed measures were analyzed into the microchannel: precisely, 10 ROIs with a dimension of 1000 μm x 1000 μm were cropped for each microchannel. In particular, for each image a scale bar was inserted by selecting the Straight Line Selection tool, and by using the scale bar tool that convert the number of pixels into μm. By means of tool Image > Colour > Split Channels, the Green Phalloidin images was selected to measure the domes structures. Then, image brightness, contrast and threshold were optimized and the Analyze Particles tool was used to select, count and measure the domes. The domes with a shape as close as possible to a circumference and a diameter greater than 20 μm were selected.
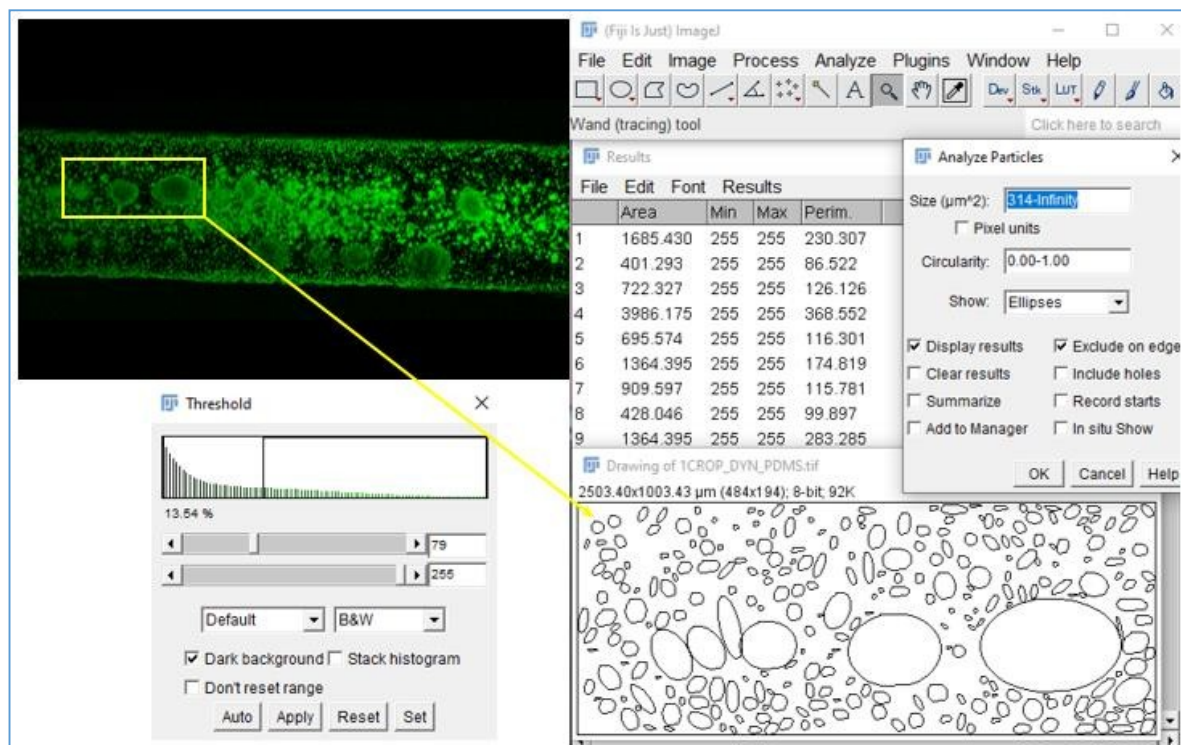
Figure 25. Example of using the Analyze Particles tool to select, count and measure the domes through ImageJ Software. Image shows both Threshold Window and found particles having diameter greater than 20 μm.

The obtained data were analyzed and processed by the Excel software. Once the number of domes and their respective diameters were calculated, they were divided into 6 categories: 20-60 μm, 60-100 μm, 100-140 μm, 140-180 μm, 180-220 μm and > 220 μm. Then, the Histogram function, was used to plot the diameter measurements and the frequency of domes diameters was estimated. The results obtained were compared to the total number of domes founded and plotted as a percentage. In addition, for the optimized Intestine on chip the height of the domes was obtained from the Z-stacks images. Scale bar was inserted into the images, brightness and contrast had optimized and 3D renderings were visualized through orthogonal views, accessed via "Image/Stacks/Orthogonal Views". This method allowed to display the XZ and YZ plane at a given point in the 3D image. When Orthogonal Views are opened, windows containing the two planes will dock alongside the original stack, with the intersection of the yellow lines on the stack indicating the point in the stack that is being analyzed. These lines were manually adjusted and positioned on the tip of the dome. The views in the XZ and YZ planes were update automatically and, by means of Straight Line Selection tool, the distance from the base to the tip of the dome was measured.
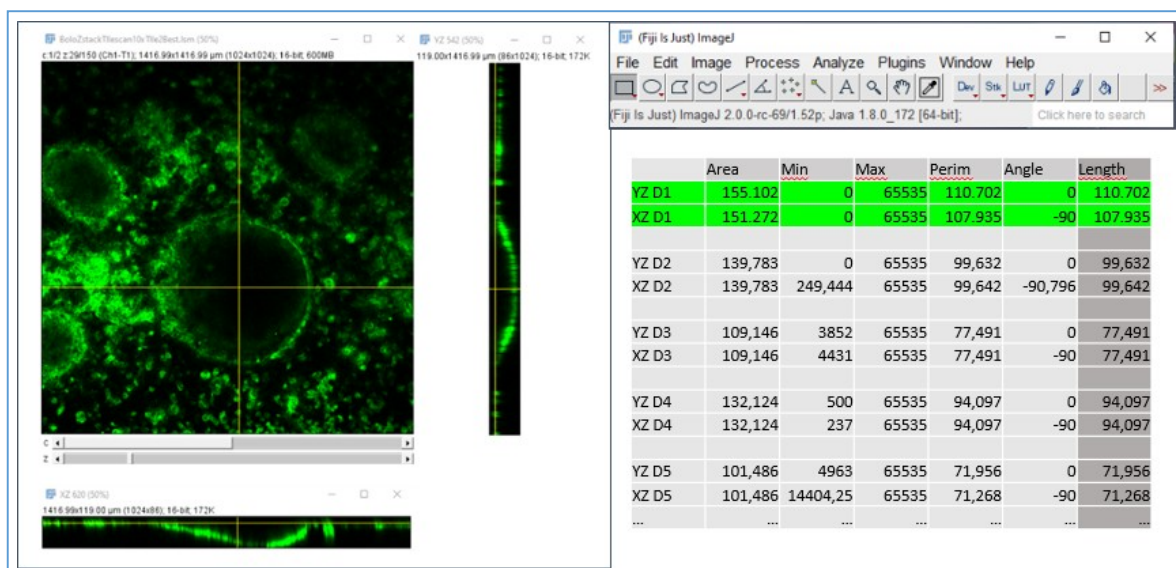
Figure 26. Example of 3D renderings visualized through orthogonal views and measure of domes height" in ImageJ Software.

3.6.2 Histological, immunofluorescence and immunohistochemical analysis

At 8th day, Caco-2 monolayer samples were fixed with 4% paraformaldehyde for 20 min and then rinsed in PBS. For the histological examination, were collected and fixed in 10% neutral buffered formalin solution overnight, dehydrated in a graded ethanol series, washed with xylene and embedded in paraffin blocks. Serial sections were stained with Hematoxylin and eosin (H/E) (Bio Optica), and Alcian Blue (Merk Millipore) staining using standard procedures. All specimens were analyzed by an optical microscope (BX53; Olympus) with a digital camera (Olympus DP 21). For immunofluorescent procedure, unstained sections from the above-mentioned paraffin blocks were deparaffinized in xylene, treated with an incremental ethanol [100, 95 and 80% ethanol/double-distilled H2O (v/v)], and rehydrated in PBS. Antigens were unmasked by heat antigen retrieval with citrate buffer, pH 6.0 for 20 min. Slides were then blocked with 5% bovine serum albumin (BSA; Sigma) and incubated with primary antibodies to Villin (1:100; Abcam), Muc-2 (1:100; Abcam), CGA (1:100; Abcam), ZO-1 (1:50; Abcam), Alpha-Smooth Muscle Actin (aSMA) (1:100; Abcam), ki67 (1:100; Abcam) and LGR-5 (1:100; Sigma), TNF-a (1:100, Abcam), IL-6 (1:100, Abcam), IL-1b (1:100, Abcam), IL-8 (1:50, Abcam) overnight at 4 C. After washing extensively, all slides were incubated with a 1:500 dilution of appropriate fluorescent secondary antibody (Alexa fluor) at RT for 1 h. Slides were rinsed, and counterstained with 40 ,6-diamidino-2-phe nylindole (DAPI) (Sigma Aldrich) at dilution ratio (1:10000 in PBS) for 10 min. Sections incubated with dilution buffer without primary antibody were used as a negative control. Confocal images were captured using a confocal laser scanning microscopy (CLSM) (TCS SP5 II femtosecond laser scanning system, Leica). The excitation/emission wavelengths were set as follows: kex = 500 nm, kem = 510–530 nm (single photon mode, for MUC-2, ZO-1, Ki67, LGR-5, IL-6, IL-8); kex = 580 nm, kem = 612–623 nm (single photon mode, for Villin, CGA, TNF-a, IL-1b); kex = 720 nm, kem = 460 ± 10 nm (two photon mode, for DAPI). The fluorescence quantifications were obtained by dividing the green/red pixels number by the cells number. The number of pixels and the number of cells were obtained by using ImageJ software. The analysis was performed in three independent experiments. For immunohistochemistry, section were dewaxed with xylene and rehydrated in PBS. Endogenous peroxide was blocked with 3% H2O2 for 10 min. After blocking non-specific reactions with 5% bovine normal serum (Sigma) in Tris Buffered Saline solution (TBS), sections were incubated with primary antibody against cytokeratin 19 (CK19) (1:100, Abcam) and Lysozyme (1:100; Sigma) at RT for 1 h. Secondary antibody conjugated with biotin, streptavidin-peroxidase and DAB used for immunostaining was from Mouse and

Rabbit Specific HRP/DAB (ABC) Detection IHC kit (Abcam).

3.6.3 Qualitative analysis of selective permeation properties

The permeability evaluation of CaCo-2 cultured In-Crypts device and PDMS conventional device was performed by measuring the trans-epithelial passage of the 3kDa FITC-Dextran solution (1 mg/ml diluted 1:100 in HBSS) (TRITC-Dextran, Molecular probes, Life Technologies). Cells monolayers were incubated for 24 h at 37°C with 5 % CO_2. 200 μL 3kDa FITC-Dextran solution were loaded on the apical side and 500 ml of HBSS/DMEM (1:1 V/V) were placed in the basolateral chamber in order to guarantee the wetting of the lower side of the membrane. The passage was analyzed by confocal imaging (Leica SP5 II Laser Scanning Confocal Microscope

3.6.4 Ultrastructural characterization Scanning Electron Microscopy

SEM analysis, the Devices was fixed with 2.5% (v/v) glutaraldehyde in cacodylate buffer. Samples were washed twice in 100 mM cacodylate buffer, pH 7.2, for 10 min at room temperature. A second fixation in 1% (w/v) osmium tetroxide, buffered in 100mM cacodylate, pH 7.2, was done overnight at 4°C. Dehydration was carried out by gradually decreasing the water concentration and increasing the ethanol concentration (10%, 30%, 50%, 70%, 90%, 100%, and 100% again, each step 30 min at room temperature). Samples were then treated with liquid carbon dioxide using a Critical Point Dryer (Emitech K850). Dried samples were mounted onto metal stubs using double-sided adhesive tape and then gold-coated using a sputter coater at 15 mA for 20min. Coated samples were then examined by scanning electron microscopy (SEM) (Leica S400).

3.7 TransEpitehlial Electrical Resistance measurements

TransEpithelial Electrical Resistance (TEER) measurements were performed to monitor the Caco-2 differentiation and barrier function exerted by the intestinal epithelium. To guarantee a good ion concentration in the solution, the culture medium was changed one hour before the analysis. TEER measurements were performed by connecting the In-Crypts device or PDMS conventional device to an AUTOLAB PGSTAT302N (potentiostat/galvanostat) by Metrohm equipped with a FRA32M module (frequency response analysis module). Impedance spectra were recorded in potentiostatic mode (0.3 V) with an amplitude of 0.01 V and frequencies

ranging from 100 kHz to 0.1 Hz between two copper electrodes. For each measurement, three readings and 50 data points (logarithmic frequency step) per reading were collected. Bode Modulus and impedance at 12 Hz were used to follow the epithelium growth as already reported in literature [28].

Figure 27. AUTOLAB PGSTAT302N (potentiostat/galvanostat) by Metrohm

Within the paracellular pathway the tight junctional proteins represent an ohmic resistance (TEER) in the circuit diagram while each lipid bilayer in the transcellular pathway, can be described as a parallel circuit of an ohmic resistance (Rmembrane) and an electric capacitance (Ccl). In addition, the surrounding medium (Rmedium) was represented as a resistance and the electrodes as constant phase elements (capacitance, CEl). RTEER was normalized for the cross sectional surface area to calculate the TEER value in Ohm x cm.

4. In-Crypts device: Results and Discussion

4.1 Microfabricated PDMS porous membrane resemble villi-crypts axis

To demonstrate that the In-Crypts device mimics the topography as well as the functionality of the intestinal crypts, we manufactured two different pore-sized membranes, the first with a thin patterned membrane on which was seeded the intestinal epithelial cells, containing an array of upside-down conical structures faithfully (from diameter of 20μm pores to 80μm pores Figure 28) reproducing the epithelial moat-like invaginations of the intestinal epithelium around the villi.
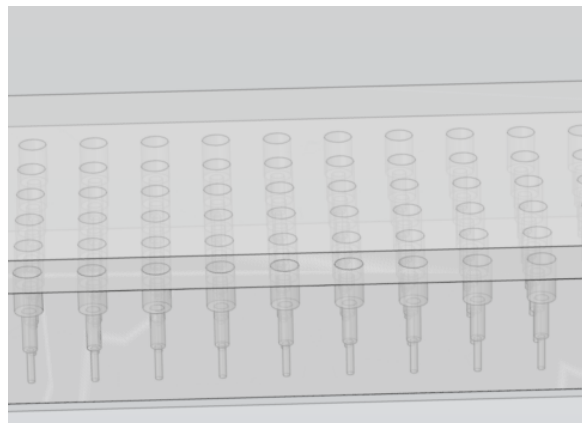
Figure 28. Scheme of In-Crypts device membrane, 80μm pores exposed and cone-shaped resemble crypts, integrated in microchannel.

The same on-made fabricated membrane that reproduce the conventional commercial membranes, was turned upside down and CaCo-2 cells were seeded on the surface with porous site of seeded 20μm. By using the micro-fabrication approach we reproduced an easy to handle and reproducible conical stepped structures, starting from a diameter of 80μm with gradually descending steps, and ending with a diameter of 20μm as shown in SEM images as shown in Figure 29.

Figure 29. Scheme of PDMS Conventional membrane, 20µm pores exposed, integrated in microchannel.

During the manufacturing of PMMA mold by carving shape with Micromilling as shown in figure (PMMA mold), it is evident that the different diameters of cone pores along the height of pillar are fundamental to obtain the robustness of each pillar (fig zoom cono). Due to the
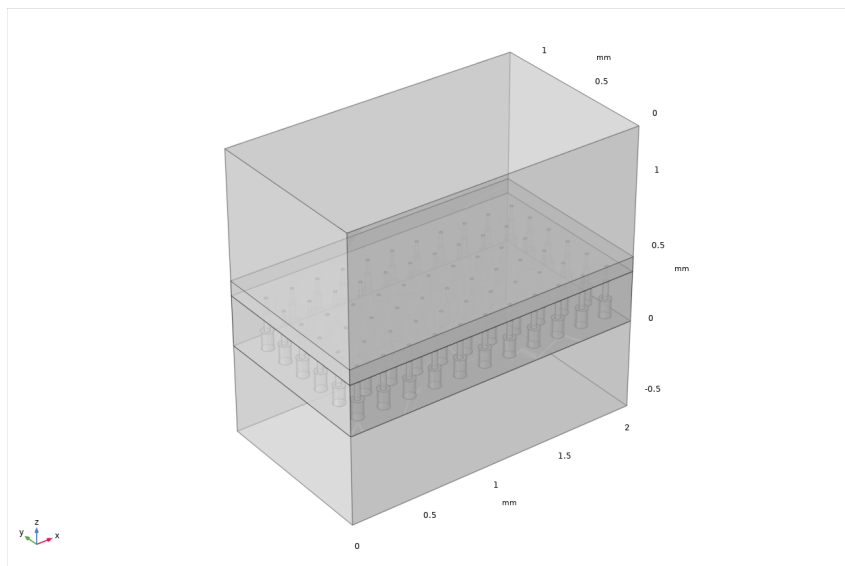
Figure 30. PDMS conventional device, focus on microchannel and integrated membrane, 20µm pores exposed, like conventional PDMS membrane.

choice of the height of the pillars according to their diameter, 20µm pores 40µm high, 40µm pores 80 µm high, 60 µm pores 120 µm high and last 80 µm pores 120 µm, as a total highness of 340µm. We ensured that pillar didn't detach from PMMA mold at the pealing-off time of the PDMS mold (membrane integrated with channel) (Figure 30) from the PMMA mold. As we can notice from figure (29-30), we can appreciate the particular structure of membrane, that has the peculiarity to be integrated with the microfluidic channel.

The peculiarity of the integrated PDMS membrane, allowed an easiest and fastest production of device, in order to obtain a high reproducibility of the device. At last, it was hypothesized that the topography of the PDMS membrane that are used in the experimental phase had influenced the coating-protein adsorption process. These factors determine the way in which the biological molecules are adsorbed by the materials. In particular, all these factors determine the orientation of the adhesion molecules and consequently may have influenced the behavior of cells connected with them. Furthermore, PDMS resulted optically transparent (in the wavelength range 240−1100nm [35]) and confocal imaging was more accessible.
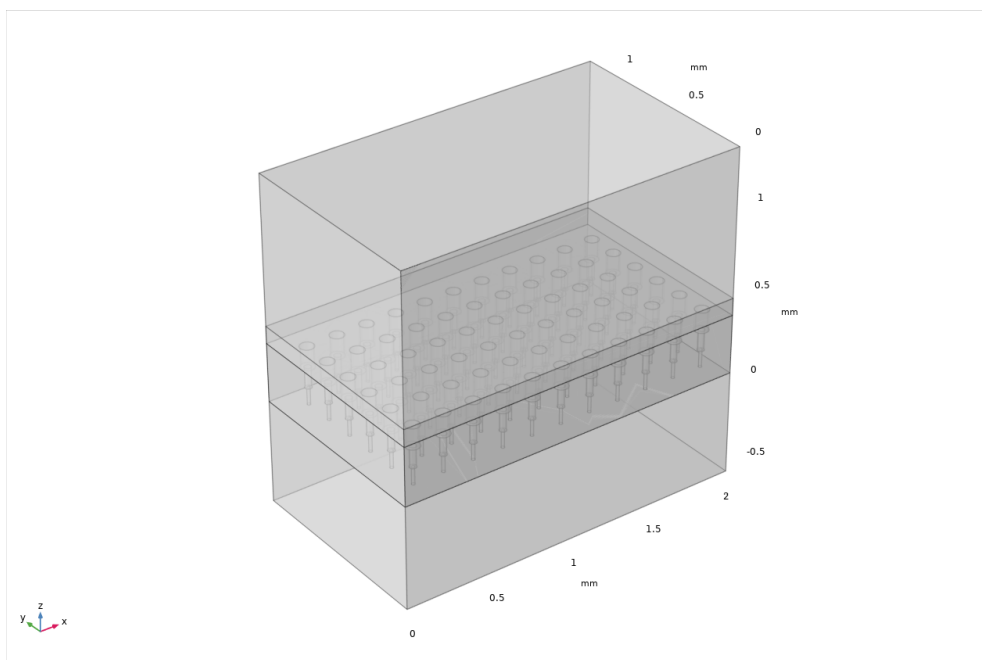
Figure 31. In-Crypts device, focus on microchannel and integrated membrane, 80μm pores exposed and cone-shaped resemble crypts.

4.2 In-Crypts CFD Comsol Multiphysics

CFD COMSOL Multiphysics was used in order to simulate the three-dimensional velocity, oxygen concentration gradient and the shear stresses both devices.
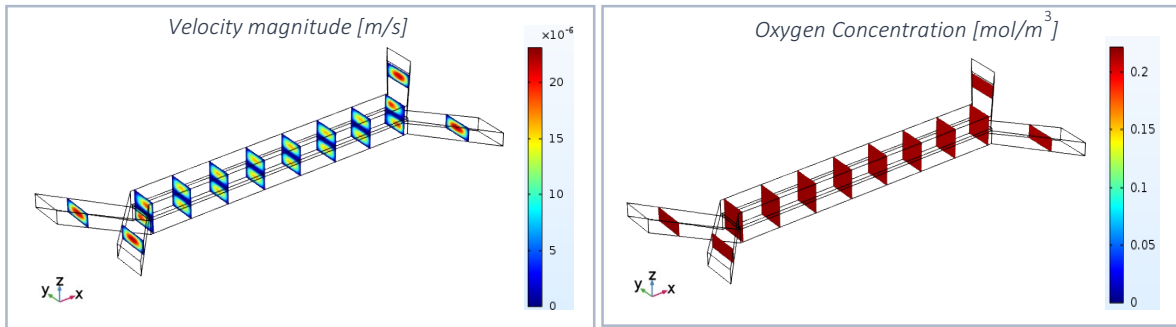
Figure 32 . CFD simulation results - Fluid velocity (left) and O2 concentration (right) along the entire length of the chip.

Figure 32 shows the velocity values for the set flow rate on the left and the O_2 concentration along the entire channel on the right. At $Q = 2$ μL/min the velocity in the middle of the channels was ~1.5×10^{-5} m/s and decreased a little bit when approaching the tissue.

In particular, CFD simulation indicated that the set flow rate, despite the oxygen consumption in the tissue, guaranteed the O_2 concentration in the culture media in the entire channel, in the same order of the initial concentration at the inlet.
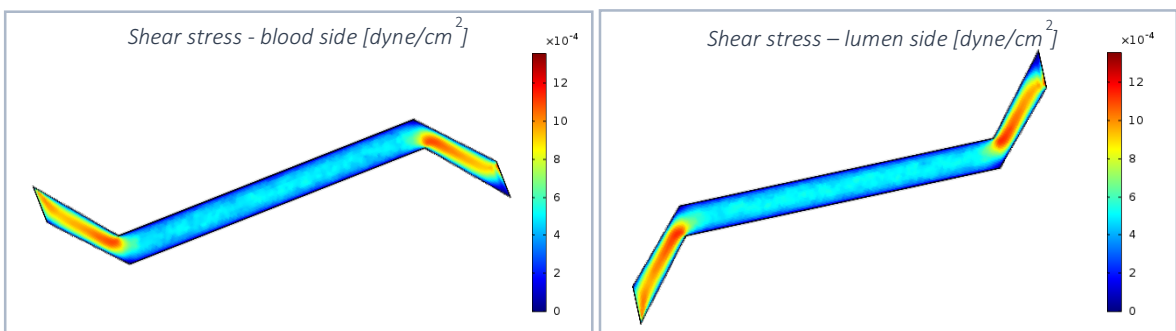
Figure 33. CFD simulation results – Shear stress exerted on the tissue in blood side (left) and lumen side (right).

At the end, the shear stresses exerted on the Caco-2 cell layer both in lumen and blood side (Figure 33) were simulated, considering that tissue differentiation can be affected by the movement of the fluid in the channels. Shear stress values were ~5×10^{-4} dyne cm^{-2} on both

sides of the tissue. It means that the set flow rate returned lower values of shear stress with respect to the physiological ones (0.002–0.08 dyne cm^{-2}) indicated by the literature [33, 34]. However, the values of the shear stress exerted on the Caco-2 cell layer both in lumen and blood side, did not damage the epithelium and stimulate the differentiation of the Caco-2 cell layer. In addition, once obtained In-Crypts device assembled, with cones-membrane shaped and PDMS conventional device, with only 20 microns exposed, we compared the amount of oxygen in static condition inside the devices. We carried out fluid dynamics simulation performed By Comsol, and we can appreciate the greater amount of oxygen in the In-Crypts device than in PDMS conventional device. In particular, as shown in the figure, the maximum In-Crypts is 0.2207 mol/m^3 than that of Conventional is 0.2197 mol/m^3 Greater amount of oxygen assured better cellular vitality and differentiation. Figure 34-35
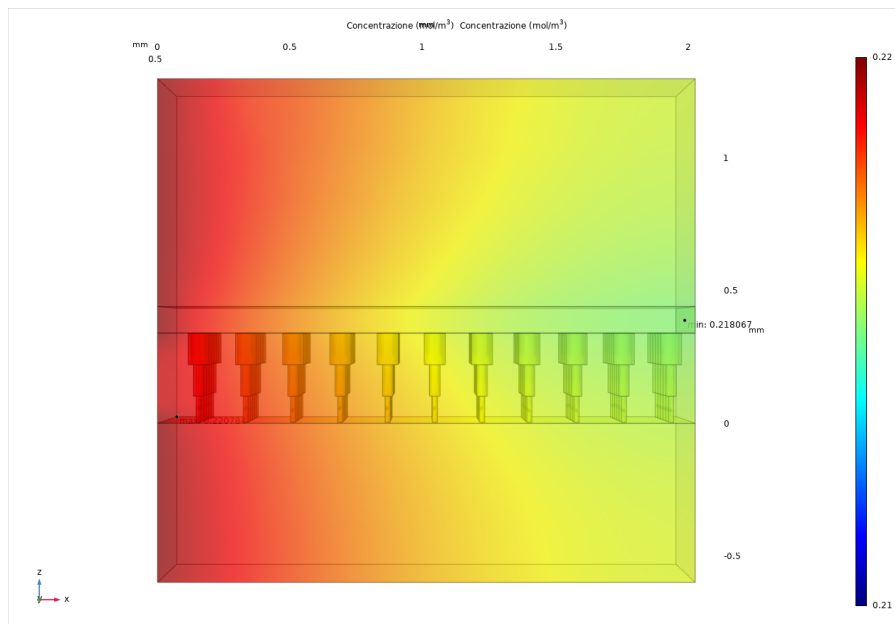
Figure 34. CFD simulation results – Oxygen amount exerted in microchannels of In-Crypts device.

In addition, the presence of large pores improved the cell viability, thanks to a great exchange of oxygen and nutrients (including growth factors) from both apical and basolateral side. Furthermore, during experimental phases, it was observed that Caco-2 cells attached and differentiated much faster to the In-Crypts Device membrane than that in PDMS Conventional device membrane. We can also have noticed, that in static condition, the In-Crypts device, show a greater amount of oxygen instead the PDMS conventional device. We already obtained, by the simulation, first result of the "custome-made" membrane. Shaped "Costume made" desing, show an increase exchanging of oxygen and also of nutrients, from the top to bottom. This can also help us to improve the oxygen condition in dynamic culture, in fact,

dynamic culture is a optimal condition of culture for device.
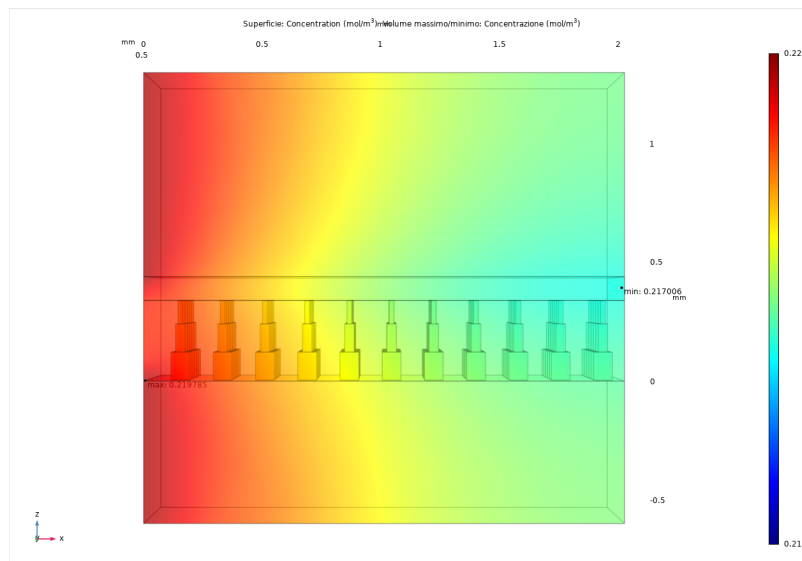
Figure 35. CFD simulation results – Oxygen amount exerted in microchannels Of Conventional PDMS device.

4.3 In-Crypts culture of Caco2 Cells

To compare the epithelial differentiation process on different porous membranes the Caco-2 cells were cultured in the devices on two different sandwiched membranes: In-Crypts device and Conventional PDMS device. The effects produced by the two membranes, whichdiffer in pores diameter and material, on the cell growth and differentiation was investigated.Moreover, different culture conditions, static and dynamic, were performed in order to evaluate also the effect of the fluid flow.

For the experimental set up, the same cell density (10^6 cells mL^{-1}) was seeded into the upper channel of the two different devices, was incubated for 2 hours in a CO2 incubator to allow the cells to attach onto the porous membrane. The cell density was carefully optimized in order to avoid the cell-cell aggregation or superposition. The cultures were stopped after 8 days from cell seeding in the experiments in static In-Crypts, static Conventional PDMS and dynamic In-Crypts. In contrast, the culture in the In-Crypts in static conditions was carried out even up to 8 days to obtain the completely differentiated epithelial layer.

The results of the Caco-2 cell culture in the In-Crypts devices and Conventional devices are shown in figure. They are tile scan and Z-stack reconstructions of a good part of the channel acquired through confocal microscope. By looking at these images,it is clearly evident that PDMS conventional has less optical accessibility compared to the In-Crypts device. For this

reason, the image C required to be zoomed in order to allow morphological analysis.
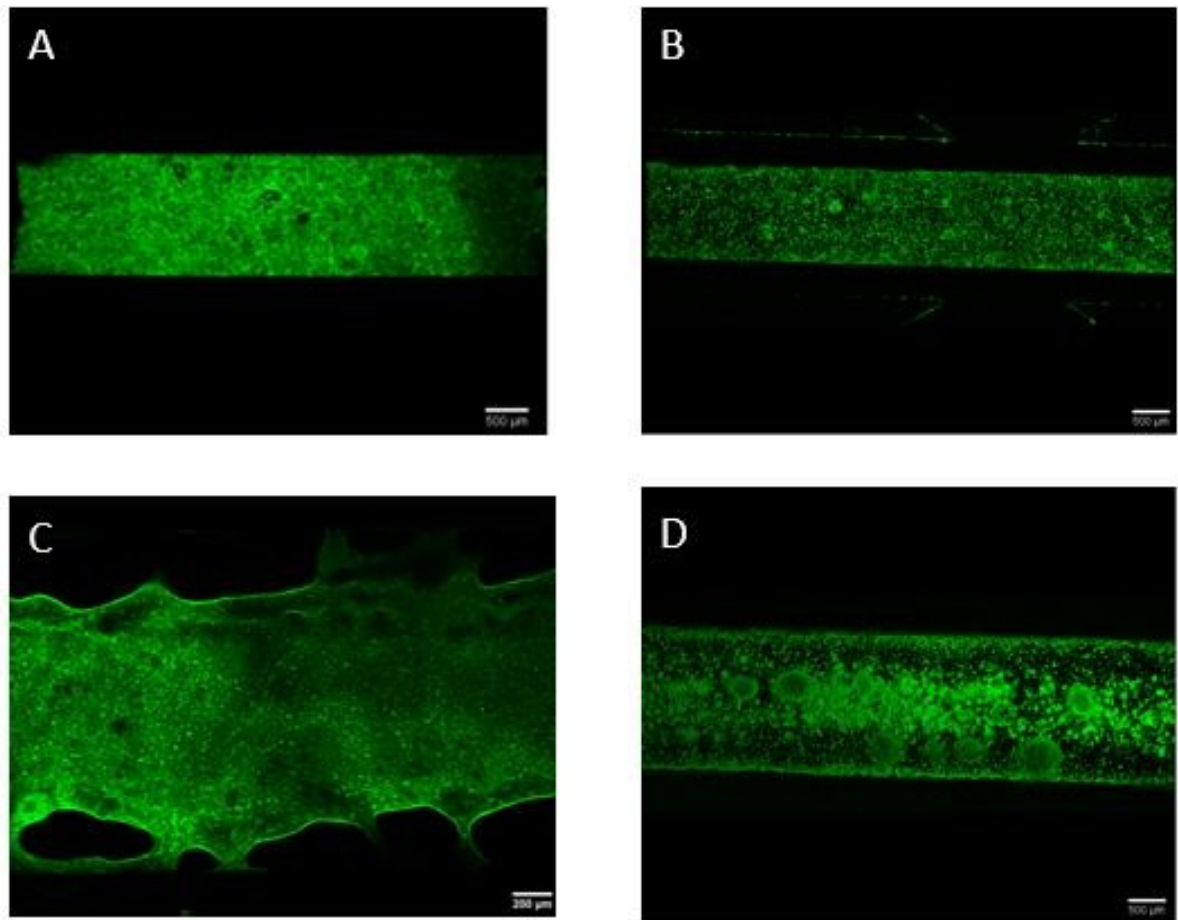
Figure 36. Confocal acquired images of Caco-2 intestinal epithelium in the Conventional PDMS microfluidic devices. The images shows results obtained in: (A) Conventional PDMS under static culture conditions; (B) In-Crypts device under static conditions; (C) the Conventional PDMS under dynamic conditions; (D) In-Crypts device under dynamic conditions – (A, B, D 500 μm scale bar; C 200 μm scale bar)

Caco-2 cells have developed a fully confluent layer over both the In-Crypts device and the PDMS conventional device, either statically or dynamically under continuous flow. They also started to polarize, however, according to the type of cell culture and of the membrane, they reached different levels of differentiation. In particular, the differences in culture times obtained for the two different membranes under static conditions correspond to a different behaviour of the epithelial cells when seeded on two different membranes supports. We can focus also that for the In-Crypts device we obtained complete confluence after only 72h of culture. These results confirmed that different materials and pore size of the porous membranes strongly affects Caco-2 cell growth and differentiation.

4.3.1 Intestinal villi formation in vitro

When Caco-2 cells were cultured in both device, PDMS conventional and In-Crypts, once they reached confluence, they begun to polarize and differentiate, forming an undulating epithelium with some raised structures that we call 'domes'. They have a morphology reminiscent of intestinal macro-villi. The function of these finger-like projections is to increase the surface area in order to maximize the absorption process. In the present study, it was determined the degree to which these 'domes' structures resemble intestinal villus in terms of size. Quantitative analyses allowed to measure the density and the diameter of these structures. In particular, the domes feature of the Caco-2 cultured on both device and different culture condition were compared.
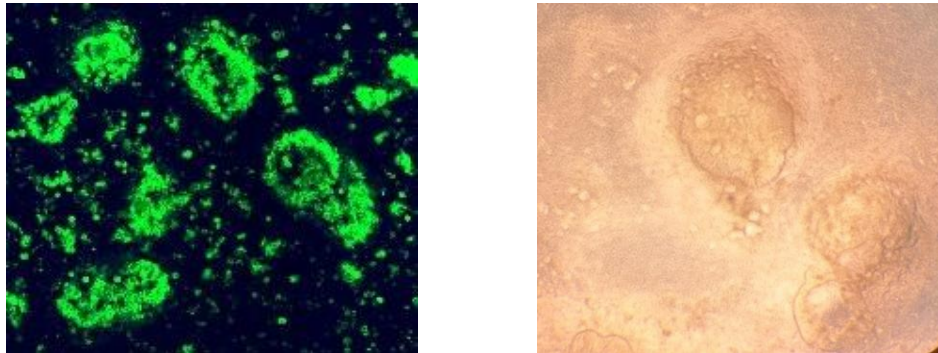
Figure 37. (A) Acquired confocal microscope image showing domes structures. (B) acquired image of domes structures.

4.4 Quantitative analysis of In-Crypts membrane *vs* conventional membrane

Quantitative analysis of the morphological features of the domes structures were carried out by using ImageJ software and the obtained data were analyzed and processed by the Excel software. ImageJ provides data on the geometry of an object represented on an image by converting the number of pixels of the scale into the unit of measurement it expresses.

First of all, analyses on the detailed characterization of Caco-2 cells culture on PDMS conventional Device and In-Crypt device.
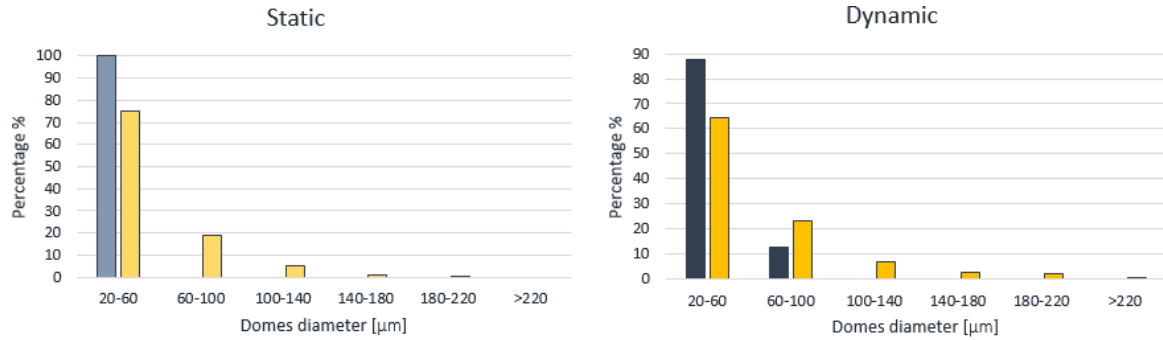
Figure 38.- Comparison between domes diameter range of Caco-2 epithelium developed on PDMS convetional device and In-Crypts device under (A) static and (B) dynamic cell culture conditions.

As reported in Fig 38 A, when Caco-2 cells were cultured in the conventional PDMS device under static conditions, 100 % of domes developed in 8 days in the first range of diameters (20-60μm), indicating that no structures with a diameter greater than 60 μm were developed. In addition, the average of diameter of this class of domes correspond to 35 μm. Under the sameculture- times and conditions, Caco-2 cells cultured in the In-Crytps device developed domes with diameters including 60-100 μm, 100-140 μm, 140-180 μm, 180-220 μm classes. Although about 70% of the domes still fall the range of the first class of diameters, the difference between the effects of the two membranes on the differentiation of the epithelium is substantial. When subjected to a dynamic culture with a constant flow rate of 2 μm min^{-1}, the cells grown on both types of the membranes developed an epithelium characterized by domes with larger diameters with respect to static culture as showed in Figure 38. This result highlighted an acceleration of the differentiation process in dynamic conditions. In particular, for the Convetional PDMS device over 10% of the domes displayed a diameter between 60-100 μm (second class), while approximately 90% was still found in the first class. In contrast,for the In-Crypts device dynamic groups, the number of domes belonging to the first class has decreased corresponding to 60% and the remaining domes falls in the second class(40%). This results demonstrated that small domes came together to form larger ones with measurements that approach the *in vivo* villi size. The quantitative characterization of the second class of domes grown in the In-Crypts device in dynamic conditions allowed to

e xtrapolate the domes density (number of domes per unit area) that correspond to 34 domes/mm^2.
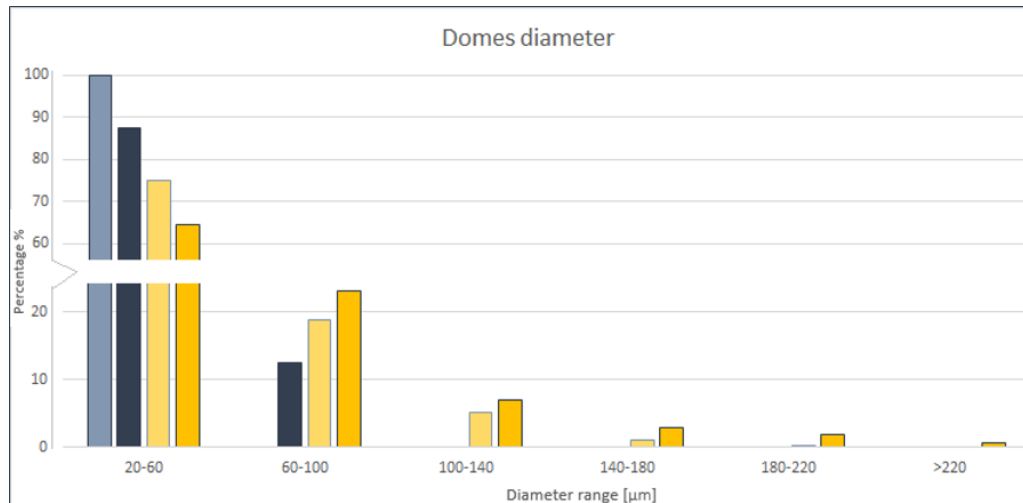
Figure 39. Histogram comparing domes diameters developed on Convetional and In-Crypts membranes under both static and dynamic conditions.

Taken together the results highlighted that the dynamic environment and the PDMS "Custom-made" membrane are essential for proper differentiation of cells by creating the correct shear stress such that the Caco-2 cells can differentiate. As it well known, the human intestinal epithelium *in vivo* is characterized by macro-villi with a diameter of 85-200 μm and a surface density of 20-40 macro-villi/mm^2. According to the *in vivo* situation, the Caco-2 cells grown in the In-Crypts in dynamic conditions developed an epithelium with the morphology closest to the intestinal macro-villi. In particular, the 40% of domes, as reported in the histogram in figure 3.11, showed the physiological diameter and villi density.

For further confirmation, long-term culture (15 days) in the Conventional PDMS device was performed. Our results displayed the better performance of In-Crypts device compared to the Conventional PDMS device in the differentiation program of the Caco-2 cells indicating that Caco-2 at 15 days of culture Conventional PDMS device not yet reached the level of differentiation that can be observed In-Crypts device in 8 days.

We assume that the integrated PDMS membrane have accelerated the differentiation process developing an epithelium with more physiological features which are attributable to different factors such as pores density, pores diameters materials of porous membranes. The commercial PC membranes, typically made by using a track-etching process, are characterized by a random placement of pores, with not uniform local pore density. In addition, membrane porosity must be kept fairly low in order to minimize the overlapping of pores. On the contrary,

the custom-made PDMS membrane displayed a better uniformityand higher porosity than the commercial PC membranes, due to the controlled pores number and distribution at the fabrication time. In addition, the small pore diameter of the conventional PDMS membrane (20 μm) determines a smooth-like surface for cell adhesion. In contrast, the PDMSmembrane with larger pores (80 μm) showed a kind of depressions on the surface of the Caco-2 cells that are able to respond differently in terms of differentiation. In fact, the cells recognized an environment more similar to the physiological one with 'invaginations' created by the pores that reminded the basal proliferative cell crypts that characterize the small intestinal epithelium. In addition, the presence of large pores improved the cell viability, thanks to a great exchange of oxygen and nutrients (including growth factors) fromboth apical and basolateral side. At last, it was hypothesized that the physical and chemical properties of the two materials that are used in the experimental phase (wettability, roughness, topography, rigidity, flexibility, porosity, etc.) had influenced the coating-protein adsorption process. These factors determine the wayin which the biological molecules are adsorbed by the materials. In particular, all these factors determine the orientation of the adhesion molecules and consequently may have influenced the behavior of cells connected with them.

Finally, while the integration of commercially available PDMS membranes in the microfluidic device was more difficult and sometimes resulted in problems such as leakage and poor bonding, PDMS membrane was easier to handle. Moreover, the PDMS highness limited optical microscopy, giving microscope-acquired images less accurate. PDMS thin integrated custom layer resulted optically transparent (in the wavelength range 240−1100nm [35]) and confocal imaging wasmore accessible.

4.5 Ultrastructural characterization of crypt-villus axis

In addition, PDMS integrated membrane SEM's acquisitions, showed the differences between the two topography of membranes. But especially we can appreciate how both membranes are engraved directly on the microfluidic channel, in order to obtain better reproducibility, faster and easier fabrication. Figure 40 showed that integrated membrane had the "conventional" literature surface exposing only pores 20μm pores in diameter. The exposed surface had a constant geometry, having for each line 6 pore of 20μm with distance of 200 μm Center-Centre. Figure 40 showed the integrated In-Crypts Membrane produced "home-made", as we can see, the surface resembles the in vivo-like dimensions and topography of crypts [].
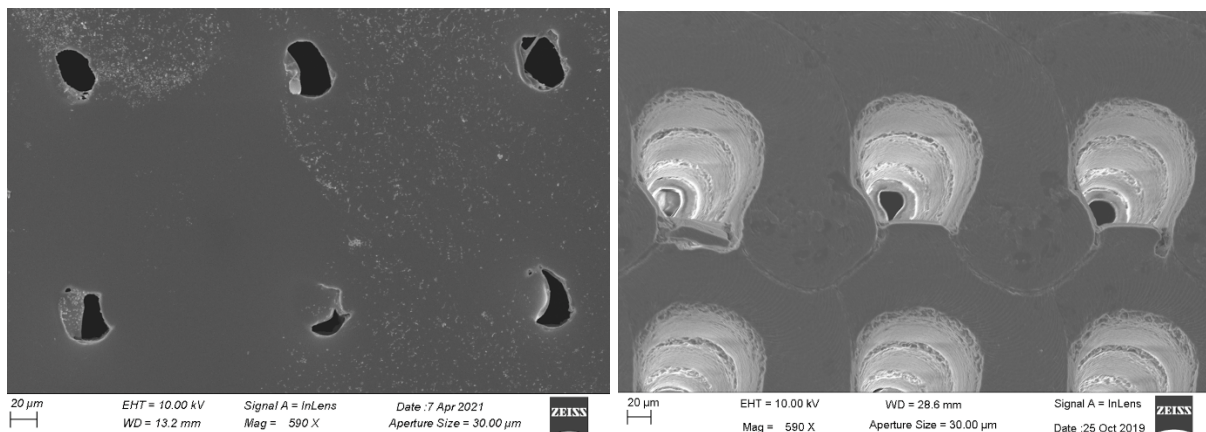
Figure 40. SEM's acquisitions of 6 pore of 20μm with distance of 200 μm Center-Centre of PDMS conventional device(left). SEM's acquisitions of 6 pore of 80μm with distance of 200 μm Center-Centre of In-Crypts device (right).

We can also appreciate the regularity of the geometry (distance C-C 200 μm) and the topography of cone-shaped pores. In-Crypts membrane is made up by 4 layer, as showed in Figure, first layer of pores 80μm, second 60μm, third 40μm and last 20μm. In-crypts membrane allowed us to increase or decrease the porosity of the membrane as we needed in order to define the best configuration for the exchange of nutrients and oxygen inside the microchannels. Furthermore, integrated membrane, overcame the difficult due to the bonding trough membrane and microchannel. To compare the epithelial proliferation and differentiation process on both porous membranes the Caco- 2 cells were cultured. Caco-2 cells were cultured in both

membranes once they reached confluence, they begun to polarize and differentiate, forming
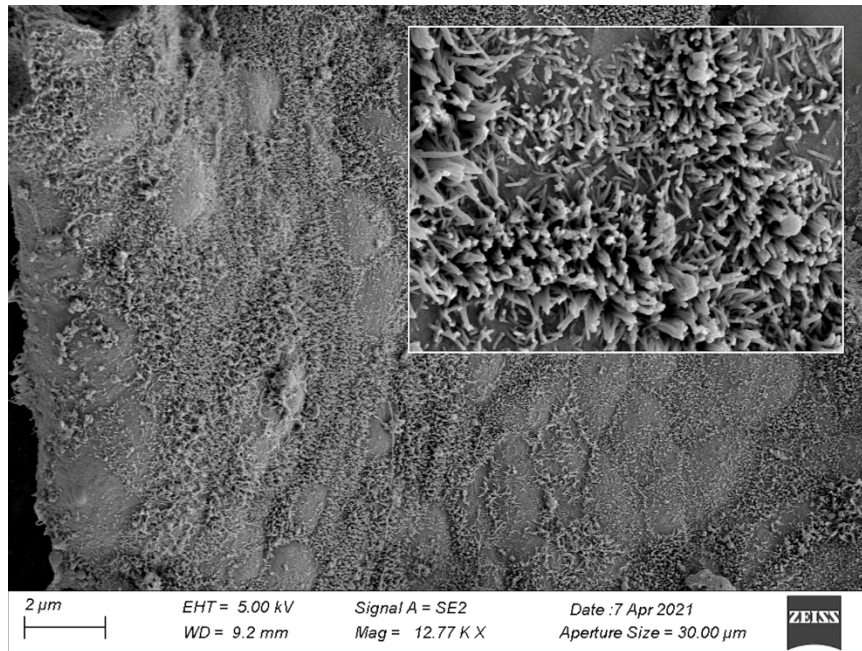
Figure 41. SEM's acquisition and focusing on epithelial layer formed after 8th day of static culture in Conventional PDMS device.

an undulating epithelium. In particular, we observed that the cells In-Crypts membrane, recognized an environment more similar to the physiological one with 'invaginations' created by the pores that reminded the basal proliferative cell crypts that characterize the small intestinal epithelium. With the In-Crypts integrated membrane, cells were sow on the bottom on cone-shaped pores in order to mimic the basal proliferation cells on crypts. Figure.41 showed the "conventional" membrane with the confluent monolayer of Caco2, presence of Microvilli and Mucus.
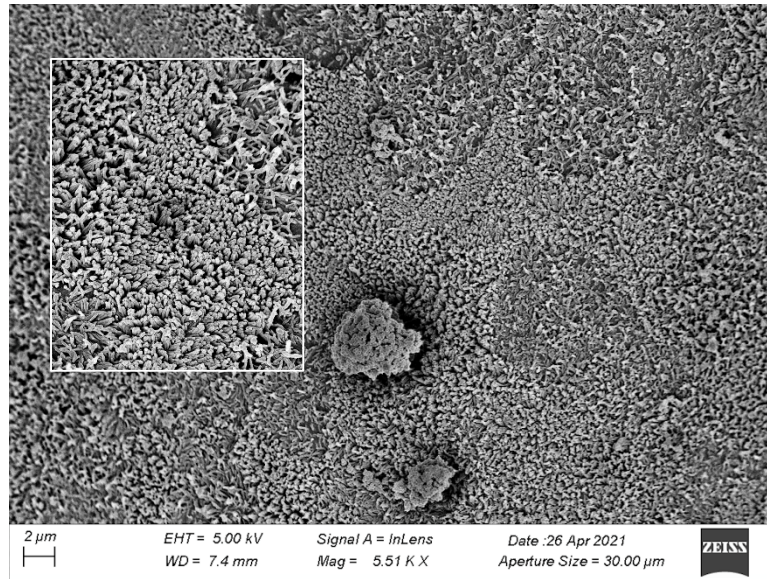
Figure 42. SEM's acquisition and focusing on epithelial layer formed after 8th day of static culture in In-Crypts device..

In the other hand, SEM's Figure 42 showed In-Crypts membrane, the presence of a completely uniform multilayer of cells. In addition, cells multilayer, completely closed the bottom of the crypt-like and close them completely.
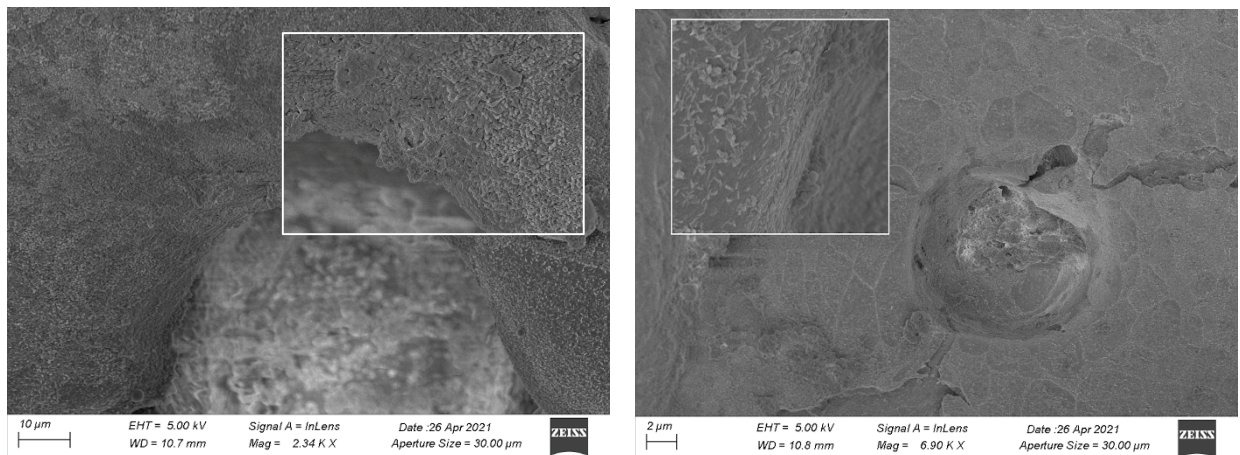
Figure 43. SEM's In-Crypts membrane. Acquisition and focusing on Crypts Epithelial layer formed after 8th day of static culture. Both focus on epithelial layer, with presence of microvilli and mucus, also presence of formed crypts.

4.6 Caco2 Transmigration and production of stem cells

The results of the Caco-2 cell differentiation in the "conventional" and In-Crypts Device are shown in Figure 43-44. Channel acquired through confocal microscope in Figure.. showed that it is clearly evident that In-Crypts Device was optical accessibility compared to the Conventional cell's culture membrane. Caco-2 cells have developed a fully confluent layer over In-Crypts Device. They also started to polarize, however, according to the type of cell culture and of the membrane, they reached different levels of differentiation. In particular, the differences in culture times obtained for the two different membranes under static conditions correspond to a different behavior of the epithelial cells when seeded on two different membranes supports. These results confirmed that different topography of the porous membranes strongly affects Caco-2 cell growth and differentiation.
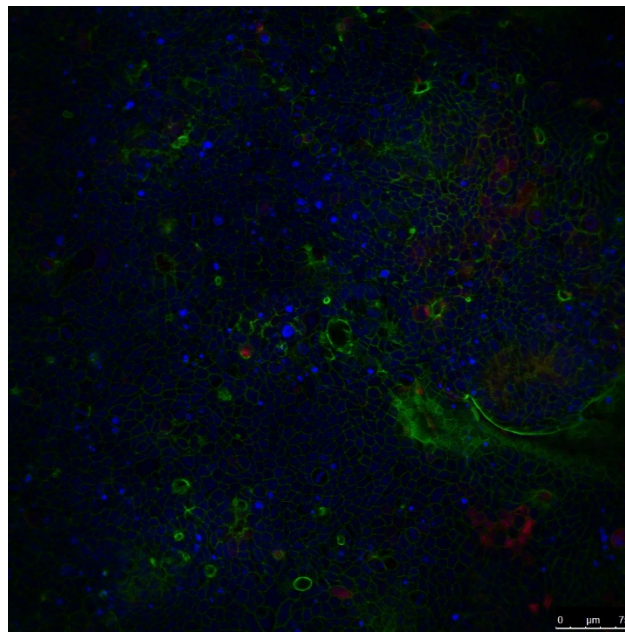
Figure 43. Confocal acquired images of Caco-2 intestinal epithelium in the Conventional PDMS device. In green tight junction, in blue nuclei in red production of mucus.

Caco-2 cell differentiation was observed by immunolabeling for specific epithelial cell differentiation markers. Epithelial layer showed that the Caco-2 cells are able to migrate along the crypt-villus axis and to differentiate into different cell types: including

- intestinal cells
- mucus cells
- neuroendocrine cells

- Paneth cells.

Villin showed by figure.. demonstrating the enterocytesphenotypes of Caco-2 cells in the apical side in only In-Crypts device, in Conventional PDMS we didn't notice relevant signal that evidence that the In-Crypts device had faster differentiation than PDMS conventional device, this means a reduction of culture time.

Other confirmation we had noticed the immunofluorescence staining for MUC-2 revealed the presence ofthe Goblet-like cells with a greater amount of mucus in In-Crypts device Fig. than in PDMS conventional device Fig. 44 Furthermore, the immunotipization for CGA and lysozyme marks respectively Enteroendocrine cells and Paneth cells phenotype, evidence only in In-Crypts device. In particular, the absorptive cells, enteroendocrine and Goblet cells were preferentially localized in the villus-like regions, whereas the Paneth cells preferentially localized to the crypt region. In addition, to deeply investigate the differentiation of both the device we analyze the LGR5 amount of cells.
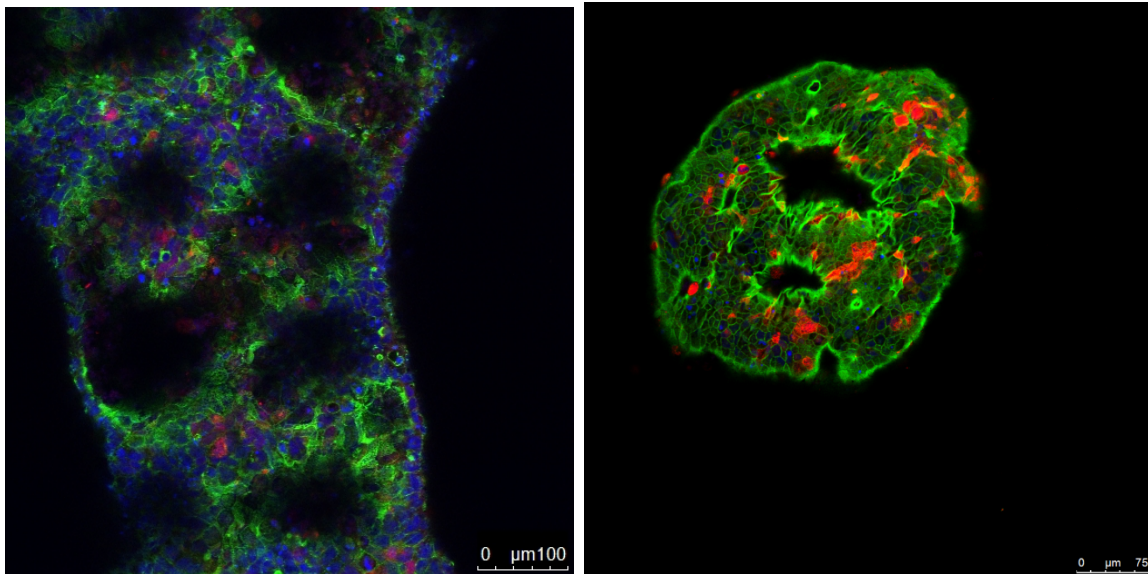
Figure 44. Confocal acquired images of Caco-2 intestinal epithelium in the In-Crypts device. In green tight junction, in blue nuclei in red production of mucus.

We noticed, also in this case, that In-Crypts device showed a greater amount of stem cells on the bottom of Crypts instead the PDMS conventional device, that lack of "Costume-made" PDMS membrane resemble the Crypts structure Fig 45.
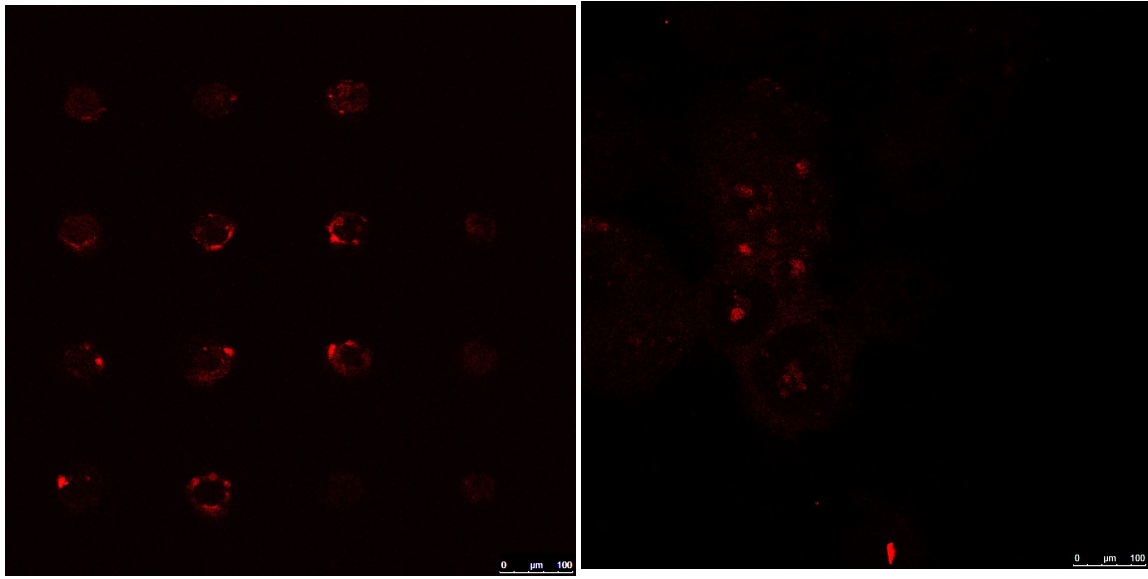
Figure 45. Confocal acquired images of Caco-2 intestinal epithelium in the In-Crypts device. In red on left Paneth cells and on right stem cells
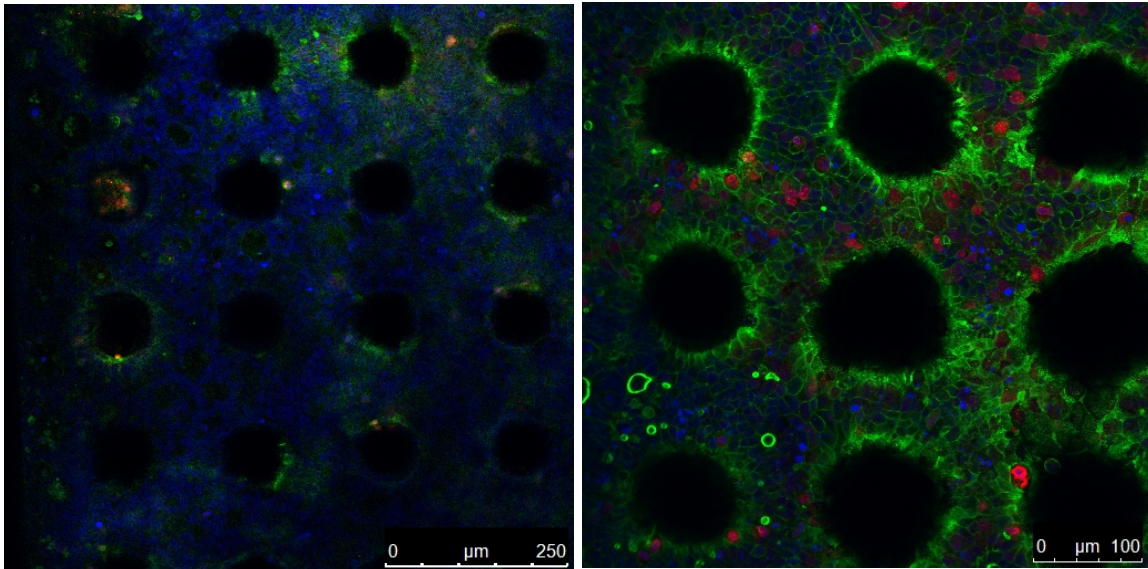
Figure 46. Confocal acquired images of Caco-2 intestinal epithelium in the In-Crypts device. In green tight junction, in blue nuclei in red cells fo proliferation.

4.7 Epithelial functionality In-crypts membrane

The tight junction (TJ) formation was detected with immunofluorescence staining highlighting the expression of a transmembrane protein of tight junction, Claudin-1 as shown in the Fig. 47 The presence of Claudin-1 confirmed that Caco-2 cells formed a confluent, differentiated epithelium with well-developed tight junctions. Tight junctions characterization is fundamental in the studies of absorption and permeability of compounds or drugs, because they form a physical barrier to the diffusion of macromolecules. The loss of the tight junction barrier leads to a higher absorption of toxin and xenobiotic compounds.
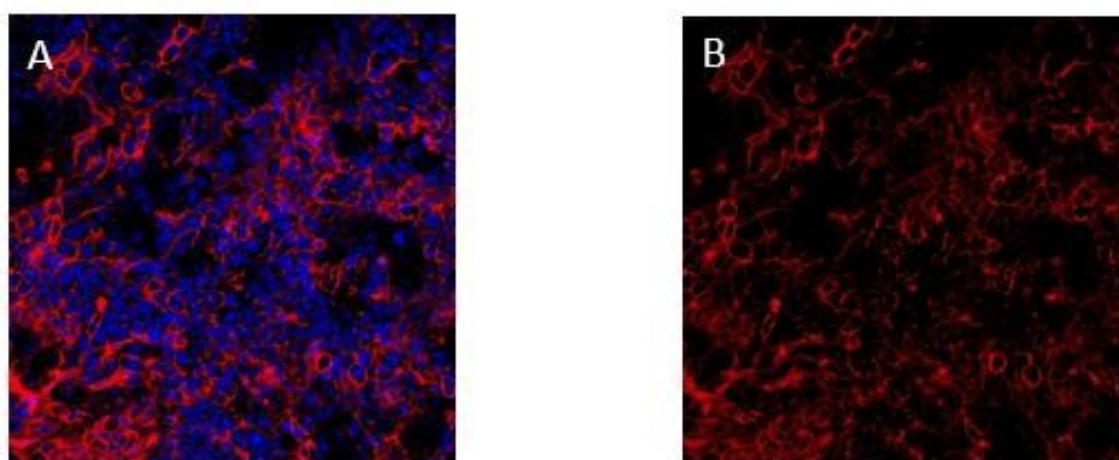
Figure 47 – Immunofluorescence images of Claudin indicate tight junction formation – (A) Claudin in red and nuclei in blue (B) Claudin.

4.8 In-Crypts permeability and TEER measurement

To monitor Caco-2 cell growth and evaluate cell-cell tight junction integrity, TEER measurements were performed directly into devices. TEER values were acquired at 0th 3th 5th 6th 8th days. As described before, TEER values were extrapolated from the fitting of the experimental data derived from the measurements with curves obtained from the equivalent model circuit. The results were plotted over time in figure. We noticed, for PDMS conventional device, after 3 days, the value of TEER is still 0, it means that Caco2 not complete confluence on the PDMS conventional device, only at day 5th we noticed complete confluence. Maximum of TEER is at 8th day, but we didn't notice a decrease of TEER, so we didn't have a peak that confirm start of complete differentiation of Caco2 cells. In the other hand, In-Crypts device,

showed by Fig. 38 an important results for us. Not only because TEER at 3th day confirm that Caco2 is complete confluence, so it means that time of culture is decrease. But also confirm a better differentiation due to the Peak at the day 5, and the decrease of value TEER at day 8. So The TEER value significantly increased with time, displaying a peak on day 5 when the cells reached confluence indicating TJ formation. This point also indicates the beginning of cell differentiation. Caco-2 cells cultured in the In-Crypts on a chip not only differentiated in terms of enterocytes, but also began to produce mucus. Mucin cells intercalated between enterocytes and resulted in a decrease in the TEER value making it closer to the physiological values of the small intestine (50-100) [28].

These results confirmed the growth and differentiation of the epithelium as well as its correct and expected barrier functions after eight days of culture only in the In-Crypts device under Static conditions. TEER values reached by the Caco-2 epithelium developed in the In-Crypts device were higher than values of native tissue: this was expected because of the lack of the stroma in the realized model [28].
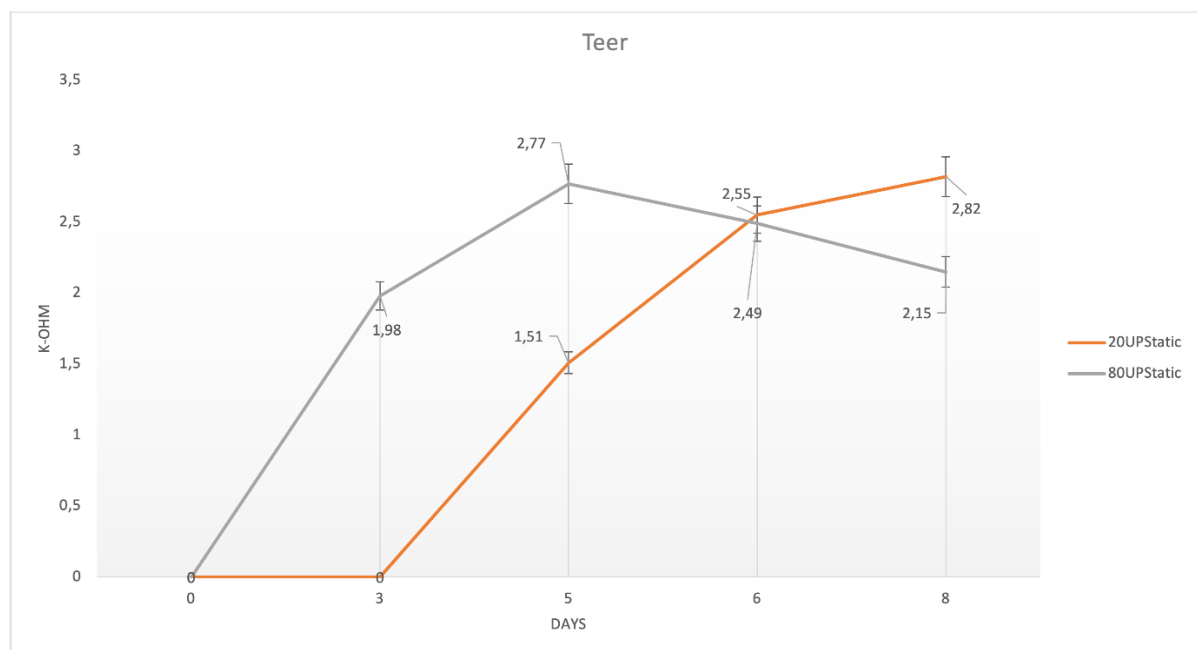
Figure 48 – TEER graphic during static culture of PDMS conventional device and In-Crypts device. TEER measurement on 0th 3th 5th 6th 8th day.

As reported in figures 48 and, the trend of the TEER values over time is very similar to the Ingber et al. model [30]: it increased over time reaching a peak when the TJs were formed. However, the peak was reached two days earlier, indicating that the differentiation process

begun earlier. In addition, all TEER values were lower than the Ingber model ones and this represented an advantage because they were closer to the physiological values of the small intestine. The variation of the TEER value and its slight decrease after the peak demonstrated the cell differentiation (not only in enterocytes, but also mucin cells) and, therefore, the development of an epithelium characterized by villi-like structures- The increase in the surface area was of great importance in the study of the absorption of molecules and compounds. Ingber et al. measured the amount of dextran particles that cross the epithelium in the unit of time and evinced an increase of steady state flux when peristalsis-like motions were introduced. They assumed that this was due to some mechanisms such as active transport, ion channels or transcytosis that probably could be activated during peristalsis. Although it was not possible to experimentally determine the steady-state flux of dextran in our device. it was possible to hypothesize its behaviour.

The steady-state flux trend was expected to be similar to that reported by Ingber in his manuscript [28].   The In-Crypts device, previously optimized, was able to reproduce an intestinal epithelium with some physiological characteristics, such as domes-like structures and well developed TJ. This device, that ensure the physiological fluid flow with relevant magnitudes,was used for preliminary permeability studies. According to the literature, In-Crypts devices have great potential in the field of pharmaceutical development and can be used in nutraceuticals to test nutrients and functional foods.
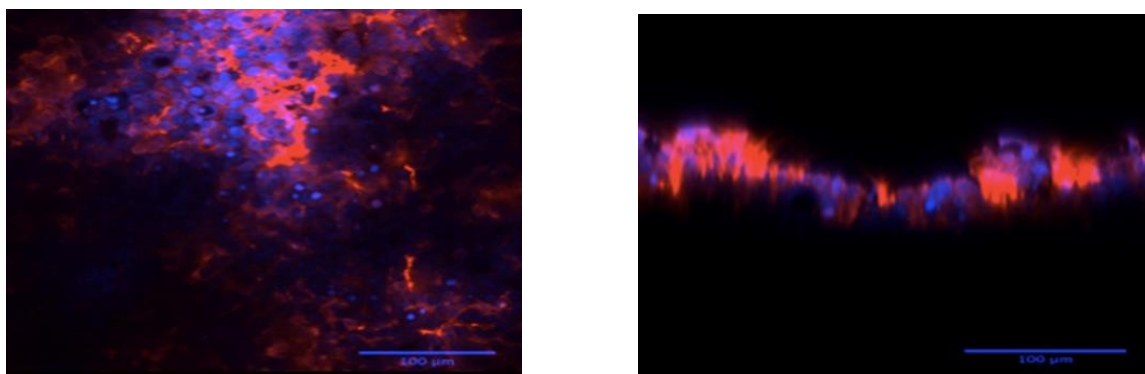
Figure 49. Fluorescent dextran on CaCo-2 monolayer displayed in the Z plane (left figure) and in the Y plane (right figure). The distribution of the compound on the apical surface and inside the monolayer is evident.

In order to select the optimal concentration and the size of the compound to perform the permeability tests, Fluorescent Dextran 3kDa FITC was added on the apical compartment ofa

Transwell system, as already described in section 2.8.

As recognized, the intestinal epithelium resulted permeable at low molecular weight molecules. According to the literature, we showed (Figure 49) the distribution of Fluorescent Dextran 3kDa FITC on both apical surface and inside the monolayer.

These preliminary studies allowed to estimate and optimize the initial apical concentration as well as duration of the experiment to perform subsequently into the In-Crypts device.Our results indicated that the initial concentration of dextran (1 mg / mL) could be diluted 1: 100 in HBSS, in order to have a homogeneous distribution and the correct intensity of the compound administrated on the apical side.

Sample aliquots (30 µL) would be collected from the apical and basolateral outlets after 2 hour, then they would be analyzed through a spectrofluorimetric analysis to quantitate the amount of fluorescent molecules transported across the Caco-2 barrier (data not shown). As reported in literature, once experimentally measured the steady state flux, itwould be possible to compute the apparent permeability coefficient:

$$P_{app} = \frac{dQ}{dt} \times \frac{1}{AC_0}$$

where:

- $\frac{dQ}{dt}$ is the steady state flux;

- dt

- A is the culture area;

- C0 the initial apical concentration.

As show in figure .. the permeability growth in exponential way, Ingber and in vivo like [].

Furthermore, to support these thesis, that the epithelial Caco2 layer resemble the in vivo barrier function we integrated TEER measurement during the 2 hour permability test. As showed in Figur.. After the 1 hours permeability has similar trend with small increase of permeability, but linear. After 90 minutes we noticed a decrease of TEER due to the striction of tight junction after the passage of Dextran trough the epithelial layer and at last a new increase at physiological epithelial Caco2 layer in to the device.

TEER CON PERMEABILITA'
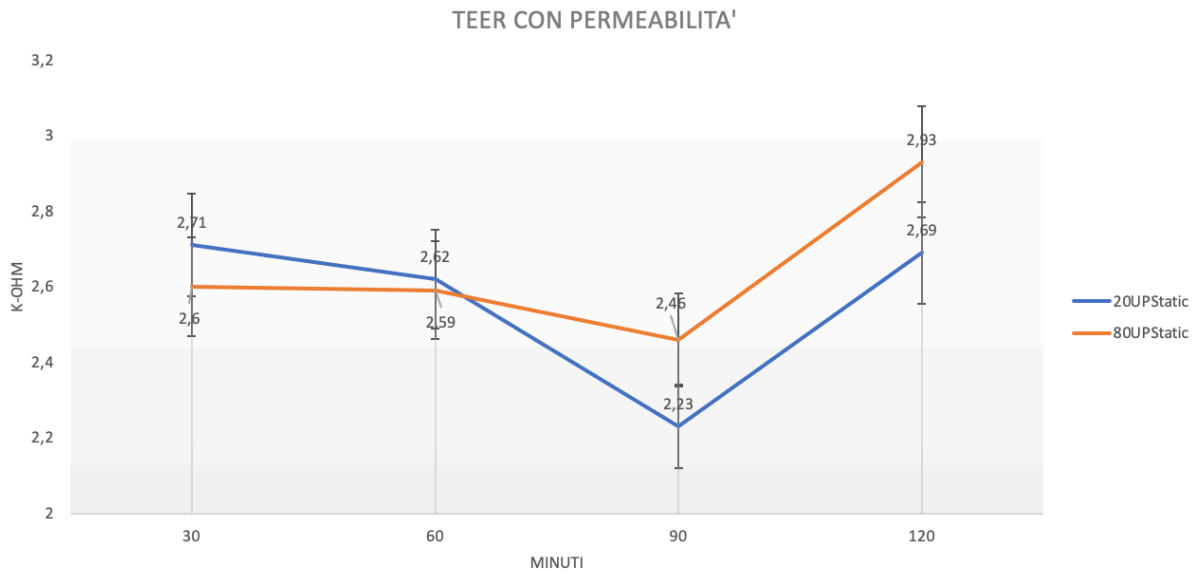
Figure 50 – TEER graphic during static Permeability test of 2 h on PDMS conventional device and In-Crypts device. TEER measurement on 30-60-90-120 minutes.

In light of the above, In-crypts device realized in this work could make a great contribution to drug and food tests. Its capability to develop an equivalent intestinal epithelium with morphological characteristics similar to the native tissue in rather faster times than those reported in the literature is a strength.

Mucin cells intercalated between enterocytes and resulted in a decrease in the TEER value making it closer to the physiological values of the small intestine (50-100) [28].

TEER values reached by the Caco-2 epithelium developed in the In-Crypts Device were higher than values of native tissue: this was expected because of the lack of the stroma in the realized model [38].

Conclusion

We demonstrated that the crypt-like pattern of the In-Crypts Device have provided the correct topographical structure for the epithelial cell differentiation resembling the microenvironment of the small intestine. We assume that the In-crypts membrane has accelerated the differentiation process developing an epithelium with more physiological features which are attributable to different factors such as pores density, pores diameters materials of porous membranes. The conventional membranes, typically made by using a track-etching process, are

characterized by a random placement of pores, with not uniform local pore density. In addition, membrane porosity must be kept fairly low in order to minimize the overlapping of pores. On the contrary, our custom-made In-Crypts membrane displayed a better uniformity and higher porosity than the conventional membranes, due to the controlled pores number and distribution at the fabrication time. In addition, the small pore diameter of the Conventional membrane (5 μm) determines a smooth-like surface for cell adhesion. In contrast, the In-Crypts Device membrane with larger pores (20 μm) showed a kind of depressions on the surface of the Caco-2 cells that are able to respond differently in terms of differentiation.

5. Peristalsis on a chip and evaluation of healthy tau

Abstract

Intestinal mucosal layer and, in general, intestinal tissues are subjected to forces that regulate and affect intestine functions. Of particular interest here, are forces generated as consequences of endoluminal chyme mechanical consistency that rise shear and pressure stress to the mucosal cells while subepithelial muscular cells induce repetitive peristaltic contraction and deformation. Luminal contents are generally minimally compressible so contraction of the muscular layers results in mucosal compression between the contracting musculature and the poorly-compressible chyme. These mechanical forces are known in literature as shear stress and Hoop (cylindrical) stress. The aim of this activity is to realize a fluidic device able to replicate the physiological behaviour of intestinal mucosa in vitro including deformation induced by chyme passage through it. The device is intended to measure and monitor relevant stress transmittal from endoluminal chyme and intestinal mucosa due to the passage induced by intraabdominal pressure due to Hoop stress (i.e. peristalsis stimulus) so to evaluate the effect of mechanical insults on intestinal epithelial damage and/or repair.

Methods and Materials

5.1 Design and fabrication of intestine on chip

The Peristalsis on chip device was fabricated from a flexible polydimethylsiloxane (Sylgard 184, Dow Corning) polymer. The device architecture consisted in two different layers, aligning only central microchannels. The lower and upper layer were prepared by casting PDMS prepolymer (10 : 1 w/w for lower layer; 15:1 w/w for upper layer; PDMS/Curing agent) on a (PMMA) micro fabricated inverse mold and polymer curing at 65° for 12 h. The PMMA master inverse mold was designed by AutoCAD and carved with micromilling machine (Minithech CNC Mini-Mill) Figure 51 making a relief positive geometry [30]. Lower PMMA mold layer design consisted in a central channel (1000μm x 6000μm) with custom made pillar (thick 150 μm). "Custom-made" cone pillar is due to the variation of their diameter along its height (section 3). Aligned centre of circular pillar changing in diameter along their height: in the first 50 μm pores diameter is 20 mm with a 200 mm spacing (centre to centre), following 50 μm 60 mm with 200 mm spacing (centre to centre), continuing for 50 μm 80 mm with 50 mm spacing (centre to centre). Upper layer design consisted in a central channel (1000 μm x 1200 μm) surrounded on either side by eight hollow chambers with chalice-shape (2500 μm x 1500 μm; 1500 μm x 3000 μm) and thin wall-layer (100 μm) on the central microchannels, that permit,

not only the application of cyclic compression and relaxation of the flexible lower central channel membrane, but also the cyclic wave compression of the eight thin wall-layer on the volume of fluid contained in the central channel. This design was inspired by the mechanism of physiological peristalsis, in living human intestine, where radial and longitudinal pressure due to smooth muscle on intestinal lumen consent the progression of Chyme along the intestine.
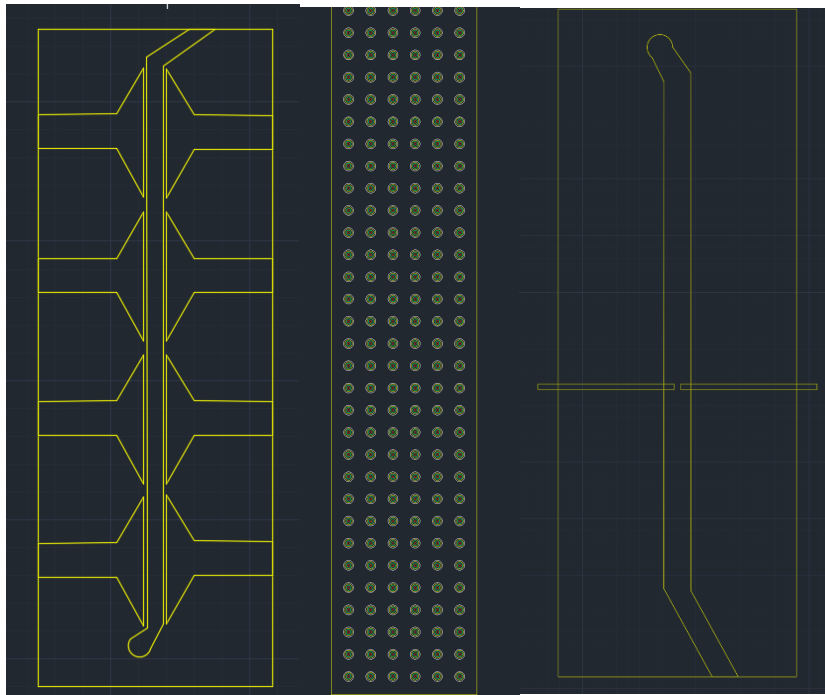
Figure 51. CAD Scheme of Peristalsis device with integrated membrane and electrodes, 80μm pores exposed and cone-shaped resemble crypts.

The PDMS Lower layer channel consented to obtain integrated PDMS membrane on the lower central channel. After peelings PDMS layers from PMMA support, upper layer was re-treated to allow the closure of eight hollow chamber. A thin layer (100 μm) of pre polymer PDMS is curing at 90° for 8 minutes. After, the upper layer was placed on thin layer and recurred at 65° for 12 h, in order to obtain the closure of the eight chamber. This type of curing and the adhesive propriety of thin PDMS layer allowed the complete closure of the eight chamber, so as to ensure, once insufflate air inside, inflation of thin wall-layer. Before the final assembly, cured PDMS on one side of central upper microchannel was cut to allow the layer's bonding. Upper layer exposed from open microchannel side and lower layers exposed from PDMS channel that contain membranes, were brushed by pre polymer PDMS and cured at 65° for 12h for the final

bonding. The PDMS biochip was sterilized by ethanol 70% for 40 minutes (protocols Ethanol Ale) and washed twice with PBS and then was filled with fibronectin (20/1; µl/ml) to allow the seeding of Caco2 cells and avoid the presence of air bubbles. The upper and lower microchannels was connected to a syringe pump trough tubes (Tygon 3350 silicone tubing, ID 1/3299, OD 3/3299, Beaverton, MI) using custom connector hub-free stainless steel blunt needles (18G; Kimble Chase, Vineland, NJ) in order to dispense medium. Eight hollow chamber was connected to air tank (type) for pressure sources trough Tubing (Tygon 3350 silicone tubing, ID 1/3299, OD 3/3299, Beaverton, MI) using connector (Male luer kit). The eight chamber connectors were assembled and tested with a brush of PDMS in order to guarantee the sealing and inflation of the pressured chamber. This set-up guarantees flow control for dynamic culture medium in the central microchannels and regulation of pressure insufflation to the chambers under Arduino control to induce cyclic mechanical wave pressure for emulate peristaltic-like wave motion. We choose the best configuration for obtain scrolling of Gelesis gel into device on the intestinal mucosa in order to better reproduce digestion microenvironment and motility.

5.2 TransEpithelial Electrical Resistance measurement (TEER)

In our experiment we chose have not used the standard TEER measurement instrument (i.e. *chopstick*) because we can only detect the value of impedance at a fixed frequency; this means that we couldn't split the contribution of electrical resistance from capacitance and inductance effect on the tissue. From the theory of chemical impedance Spectroscopy, we know that these are very relevant contribution that play different role depending on the frequency range that we consider. For these reasons we chose to use a potentiostat/galvanostat by Metrohm. This provides a more accurate measurement both for the quality of the instrument (it uses four electrodes instead of two of the chopstick) and to the quantity of parameters that can be set in our experiments: for example, we are able to set the current and the voltage range.

We found that for our application, potentiostatic mode provides more accurate results. In addition, in this mode we can choose very small value of current in order to avoid barrier damage. Other advantages are that we can directly use the measurement to digitally fit the values and estimate our values.

TransEpithelial Electrical Resistance (TEER) measurements were performed to monitor the Caco-2 differentiation and barrier function exerted by the intestinal epithelium. To guarantee a good ion concentration in the solution, the culture medium was changed one hour before the analysis.

TEER measurements were performed by connecting the SI-on-Chip microfluidic device to an AUTOLAB PGSTAT302N (potentiostat/galvanostat) by Metrohm equipped with a FRA32M module (frequency response analysis module). Impedance spectra were recorded in potentiostatic mode (0.3 V) with an amplitude of 0.01 V and frequencies ranging from 100 kHz to 0.1 Hz between two Platinum electrodes. For each measurement, three readings and 50 data points (logarithmic frequency step) per reading were collected. Bode Modulus and impedance at 12 Hz were used to follow the epithelium growth as already reported in literature. A typical output of the measurement is shown in figure 52. It is a Bode plot, in which the red line represents the module of impedance and the blue one, the phase. It is important to underline that this kind of parameters estimation is more precise because it is the result of a measurement at each frequencies of interest.
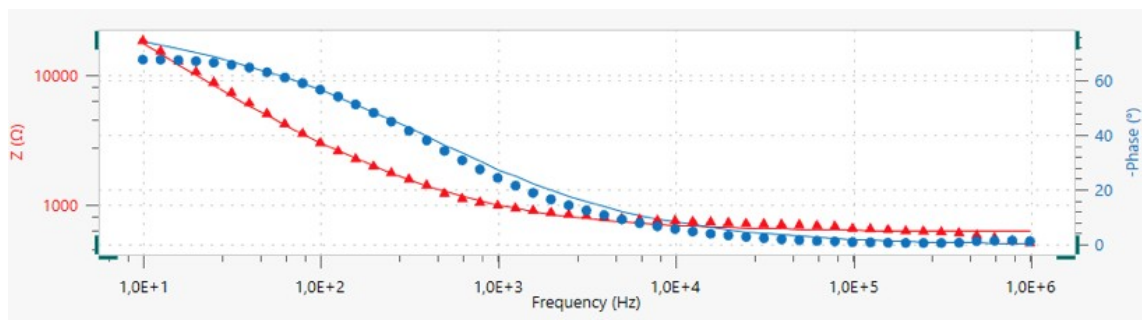
Figure 52 - A typical measurement performed with Metrohm Autolab. Red line represents the module of impedance while the blue one represents the phase.

Measurements were directly used to digitally fit the values and estimate our results. In particular, the least-square optimization method was used to fit the measured impedance data to an electrical equivalent circuit model, reported in Figure 53.
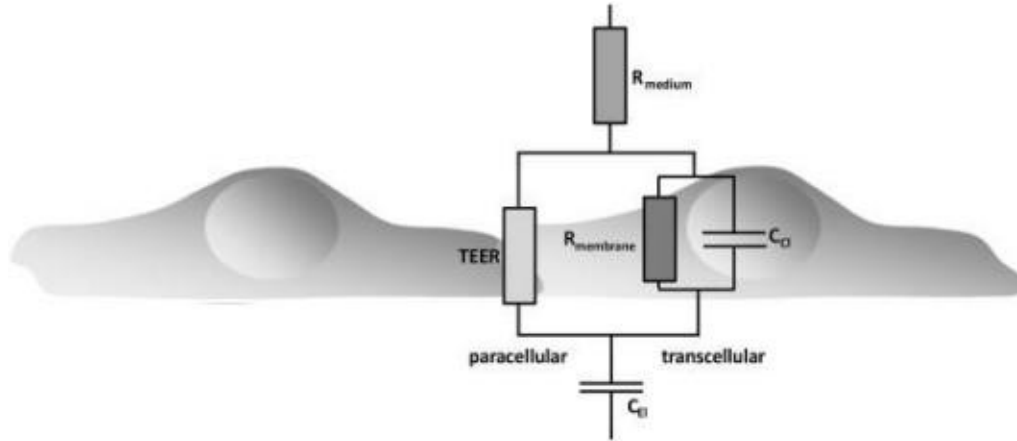
Figure 53- Electrical equivalent circuit model.

Within the paracellular pathway the tight junctional proteins represent an ohmic resistance (TEER) in the circuit diagram while each lipid bilayer in the transcellular pathway, can be described as a parallel circuit of an ohmic resistance (Rmembrane) and an electric capacitance (Ccl). Within the considered frequency range, the high resistance of the membrane causes the current to flow predominantly across the capacitor and allows, in first-order approximation, to ignore the membrane resistance. In addition, the surrounding medium (Rmedium) was represented as a resistance and the electrodes as constant phase elements (capacitance, CEl). RTEER was normalized for the cross sectional surface area to calculate the TEER value in Ohm x cm^2.

5.3 Induction of controlled stress acting on the chip

5.3.1 Realization of hardware setup

To emulate the peristalis through a system of pneumatic actuators had already been made during the design phase of the layout of the device: in fact device had eight calici-shaped bedrooms arranged according to a 2x4 matrix, which stimulate Caco2 layer in the interposed channel, if properly inflated and deflated (Fig. 54).

In order to carry out these operations, due to the small size of the chambers, it was essential to use an air cylinder coupled with a pressure reducer with an adequate resolution (0.1 bar). In addition, it was necessary to coordinate the chambers in order to facilitate the passage of the bolus within the canal and to realize the peristalsis movement. The air flow was regulated in each bedroom by a set of electrovalve driven by a microcontroller by means of a circuit with special transistors.
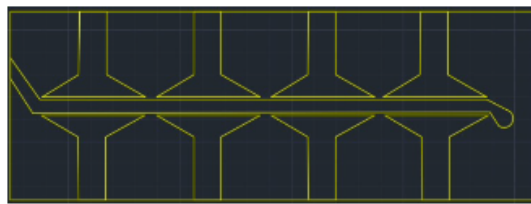
Figure 54. CAD Scheme of 8 chamber that will be inflated.

Electrovalvances are valves whose state can be electrically controlled by applying an appropriate potential difference to the clamps. Inside they have a solenoid that, due to the generated magnetic field, attracts a moving nucleus and a shutter: this shutter lifting up consent the passage of the fluid. An appropriate spring closes the valve when the current is interrupted. On the market there are several types of valves, that are different in electrical characteristics or different depends of fluid that they had to bring, at least they are different due to the exercise pressure and temperature that its worked.
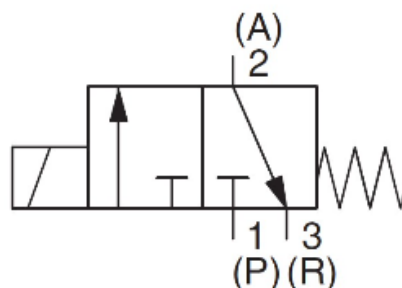
Figure 55.Pneumatic scheme of valves type that we chose for Peristalsis on a chip Model.

5.3.2 Electrovalves choice

The requirements for our application required that the electrovalves should be:

• 3-way and 2-position. Number of routes is the number of attacks with which the valve interfaces with the outside. For our needs it was necessary to have:

1. a route to the pneumatic supply source (compressed air) usually indicated in the diagrams with the letter P2.
2. A discharge route left to atmospheric pressure (not connected) to allow the chambers to deflate, usually indicated in the diagrams with the letter R3.
3. A way to connect the valves to the chambers (line of use) with either with P or with R depending on the state of the valve; is usually indicated in schemes with the letter A.

The number of positions is the number of states in which the valve can be located: in our case one state is responsible for inflating the chambers (the power supply is connected to the utilization line) and another for deflation (the utility line is connected to the exhaust).

Figure 56. Pneumatic diagram of the type of valve used in this project.

• **normally open.** An electrovalve is defined as N.A. if, in the absence of electrical wings, the line of use is disconnected from source P. It can be inferred from Figure that the valve in question is normally open because the spring is in a state of rest (absence of electrical voltage) and A is connected with R. In some applications where it is more common to break a flow than to establish it, you may have the opposite behavior.

• **small.** In fact, the external diameter of the utilization line had to be compatible with that of the tube entering the bedrooms of φ 3 mm.

• **modular.** With this construction feature, the set of valves is fixed on a common base in order to form a single block with the pneumatic supply and the common discharge, from which each valve can draw separately. This was essential to reduce the number of pipes to be used and to greatly reduce the footprint of the setup.

• **operated with DC current.** In this way it is easier to interface the electrovalves with a microcontroller (which generally uses TTL logic) and which works more easily with continuous voltage rather than alternating.

• **low power absorption.** In fact, the purpose was to power the electrovalve with a stack, in order to make the setup more portable. Following market research, it was found that the company SMC@R produces a line of electrovaldes that is fully compatible with the desired specifications, as well as offering assistance directly in the territory.

Figure 57 Platform of Arduino Uno and its specifically components

The S-070 series, in addition to being 3-way and 2-position, was found to be compliant with dimensional specifications both in terms of the diameter of the attachment of the utilization line (φ 3.2 mm) and for the size of the entire valve set (73mm x 25mm x 12mm); SMC@R also makes the modular version available as shown in Figure 57. In addition to a reduced power absorption (0.35W) it was possible to choose the version with the power supply of 5V in continuous.

5.3.3 Choice of microcontroller and circuit

Since the computational power required was not high, the choice of board converged on the widespread Arduino UNO (Figure 57) It is an embedded device on which you can upload a program via USB interface (appropriately written and compiled on external PC), which will run in loops.

It is a board equipped with microcontroller (ATmega328P) and some peripherals such as Analog to Digital Converter 10 bits (for the detection of analog voltage signals), communication devices (such as serial), 14 General Purpose Input Output that allow to establish or detect a voltage of 0 or 5 V and a voltage regulator that establishes between the 5V and GND pins, a continuous voltage of 5V.

However, this was not enough for our applications, in fact:

• 5V and GND pins can power the electric cables but cannot "turn them off" since the voltage regulator cannot be turned off;

• GPIO ports can be controlled both on and off but cannot deliver a proper current intensity to power the electrics.

For these reasons it was necessary to interpose a circuit between Arduino and the electrovalve, which is shown schematically in Figure 58 for a pair of electrovalve.
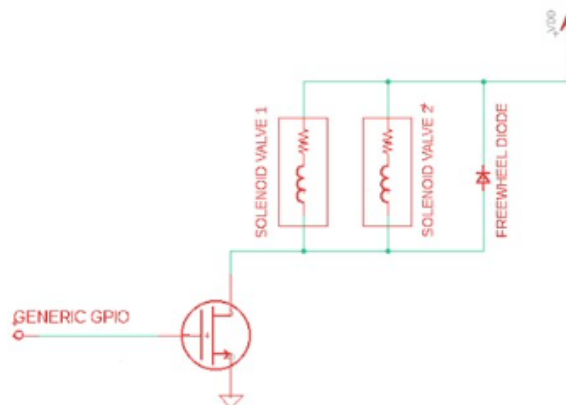
Figure 58 Schematic view of electrovalve control circuit

5.3.4 Mini compressor

Since no special air filtration operations are required it was thought that the air present in the environment would be used: to do this, a compressor was used to take air out of the environment and enter it into the fluid circuit at a higher pressure. In the absence of stringent specifications on flow quality and the need for a simple and cost-effective solution, a membrane pump has been chosen, the operation of which is exemplified in Figure 59 :

- an engine (usually brushed or brushless direct current) has a shaft that has a certain eccentricity.
- an elastic membrane is urged by the eccentric motion of the motor to curve downwards and downwards
- a chamber is placed adjacent to the membrane; when the latter is curved downwards the chamber fills with air while when it is curved upwards, the air tends to flow with some pressure towards the outlet orifice.
- a set of two valves takes care not to reverse the direction of flow in the moments of time when the membrane is in rest conditions.
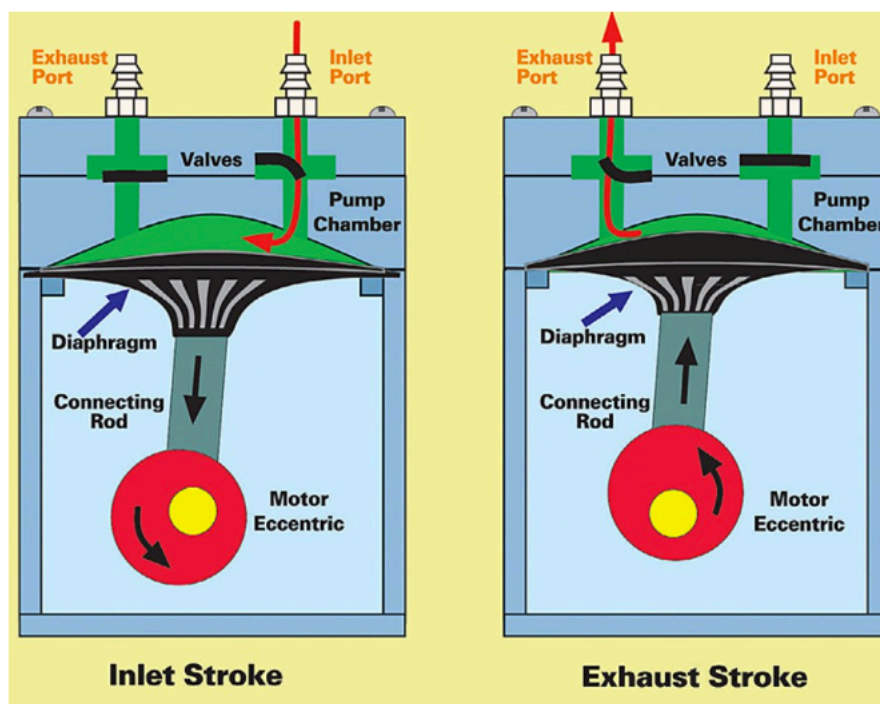
Figure 59. Membrane pump schematic type of working scheme

The compressor that has been selected for this purpose is the KNF NMP830KNDC model, shown in Figure... The characteristics of this compressor which led to its use in this application lie in the reduced dimensions of application zone, the characteristic flow-back pressure (shown in Figure 60 for 12V power supply) and the good lineriness of the flow rate as the current changes.

Figure 60 Mini compressore KNF NMP830KNDC model

It can be seen from Figurev62 that the pump can work up to 1.4 bar and this allows on the one hand to take full advantage of the range of pressures required by the peristaltic motion and on the other to protect the device in case of malfunction, since too high pressures are not reached. In addition, since the feature has a considerable slope, the compressor reduces the flow to a minimum once the chambers have inflated: this allowed to use it in continuous mode taking advantage of the inevitable load losses due to air leaks in the connections (which at full speed constitute the minimum flow of the compressor). This simplifies the control of the compressor and preserves its life time that would otherwise have been affected by the frequent high currents at start-up.
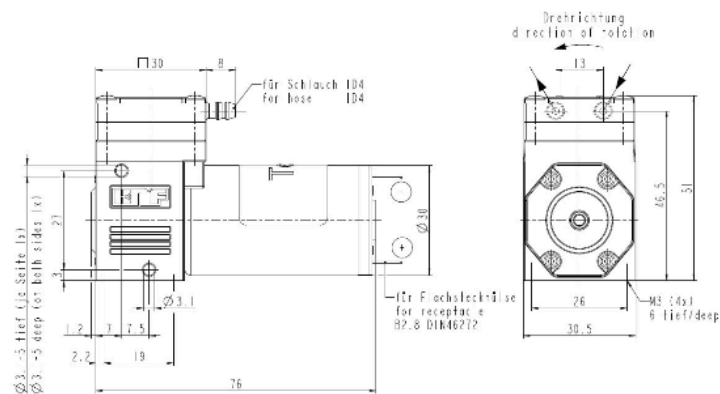
Figure 61. schematic dimension of KNF compressor

As regards the linearity of the flow with the current, this derives from the properties of the direct current motor: since Arduino does not allow to have a continuous variable voltage at the output, the flow has been adjusted with the Pulse Width Modulation technique through the appropriate pins of the board. To achieve this technique, it is necessary to have a component that acts as an electronically piloted interrupt and in this case a Mosfet type N. Fundamental has been used is the current recirculation diode necessary to have a non-zero current even when the mosfet is in interdiction. Given the inductance of the engine, it was sufficient to carry out modulation at 976 Hz, frequency directly available in certain board pins.
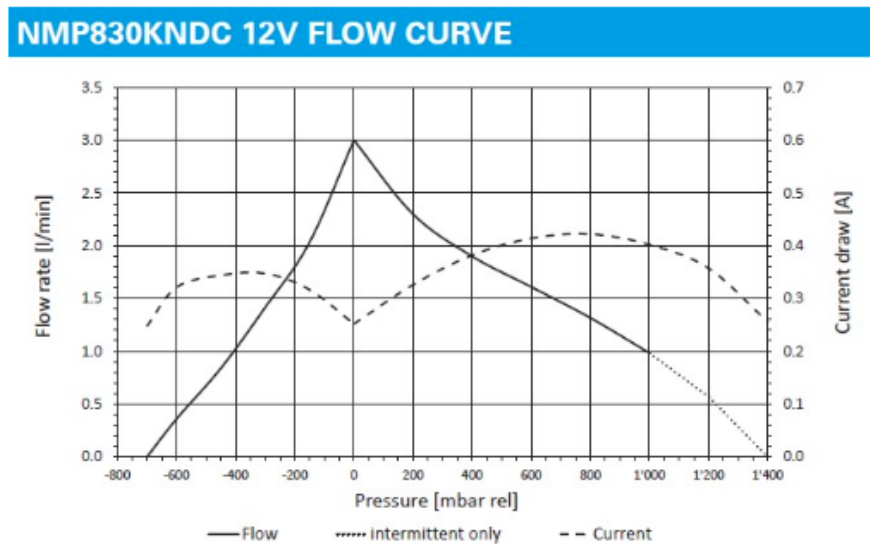
Figure 62 Schematic graphic of flow curve, Flow rate [l/min] of air vs Pressure [mbar]

For the 12V power supply of the compressor, it was chosen to use a particular type of powerbank to facilitate the portableness of the device. In particular, since the usual powerbanks only have the USB output that allows you to have 5V output, the choice fell on the mini UPS shown in Figure 63 It is a modem UPS unit that is designed to be interposed between the home electrical network and the Bluethoot: when power is lost, it powers the modem with a series of batteries that ensure continuity compared to the previous regime. However, if previously charged, it becomes a powerbank that allows you to power mobile devices, including the compressor of this application.

Figure 63 modem UPS unit that is designed to be interposed between the home electrical network and the Bluetooth

5.3.4 Bluetooth and Matlab Application

Finally, although arduino can be controlled at any distance, it was observed that the main usage was carried out in the same setup environment or in any case in the same structure. For these reasons it was decided to opt for Bluetooth technology that, in addition to a simplicity of programming and use, would allow you to free yourself from the particular WiFi network and make the device usable in different laboratories. The module used is named HC-05 and is shown in Figure 64.
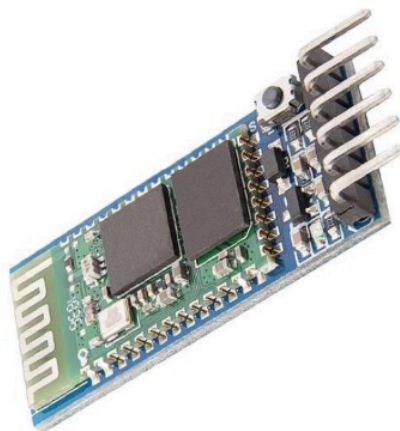
Figure 64 Bluetooth module used HC-05

It allows a flow of information both in and out of Arduino up to a distance of 10 meters. The peculiarity of this board lies in the fact that it communicates with Arduino using a serial protocol and that is easily integrated with the appropriate pins and libraries that the microcontroller is equipped with.The communication implemented through HC-05 is necessary to provide Arduino with a series of signals to change the execution of the program according to the needs of the user, and to do this a numerical coding of the commands has been carried out: for example, the number 0 is associated with the interruption of the peristalism motion while the signal -1 is associated with the request to exclude the first valve from the motion.Later, to relieve the user of knowledge of such coding, a graphical interface was created in matlab environment. This is shown in Figure 65 and allows you to activate and disable the peristaltic motion and set the choice of timing.
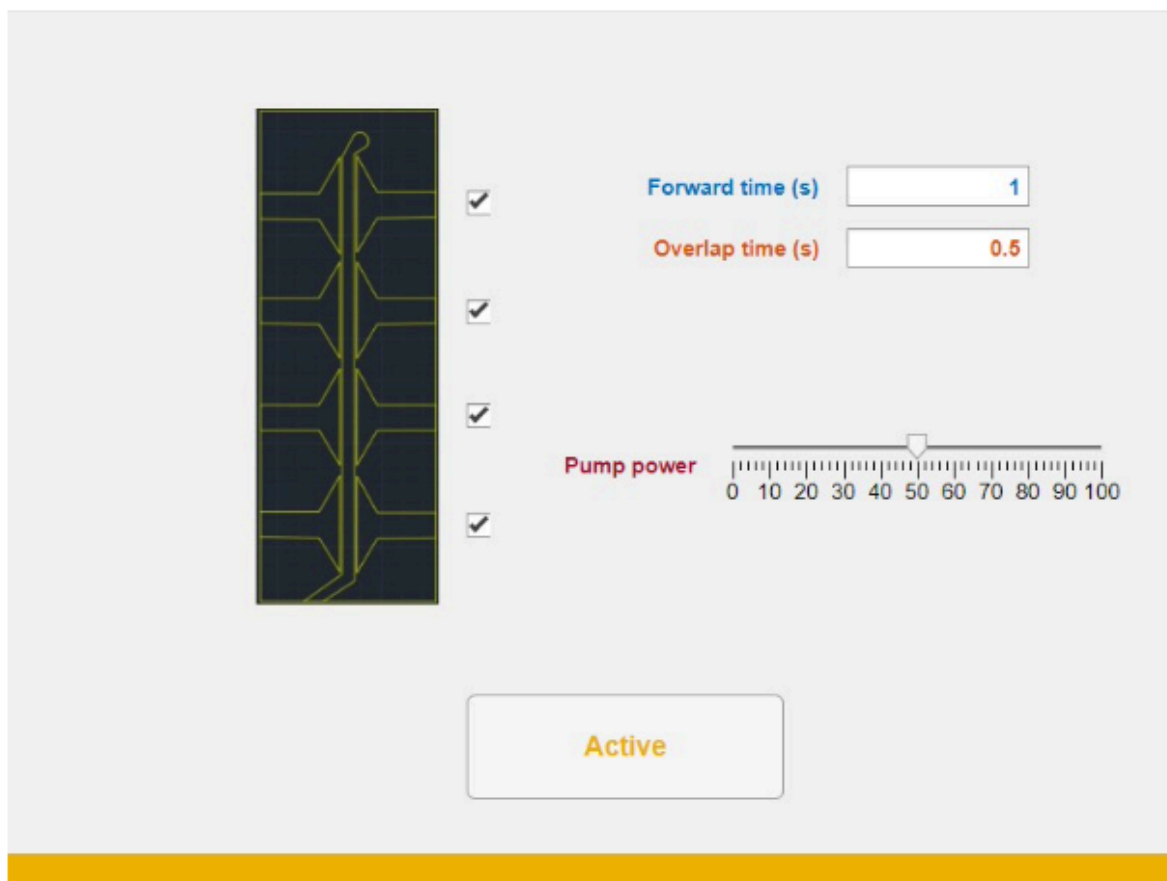
Figure 65 Matlab Application for manage device. Open and close chamber air inflated, forward time and overlap time for air inflaterd, pump power air.

Futhermore to the previously made version, there is a slider that allows you to control the duty cycle of the minicompressor and ultimately the respective power output in order to change the characteristics of the flow. In addition, the possibility of excluding certain valves from the algorithm has been inserted: this choice was motivated by the numerous situations in the experimental phase in which a bedroom, either due to a production defect, or accidental damage, was damaged and lost air.
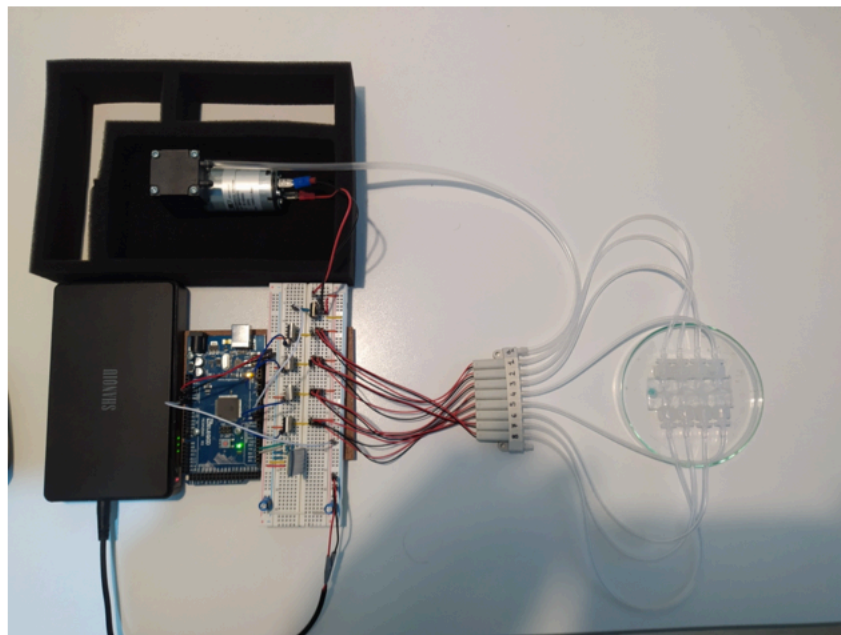
Figure 66 Complete scheme: Minicompressore, power bank, Arduino Uno and connector, electrovalves and tubing inside chamber of Peristalsis on chip.

5.3.5 Reproduction Hoop stress

The tools described above are sufficient to implement the movement of peristalsis in the manner shown. However, the proper functioning of this mechanism implies, by its definition, a net displacement of a certain portion of fluid until it is ejected from the fluid duct (on the left in Figure). The material used to emulate the bolus is a granular gel (produced by Gelesis) and flows quite slowly inside the channel due to friction. Despite this, after part of the gel has been expelled, the channel tends to empty and ceases the motion of the bolus: it is essential, therefore, to supply the channel with additional material.

Figure 67 Syringe pump, Hardvard apparatus.

The solution adopted in this first phase was to use a syringe pump (Figure 67), i.e. a device that behaves like a flow generator: a syringe is arranged on the upper side and a piston compress it in such a way as to determine a certain flow previously inserted by display (to do this it is also necessary to insert the diameter of the syringe).This has solved the problem, although not completely satisfactory: in fact, the net outflow to the channel depends not only on the work of the bedrooms but also partly on the contribution of the syringe pump. To overcome this, in future experiments, it is possible to replace it with an equivalent of a pump, which generates a constant pressure difference on the sides of the channel: this is possible either by placing a column of fluid of a predetermined height or using an air cylinder with a pressure gauge.
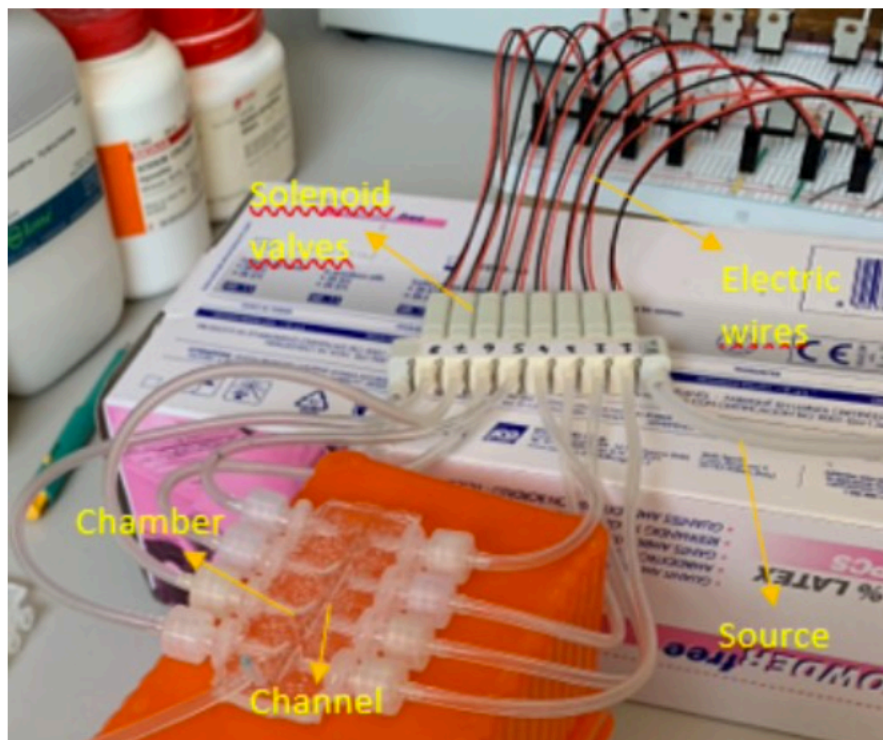
Figure 68. Complete scheme: Arduino Uno and connector, electrovalves and tubing inside chamber of Peristalsis on chip.

After the design phase of the hardware setup, we moved to identify a correct feed rate of the bedrooms to be performed by the microcontroller, in order to realize the peristaltic movement. Figure 69 shows the pattern of the first experimentally tested algorithm over time: in particular, the device strokes highlighted in red correspond to the active (swollen) chambers while the adjacent images refer to consecutive intervals of time, of the same duration. Although it is a simple, intuitive solution that reproduces the spread of a muscle stimulus on the walls of the canal, it has not been adequate for our purposes. In fact, it was noted that the inflation of a single pair of bedrooms could not give such a stress as to advance the bolus clearly; moreover, in the transition phase between two different stages (consecutive frames of Figure 69), the gel uneathed a retrograde motion due to the sudden contraction of the channel.In order to try to solve these problems, a different algorithm has been tested (illustrated with the same notation in Figure 70), by which it was possible to obtain a clear bolus passage: as you can see, in fact, the simultaneous force of all the chambers.
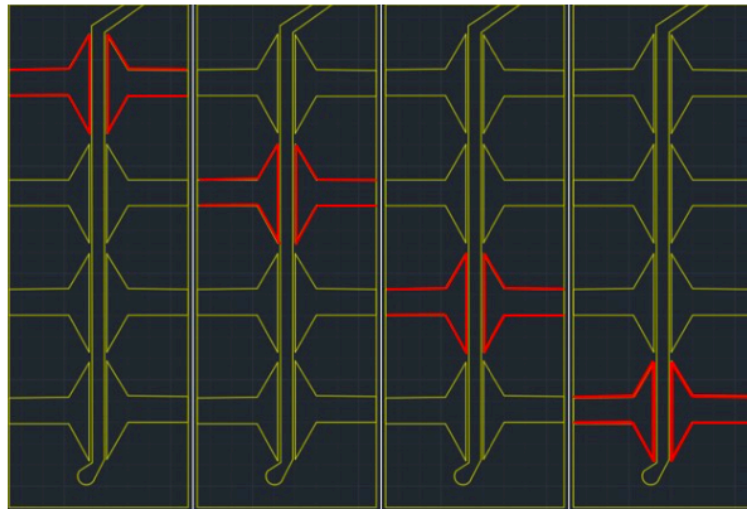
Figure 69. First algoritm utilized for the Peristalsis stimuli to the chamber

Nevertheless, at a time when all the chambers deflated simultaneously (last frame), there was a considerable retraction of the gel inside the channel due to the abrupt geometric variation suffered by the channel. Finally, this movement differed greatly from the sought-after waving movement. It was therefore understood that, in order to hinder the retrograde motion of the bolus, it was necessary to deflate only a few chambers at a time, keeping others active in order to hinder retraction.
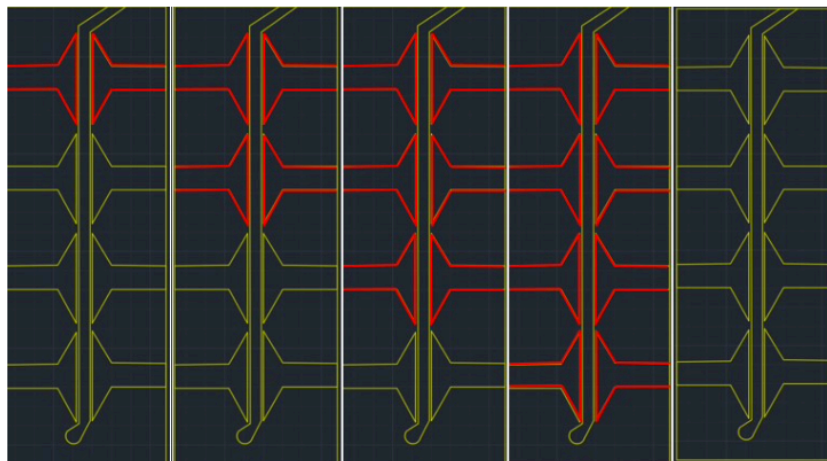
Figure 70. Second algoritm utilized for the Peristalsis stimuli to the chamber
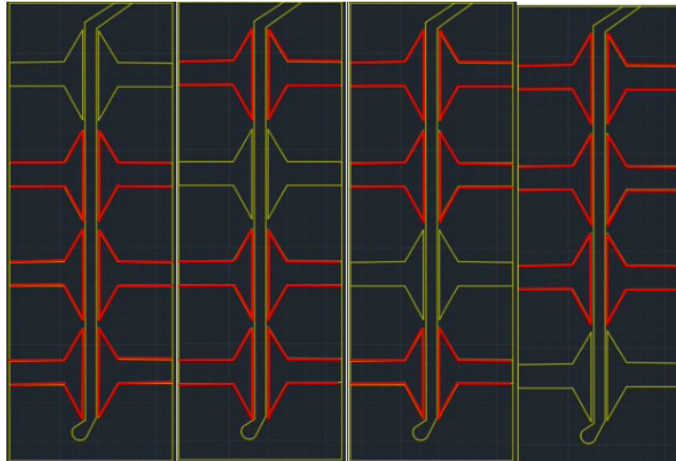
Figure 71. Definitive algoritm utilized for the Peristalsis stimuli to the chamber

We have therefore moved on to experimenting with the algorithm shown in Figure 71: this can be interpreted as the complement to the first algorithm described; the merits of this solution lie in the fact that:

• in order to facilitate the passage of the bolus, when a pair of bedrooms becomes active, the next pair deflates; however, this occurs only after a certain time interval in which, in order to avoid abrupt contemporary variations, both pairs are active.

• the wavy feature of the bike returns

• as in the second algorithm reported, there are multiple active pairs in order to give an adequate stress to advance the bolus

• when a pair of bedrooms deflates there is at least one other consecutive active torque such as to prevent retrograde motion

5.3.6 Arduino programming

Once you have established the algorithm to be used, you have moved on to implement it on the microcontroller. Due to the presence of time specifications within the program and the need to manage multiple communications with peripherals and the WiFi module, it was considered appropriate to use Free RTOS. It is a real-time operating system designed for the embedded world and therefore offers the basic functionality of an RTOS, with reduced memory occupancy. It is equipped with a scheduler that allows multitasking programming and

ensuresthe satisfaction of time constraints by increasing their reliability.With the following primitives, two tasks have been created, one for managing electrovalvancesand one for communication with the module ESP8266-01 which, by launching more frequently, has been set with higher priority (Rate Monotonic algorithm).xTaskCreate(fun_valve, "Electrovals", 100, NULL, 1, NULL);xTaskCreate(fun_comunication , "Communication", 100, NULL, 2, NULL);

5.3.7 Reproduction Shear stress

In order to conduct the sperimental phase of the calculation of τ, we chose as the first bolus-like, gel Gelesis. This gel for its properties has been assimilated to Bingham fluid. A viscous fluid that possesses a yield strength which must be exceeded before the fluid will flow. To reproduce real viscosity of Chyme inside the lumen of small intestine we tested different viscosity of Gels. Gels were prepared by dissolving the hydrogel material with three different granulometries (G1, 400÷250 μm, G2, 600÷400 μm, G3, 600÷850 μm) in DMEM cell culture medium with a high content of glucose (4500 mg/l) at three different final concentrations of 0.5%, 0.7% and 1% w/v. The rheological properties of gels were evaluated by small-amplitude oscillatory shear experiments to measure of the dynamical response of the samples within their linear viscoelastic region. To this aim, the tests were performed by using a rotational rheometer (Anton Paar, MCR 302) equipped with a double couette geometry. The instrument was preheated to 37±0.01°C and maintained at a constant temperature throughout the test. Dynamic strain sweeps were performed at a frequency of 1 Hz with strain amplitude ranging from 10^{-2}% to 10%. Dynamic frequency sweeps were performed at a strain of 10^{-1}% with frequency ranging from 1 to 100 Hz. Flow curves were measured as a function of shear rate ranging from 10^{-2}% to 10^{2}% s^{-1}.

5.4 Mathematical model CFD simulation

It was used two physics, first physic is Free and Porous Media Flow Interface and it is useful for equipment that contain domains where free flow was connected to porous media. The equation used was the Brinkman, that equations extend Darcy's law to describe the dissipation of the kinetic energy by viscous shear, similar to the Navier-Stokes equation. Consequently,

they were well suited to transitions between slow flow in porous media (domain t "Caco-2 like tissue"), governed by Darcy's law, and fast flow in channels described by the Navier-Stokes equations (domain f "fluid"). The second physic was the Transport of Diluted Species interface is applicable for solutions (either fluid or solid) where the transported species have concentrations at least one order of magnitude less than their solvent. And it is chosen chemical species transport through diffusion (Fick's law) and convection. Navier-Stokes equation:

$$\rho(u \cdot \nabla)u = \nabla \cdot [-pI + \mu(\nabla u + (\nabla u)^T)] + F$$

$$\nabla u = 0$$

where ρ is the fluid density, μ is the dynamic viscosity, u is the fluid flow velocity, and p is the hydrostatic pressure, the value as shown in Tab 1 (f refers to the fluid). Brinkman equation:

$$\left(\frac{\mu}{\kappa} + Q\right)u = \nabla \cdot \left(-pI + \left(\frac{1}{\varepsilon}\right)\left(\mu(\nabla u + (\nabla u)^T) - \left(\frac{2\mu}{3} - \kappa_{dv}\right)(\nabla \cdot u)I\right)\right) + F$$

$$\nabla \cdot u = \frac{Q}{\rho}$$

The t refers to the fluid in the tubular-construct, κ^t is the hydraulic permeability, μ^t is the effective viscosity, ε is the porosity of the material, Q is the source term, κ_{dv} is the dynamic permeability and p is the pressure. The oxygen concentration within the system was evaluated by means of the following mass balance equation:

$$\frac{\partial C}{\partial T} = D\nabla^2 C - \nabla(Cu) + R$$

where C is the oxygen concentration, u is the fluid flow velocity field that was set equal to u^f in the domain "f" and u^t in domain "t" in order to match the Multiphysics; D is the diffusion coefficient of the oxygen that was set as a D^t in the domain "t" a D^f in the domain "f" respectively. R is the volumetric oxygen consumption rate expressed by the Michelis-Menten law and according to following:

$$R = \rho \frac{V_{max} \, C}{K_m + C}$$

where the V_{max} is the maximum oxygen consumption rate and K_m is the concentration at which the oxygen consumption rate is half of V_{max}, ρ is the cell density in the bioreactor obtained by taking into account the number of μTP loaded in the bioreactor. R was set to 0 only in the domain "f", since the cells were confined in the domain "t". All the variables used in the simulation are reported in detail in Table 1 [1].

Variable	Description	Value	Source
μ^f	Dynamic viscosity of the culture media (Pa s)	0.001	1
μ^t	Effective viscosity in the fluid (Pa s)	0.0016	1
ε	Porosity of the tissue	0.7	1
κ^t	Effective hydraulic conductivity (m^2)	10^{-11}	1
D^f	Oxygen diffusivity in the culture media $(m^2 s^{-1})$	10^{-9}	1
D^t	Oxygen diffusivity in the tissue $(m^2 s^{-1})$	10^{-10}	1
C_0	Equilibrium oxygen concentration in the culture media (μM)	0.22	1
ρ_{HD}	Cell per μTPs (cell m -3)	0.2 1014	2
V_{max}	Maximum rate of oxygen consumption ($\mu mol\ per\ cell\ per\ s$)	10 -18	2
K_m	Oxygen concentration at $\frac{V_{max}}{2}$ (mol m -3)	10 3	2
κ_{dv}	Dynamic permeability (m2)	0	2
Q	Source term (kg m -3 s -1)	0	2

Table 1: Values of the variables used in the mathematical modelling.

The following are the boundary condition:

$$u^f = \frac{Q_{in}}{A} \; ; C = C_0 \text{ At the inlet}$$

where Q is the flow rate imposed by the peristaltic pump and A is the cross area of pump connections at the inlet and outlet. Fully developed Poiseuille velocity profile was specified at inlet.

$$P^f = 0 \; ; C = C_0 \text{ At the outlet}$$

$$P^f = P^t ; u^f = u^t ; J^f = J^t \text{ At the interface of the f/t domains}$$
where J is the total (convection + diffusion) oxygen flux;

$$u = 0 \; ; J = 0 \text{ At the confining boundaries}$$

The symmetry condition in order to respect the axial symmetry and to gain a computational cost. The simulation was performed using commercially available software COMSOL MULTIPHYSICS, by means of Momentum Transport-Steady State/Navier-Stokes/Brinkman application mode [36]. In order to reproduce also the swalling of chamber, was implemented another CFD Comsol module: Fluid-Structure Interaction. This model exemplifies the solution of fluid-structure interactions problems in COMSOL Multiphysics. Viscous forces and the system's pressure impose forces to the surface of a structure. The deformation of the soft structure is significant and the fluid regime will therefore dynamically change.

Fluid-structure interaction (FSI) is a multiphysics coupling between the laws that describe fluid dynamics and structural mechanics. This phenomenon is characterized by interactions – which can be stable or oscillatory – between a deformable or moving structure and a surrounding or internal fluid flow. When a fluid flow encounters a structure, stresses and strains are exerted on the solid object – forces that can lead to deformations. These deformations can be quite large or very small, depending on the pressure and velocity of the flow and the material properties of the actual structure. If the deformations of the structure are quite small and the variations in time are also relatively slow, the fluid's behavior will not be greatly affected by the deformation, and we can concern ourselves with only the resultant stresses in the solid parts. However, if the variations in time are fast, greater than a few cycles per second, then even small structural deformations will lead to pressure waves in the fluid. These pressure waves lead to the radiation of sound from vibrating structures. Such problems can be treated as an acoustic-structure

interaction, rather than a fluid-structure interaction. Yet, if the deformations of the structure are large, the velocity and pressure fields of the fluid will change as a result, and we need to treat the problem as a bidirectionally coupled multiphysics analysis: The fluid flow and pressure fields affect the structural deformations, and the structural deformations affect the flow and pressure. In design, you may either want to exploit or avoid significant effects of fluid-structure interactions. Devices such as peristaltic pumps, for example, exploit significant structural deformations to gently pump blood without damaging living cells. Such pumps are a combination of flexible tubing and rigid rollers, and the designer must be concerned with the fluid velocities, shear rates in the fluid, and the stresses and deformation in the tubing. (See this paper for an example of a peristaltic pump FSI analysis: "Fluid-Structure Interaction Analysis of a Peristaltic Pump".) Industrial mixers, on the other hand, have moving parts, but the stirrers can be considered essentially rigid parts that agitate a fluid. When analyzing such systems, the mixing efficiency is the most important quantity to compute. It is possible to compute the stresses in the stirrers, if the designer is concerned with that. The solid structures can even be treated as entirely stationary obstructions in the fluid flow, with an objective of computing the stresses in the solid materials. When modeling such systems, there are a variety of appropriate modeling approaches available. You may need to model both the Navier-Stokes equations for fluid flow as well as the solid mechanics equations for the deformation of a solid body. The Navier-Stokes equations can be solved in various forms for different flow regimes. It may even be possible to simplify the modeling of the flow as a thin film to model lubricating films. The structures can be treated either as rigid, experiencing small deflections that are negligible to the fluid flow problem, or as having large deflections that significantly affect the fluid flow.

5.5 Rheological Model

Our study is designed to obtain the better estimation of the shear stresses that the gel exerts on cell sheet when it passes into the device, through high-resolution measurements of local fluid velocities.

To this end, we decide to use the well-known Bingham rheological model that describes the flow curve of a material with a yield stress τ_0 (the force at which the fluid must be exposed to in order to start flowing) and a constant viscosity at stresses above the yield stress. The yield stress (τ_0) is the shear stress (τ) at zero shear rate (γ) and the viscosity (η) is the slope of the curve at stresses above the yield stress:

$$\tau = \tau_0 + \eta\gamma$$

Naturally, to evaluate the shear stresses exerted by the gels on cells we can use the viscosity extrapolated from flow curves at certain values of shear rates. To determine the wall shear rate at which the gel is sheared during the flow inside the device, we performed microparticle tracking velocimetry (μ-PTV) experiments. Fluoresbrite YG polystyrene microspheres (4.5 μm diameter; Polysciences, Warrington, PA) are suspendend in DMEM cell culture medium at a final concentration of 0.002% and sonicated for 10 min. Then gel was prepared by mixing hydrogel material with the granulometry G1 at a final concentration of 0.5% w/v. The gel will be allowed to pass inside the device and video of microparticles will be recorded using a digital camera (Hamamatsu, ORCA-Flash 2.8) attached to a PC and Cam control video capture software mounted on an inverted fluorescence microscope (Olympus IX81) equipped with a fluorescent mercury lamp (Olympus U-LH100L-3) for a total of 5 min at 10 fps.

The microparticle trajectories was generated by using a custom built Matlab code and velocities will be calculated by dividing the total displacement by the total duration of the video. The shear rates were calculated in the proximity of the wall by dividing the velocity by the perpendicular distance of the microparticles from the wall.

5.6 Staining and histological analysis

5.6.1 Cell staining

To compare the epithelial differentiation on different porous membrane in the In-Crypts device and in the Conventional PDMS device, the samples were fixed and stained. Briefly, the culture medium was removed and PBS was perfused through upper and lower channel of the both devices. To allow histological analysis, the samples were fixed by flowing Paraformaldehyde (PAF) solution 4% for 20 minutes. The micro-channels were washed 2-3 times by flowing 0.2% Triton in PBS solution for 15 minutes to increase cell permeability and allow dye penetration. The samples were rinsed with PBS and, then, a Phalloidin-PBS solution (1:200) was added and incubated for 40 minutes. After rewash, DRAQ5-PBS solution (1:1000) was inserted and incubated for 15 minutes. During staining procedures, the entire device was covered with aluminium foil to preserve fluorescence. The In-Crypts device and conventional PDMS device were analyzed with Leica SP5 II laser scanning confocal microscope.

5.6.2 Histological, immunofluorescence and immunohistochemical analysis

At 8th day, Caco-2 monolayer samples were fixed with 4% paraformaldehyde for 20 min and then rinsed in PBS. For the histological examination, were collected and fixed in 10% neutral buffered formalin solution overnight, dehydrated in a graded ethanol series, washed with xylene and embedded in paraffin blocks. Serial sections were stained with Hematoxylin and eosin (H/E) (Bio Optica), and Alcian Blue (Merk Millipore) staining using standard procedures. All specimens were analyzed by an optical microscope (BX53; Olympus) with a digital camera (Olympus DP 21). For immunofluorescent procedure, unstained sections from the above-mentioned paraffin blocks were deparaffinized in xylene, treated with an incremental ethanol [100, 95 and 80% ethanol/double-distilled H_2O (v/v)], and rehydrated in PBS. Antigens were unmasked by heat antigen retrieval with citrate buffer, pH 6.0 for 20 min. Slides were then blocked with 5% bovine serum albumin (BSA; Sigma) and incubated with primary antibodies to Villin (1:100; Abcam), Muc-2 (1:100; Abcam), CGA (1:100; Abcam), ZO-1 (1:50; Abcam), Alpha-Smooth Muscle Actin (aSMA) (1:100; Abcam), ki67 (1:100; Abcam) and LGR-5 (1:100; Sigma), TNF-a (1:100, Abcam), IL-6 (1:100, Abcam), IL-1b (1:100, Abcam), IL-8 (1:50, Abcam) overnight at 4 C. After washing extensively, all slides were incubated with a 1:500 dilution of appropriate fluorescent secondary antibody (Alexa fluor) at RT for 1 h. Slides were rinsed, and counterstained with 40 ,6-diamidino-2-phe nylindole (DAPI) (Sigma Aldrich) at dilution ratio (1:10000 in PBS) for 10 min. Sections incubated with dilution buffer without primary antibody were used as a negative control. Confocal images were captured using a confocal laser scanning microscopy (CLSM) (TCS SP5 II femtosecond laser scanning system, Leica). The excitation/emission wavelengths were set as follows: kex = 500 nm, kem = 510–530 nm (single photon mode, for MUC-2, ZO-1, Ki67, LGR-5, IL-6, IL-8); kex = 580 nm, kem = 612–623 nm (single photon mode, for Villin, CGA, TNF-a, IL-1b); kex = 720 nm, kem = 460 ± 10 nm (two photon mode, for DAPI). The fluorescence quantifications were obtained by dividing the green/red pixels number by the cells number. The number of pixels and the number of cells were obtained by using ImageJ software. The analysis was performed in three independent experiments. For immunohistochemistry, section were dewaxed with xylene and rehydrated in PBS. Endogenous peroxide was blocked with 3% H_2O_2 for 10 min. After blocking non-specific reactions with 5% bovine normal serum (Sigma) in Tris Buffered Saline solution (TBS), sections were incubated with primary antibody against cytokeratin 19 (CK19)

(1:100, Abcam) and Lysozyme (1:100; Sigma) at RT for 1 h. Secondary antibody conjugated with biotin, streptavidin-peroxidase and DAB used for immunostaining was from Mouse and Rabbit Specific HRP/DAB (ABC) Detection IHC kit (Abcam).

5.6.3 Ultrastructural characterization Scanning Electron Microscopy

SEM analysis, the Devices was fixed with 2.5% (v/v) glutaraldehyde in cacodylate buffer. Samples were washed twice in 100 mM cacodylate buffer, pH 7.2, for 10 min at room temperature. A second fixation in 1% (w/v) osmium tetroxide, buffered in 100mM cacodylate, pH 7.2, was done overnight at 4°C. Dehydration was carried out by gradually decreasing the water concentration and increasing the ethanol concentration (10%, 30%, 50%, 70%, 90%, 100%, and 100% again, each step 30 min at room temperature). Samples were then treated with liquid carbon dioxide using a Critical Point Dryer (Emitech K850). Dried samples were mounted onto metal stubs using double-sided adhesive tape and then gold-coated using a sputter coater at 15 mA for 20min. Coated samples were then examined by scanning electron microscopy (SEM) (Leica S400).

5.7 Qualitative analysis of selective permeation properties

The permeability evaluation of CaCo-2 cultured on Transwell permeable supports (24-well plates with polyester membrane 0.4 μm, Corning® Costar) was performed by measuring the trans-epithelial passage of the 3kDa FITC-Dextran solution (1 mg/ml diluted 1:100 in HBSS) (TRITC-Dextran, Molecular probes, Life Technologies). Cells monolayers were incubated for 24 h at 37°C with 5 % CO2. 500 μL 3kDa FITC-Dextran solution were loaded on the apical side and 500 ml of HBSS/DMEM (1:1 V/V) were placed in the basolateral chamber in order to guarantee the wetting of the lower side of the membrane. The passage was analysed by confocal imaging (Leica SP5 II Laser Scanning Confocal Microscope) and the fluorescence emission (λ_{ex}=555 nm).

6. Peristalsis on a chip and evaluation of healthy tau: Results and Discussion

6.1 Peristalsis device fabrication

In this work, a microfluidic device was designed and fabricated in order to replicate the dynamic intestinal microenvironment, support perfusion-based cell culture and enable analysis of intestinal epithelial barrier functions *in vitro*. A schematic representation of the assembled microfluidic device is reported in figure 72.
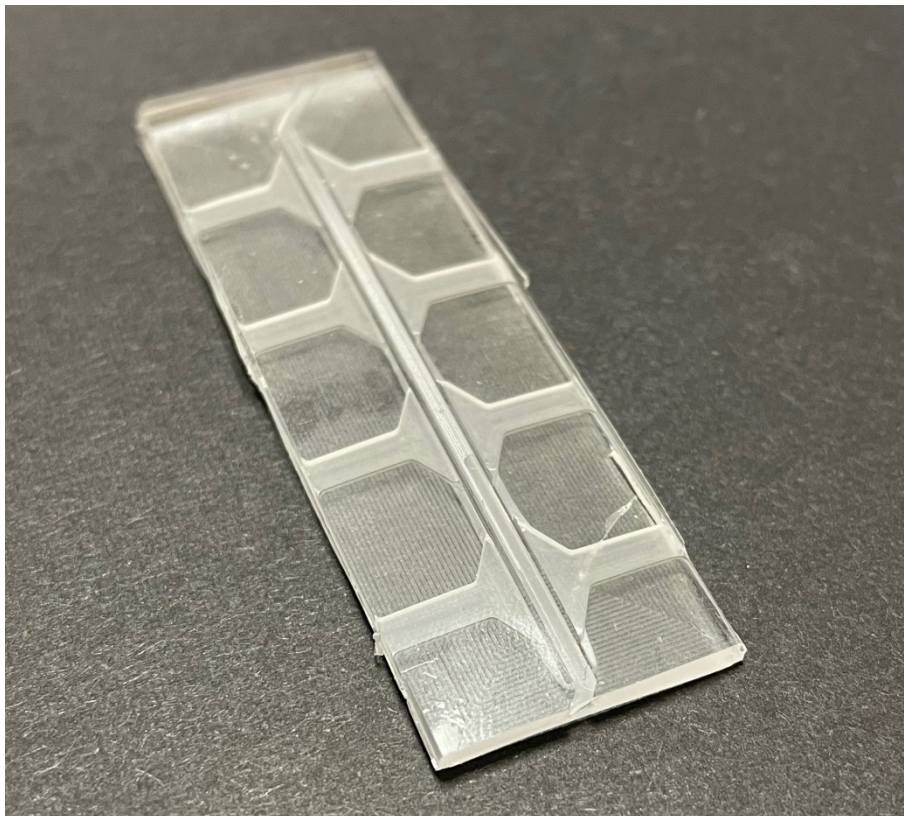
Figure 72. Schematic representation of the assembled Peristalsis on chip.

To achieve these goals, the peristalsis was developed overlayingtwo layers of the single channel PDMS and separating the two corresponding channels by athin porous PDMS (80 μm pore size custom-made PDMS membrane, 150 μm thickness). The figure 72 shows both schematic representations of the Peristalsis on a chip.

Figure 73. Schematic representation of 'Peristalsis on a chip' with integrated PDMS membrane.

Preliminary studies were performed in order to integrated the PDMS "custome made" membranes that reach half of the branches on the apical and the correspondent basal microchannels to prevent the membrane breaking as well as to avoid the medium mixing after the cell seeding (Figure 73). To provide peristaltic movement, hollow chambers were integrated next to the top channels in the upper PDMS layer (Figure72-73).

The selection of this synthetic polymer as substrate material for the peristalsis allowed to obtain a desired degree of mechanical rigidity or flexibility, ensuring expansion and contraction of the chambers. In addition to its ability to be functionalized with chemical moieties for modulation of cell – surface interactions and its high oxygen permeability that allows sufficient oxygen supply to the cells in the microchannels, the PDMS made possible the realization of a device optically accessible for cell imaging [31].
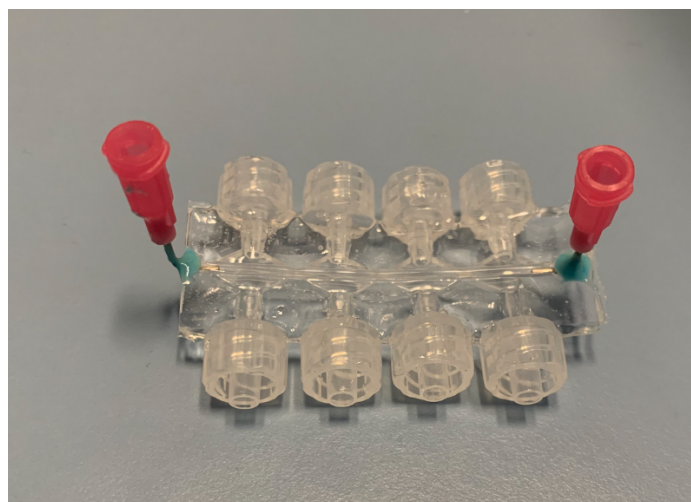
Figure 74. A photographic image of Peristalsis on a chip with inlet and outlet tubing.

The upper and the lower microchannels of the Peristalsis on a chip reproduce the lumen and the capillary side of the small intestine, respectively. The porous PDMS membranes were coated with Fibronectin to ensure the optimal Caco-2 cell adhesion and spreading. Once full confluence was reached into the Peristalsis a barrier between the intestinal lumen and the blood was established reproducing the protective barrier towards harmful agents of the digestive tract and regulating the uptake of nutrients from ingested food [32].

6.2 Peristalsis-like mechanical stimuli

The Peristalsis was designed to reproduce the intestinal dynamic microenvironment *in vitro*, which comprises the flow fluid shear stresses as well as the substrate deformations. The latter, in particular, have been made by using pneumatic. Eight solenoid valves and a computer-controlled system are responsible for the activation of the 8 lateral chambers.
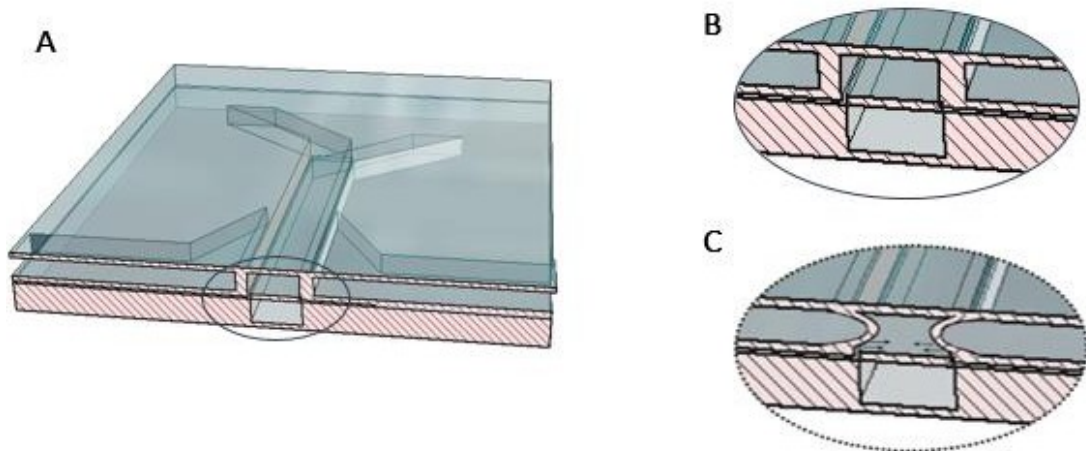
Figure 75. (A) A schematic cross-sectional representation of the Peristalsis on chip device in correspondence of the side, hollow chambers. Zoom on the middle channel when lateral chambers are inflated (B) and deflated (C).

According to the work of the valves, the symmetrical andcoordinated expansion (75 c) and contraction (Figure 75 b) of the side chambers leads to a rhythmic approach of the upper sidewalls at that specific point of the channel. Thismotion, clearly illustrated in figure 75, induces local stress on the Caco-2 cell monolayer that simulate the circumferential (Hoop) stress experiences by intestinal epithelium.

Other researchers introduced full-height hollow chambers in microfluidic devices mimicking the epithelial stretching by applying vacuum. This mechanism, originally designed for the Lung-on-Chip, has been reported to be helpful to simulate breathing motions. Therefore, this stretching is not appropriate for simulating the complete peristalsisof the small intestine [28]. Our Peristalsis on chip, instead, proposed the reproduction of a more physiological peristalsis-like motion:

- when the state of the valves is on, side chambers expand and the lateral walls of the channel deform inducing a contraction of the membrane and therefore of the epithelium;
- when the state of the valves is off, side chambers deflate and the walls of the channel come back to the initial position, resulting in a relaxation of the epithelium.

6.3 Peristalsis on a chip CFD Comsol Multiphysic

To assess the optimal flow rate, we developed a COMSOL Multiphysics simulation. We selected the range of flow rates that ensured both cell attachment, vitality and growth.

Figure 3.8 shows the velocity values along the entire channel for the set flow rate when one single lateral chambers are deflated (on the left) and inflated (on the right). In both cases, the viscosity of the upper fluid domain was set to 10^{-2} Pa s, that is the zero-shear viscosity valueof the bolo in vivo (taken from literature, [39]). As expected, the velocity at the chamber increased up to $\sim 2.34 \times 10^{-5}$ m/s when the wall deformed.

Moreover, the values of the shear stress exerted on the Caco-2 cell layer in lumen side (Figure 3.9, right) increased up to $\sim 8 \times 10^{-3}$ dyne cm^{-2} with respect to the simple geometry $\sim 4 \times 10^{-3}$ dyne cm^{-2} (Figure 3.9, left), while they remains unchanged in the blood side.
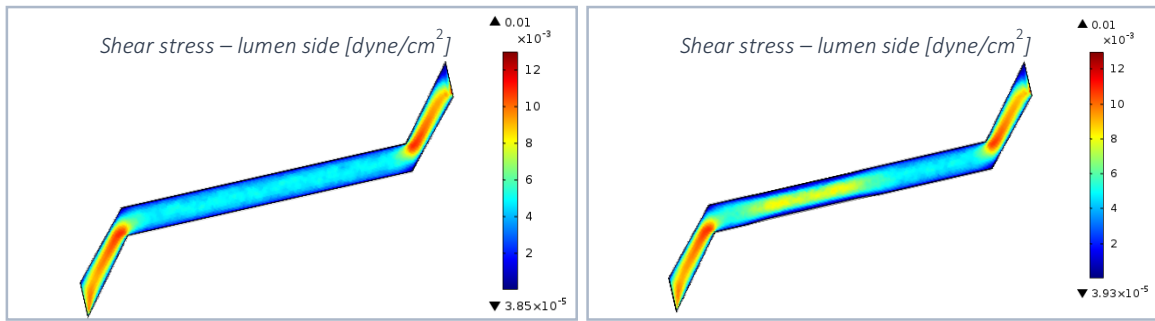
Figure 76. CFD simulation results – Shear stress exerted on the tissue in the lumen side when chambers are deflated (left) and inflated (right).

In conclusion, the deformation of channel sidewalls at chambers during their expansion contributed to increase stimulation of Caco-2 differentiation, avoiding disruption of Caco-2 layer itself.
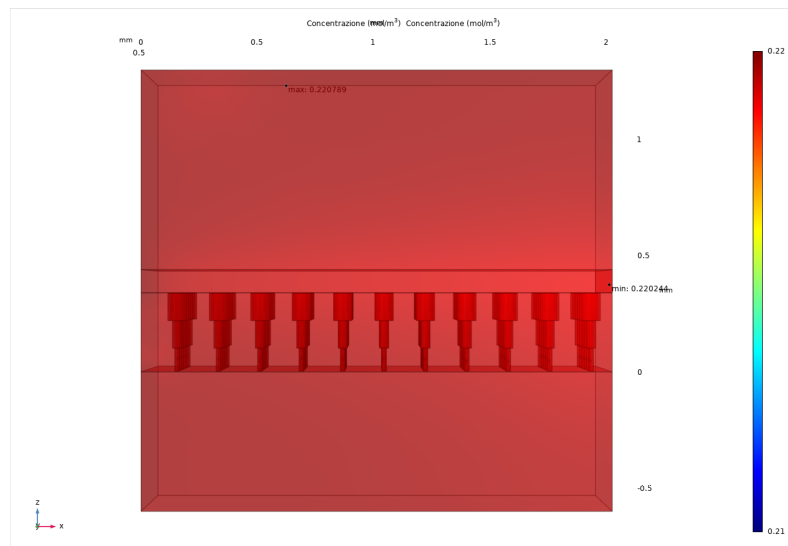
Figure 77. CFD simulation results – Oxygen amount exerted in microchannels of Peristalsis on a chip.

In addition, the presence of large pores improved the cell viability, thanks to a great exchange of oxygen and nutrients (including growth factors) from both apical and basolateral side. Furthermore, during experimental phases, it was observed that Caco-2 cells attached and differentiated much faster to the static In-Crypts device (section 3). We can also noticed, that in Dynamic condition, Peristalsis on chip, show a greater amount of oxygen instead.
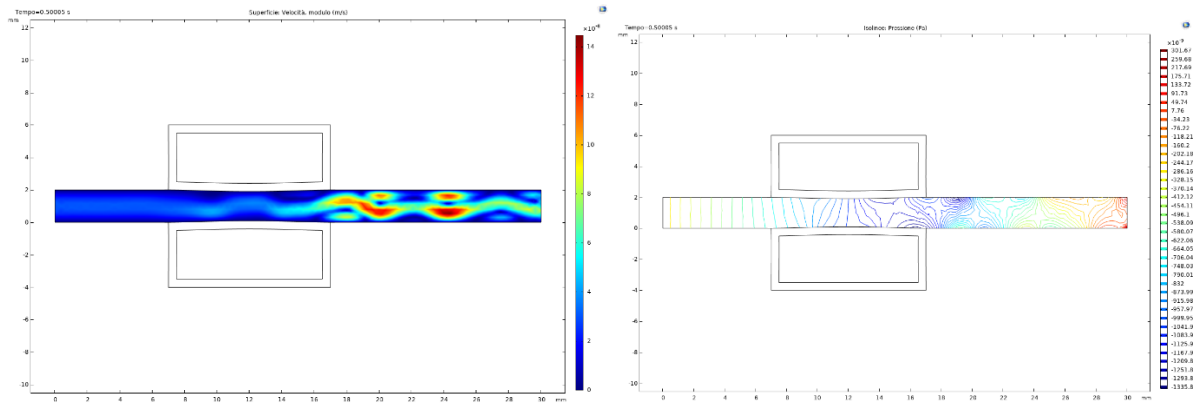
Figure 78. CFD simulation results – Velocity and pressure field in microchannels of Peristalsis on a chip during peristalsis stimuli-like.
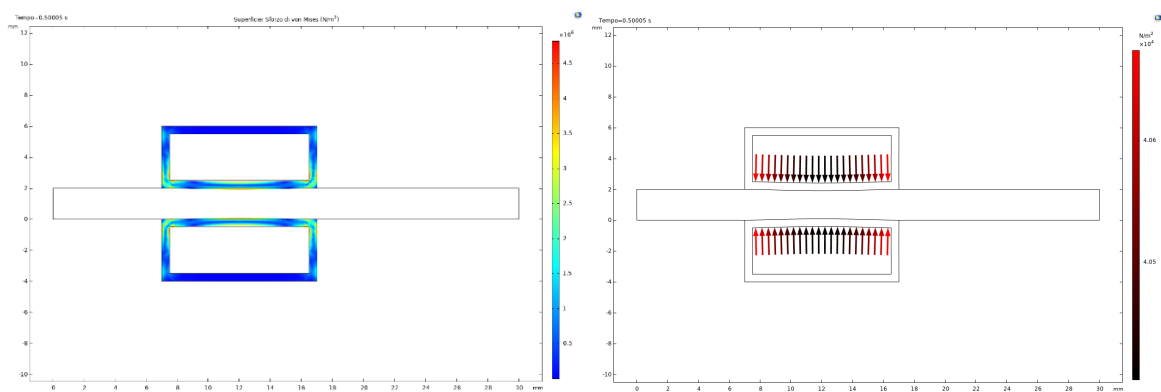
Figure 78. CFD simulation results – Strain on chamber in Peristalsis on a chip during peristalsis stimuli-like.

So, we already obtained, by the simulation, first result of better culture condition, in terms of amount of oxygen and nutrient, for viability and vitality of cells, and in terms of shear stress that reduced the time of confluence and differentiation, so reduced the global culture time.

6.4 Reproduction of intestinal epithelial

To reproduce a well differentiated and polarized intestine epithelial layer, we seeded intestinal epithelial Caco2 cells on central channel of the microfluidic device. Prior to the cell seeding, porous PDMS "custome made" membrane was coated with fibronectin to enhance the cell adhesion. Preliminary experiments were carried out to optimize the percentage of cells to seed on the porous membranes to achieve the best cell confluence into the channel (data not shown).

10

Once the percentage of the cell to seed into the channel was optimized (5 x 10^5 cell/0.5 ml), preliminary tests were carried out on a differentiated epithelium that cover the entire channel with high density of domes that indicates the epithelial polarization as reported in Figure 10. Then, the polarized epithelium was exposed to dynamic flow on the apical side by flowing the culture medium and/or Gelesis at a microgranulation selected. In particular, we choose the viscosity of Gel that resemble the real viscosity of bolus on the lumen of small intestine,that is very similar to water like viscosity, granulometry of Gelesis < 0.100 da controllare [10].

Figure 79. A photographic image of Peristalsis on a chip with testing of Gelesis (Central) or Medium (on right).

Preliminary results already indicated that the mechanical consistency of chyme has a profound effect on cell shape and behavior [10]. Remarkable differences in cell shape, differentiation and polarization was reported when the epithelial layer was flushed with the medium alone or with gelesis. In particular, after the Gelesis flown the Caco2 cells exhibited better differentiation that resulted in a greater amount of Domes. In particular, the Domes produced after the Gelesis flown were in larger numbers and with greated height compared to samples flowed with culture medium. These results were obtained after the visualization of 3D recontruction of nuclear and citoskeleton staining slice observed under confocal microscope. Figure 80-81
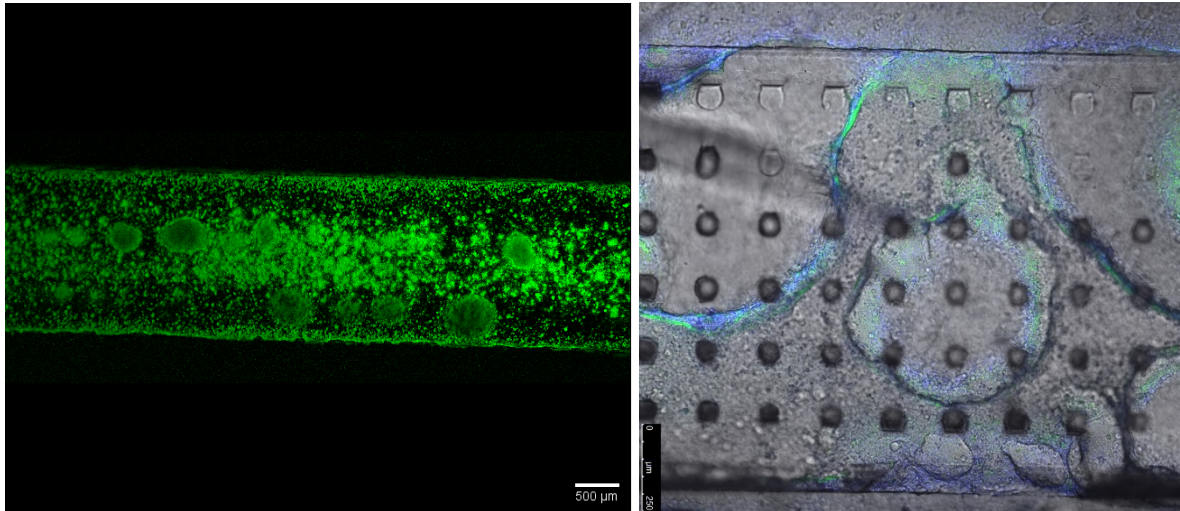
Figure 80. Confocal acquired images of Caco-2 intestinal epithelium in the Peristalsis on chip.. In green tight junction, in blue nuclei. On right focus on Nuclei.
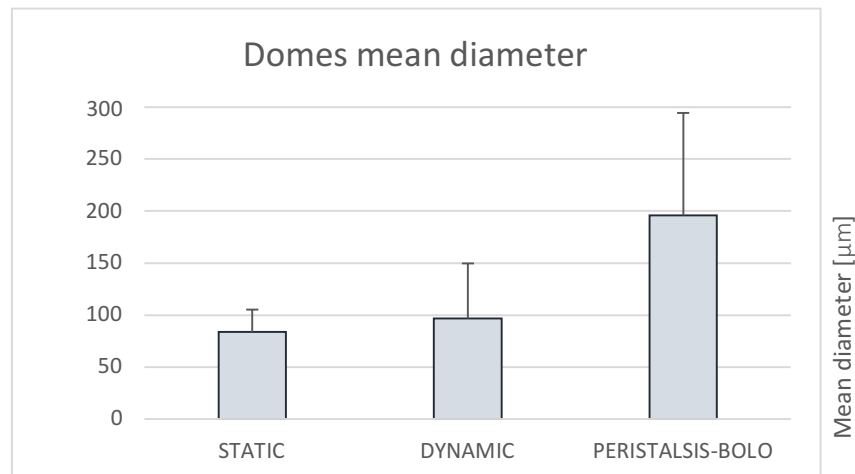
Figure 81. Graph on Domes mean diameter in the three critical condition analyzed. Static, 8 days of dynamic culture, 8 days of dynamic culture plus 2 hours of peristalsis.

After the dynamic cell seeding, in 8 days we obtained a complete confluence and differentiated intestinal epithelium. Different from the othe researcher [40] we obtained a complete confluence after only 3 days of dynamic culture (2ul/min). Furthermore, a deeper morphological characterization of the epithelial differentiation was performed by histological and ultrastructural SEM analysis. First, the trasversal section of the H&E stained sample shows the epithelial polarization of Caco2 adhese on porous membrane after culture (Figure 82 left). SEM micrograph indicates the microvilli structures that coverthe free surface of the epithelial cells (Figure 82 right).
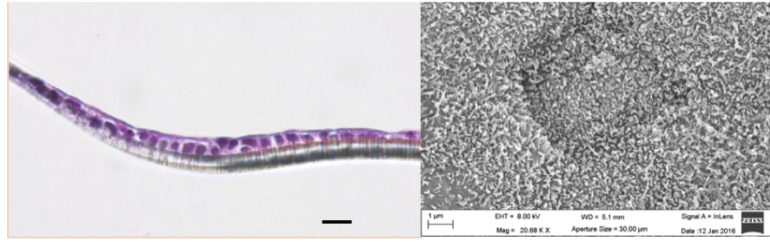
Figure 82. Histological and ultrastructural SEM analysis on Caco2 Epithelial layer in Peristalsis on a chip after 8 days of dynamic culture.

Once defined the operative conditions, we evaluated the effect of shear stress at the chyme-epithelial layer interface on the intestine function and properties. In the following activities we reported on the first combined data the possible correlation between mechanical consistency of chyme (simulated by gelesis gel) and Caco2 epithelial morphology and function with particular interest on damage and repair (TEER, histology and mucus amount).

6.5 Gel (Bolus-like) Rheological properties

From a dynamic point of view, all the tested gels present flat dynamic elastic (G') and viscous (G'') moduli curve until 1% strain and 1 Hz. As expected, dynamic moduli increase by increasing both concentration and granulometry of hydrogel material.
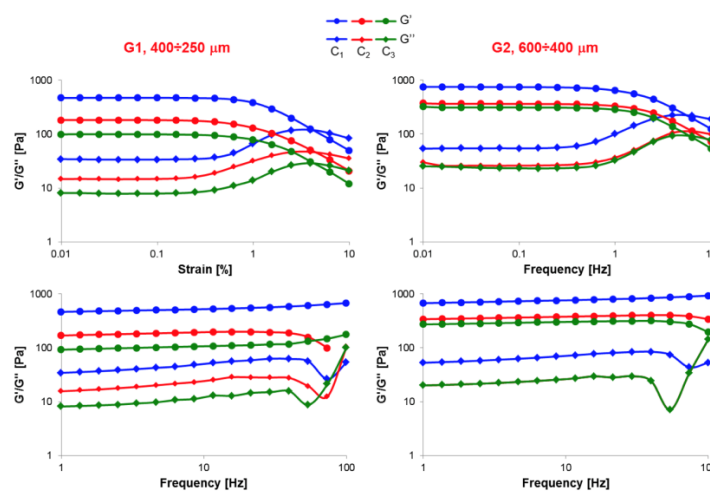
Figure 83. Gel rheological Proprierties

In accordance with rheological moduli, flow curves show that viscosity increases as concentration and granulometry increase. All gels exhibit an extrensional strain-rate thinning viscosity behavior typical of complex fluids.

6.6 Effect of peristalsis on epithelium differentiation

Once established that the porous PDMS membrane together with continuous perfusion of DMEM had enhanced the differentiation of the Caco-2 cells, other features of the PDMS membrane were evaluated which improve the complexity of the Peristalsis on chip due to the high compliance/elasticity (with an elastic modulus of 1-3 Mpa [36]) of the PDMS and its capability to be irreversibly bonded to other PDMS layers, was a suitable tool to mimic peristalsis movement and induce mechanical stimuli.

In this perspective, the solenoid valves, which inject the air into the chambers and the additional syringe pump, which make the bolo-like gel flow were integrated into the Peristalsis on chip and were activated for two hours.
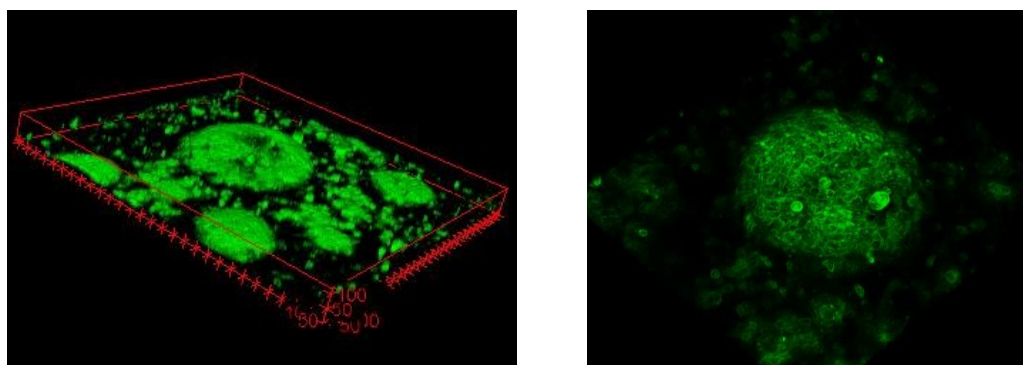
Figure 84. 3D view reconstructed through ImageJ Software – (A) Caco-2 intestinal epithelium developed in Peristalsis on chip under dynamic conditions and after 2 hours of peristalsis-like motion and Gelesis passage.

All Caco-2 epithelia developed on Peristalsis on chip device were fixed, stained and analyzed to study the effects of peristalsis after the bolus-like administration. The results obtained after the peristaltic-like movement were encouraging. Firstly, the average of the domes diameter was almost doubled, as histogram in figure 84 shows. Secondly, the height of the domes, calculated from Z stack images by plotting Orthogonal views, showed a height of about 200μm compared to the dynamic conditions without peristalsis 110 μm. Although the height of the domes was lower than the physiological one, it was hypothesized that an extension of the culture time in the presence of peristalsis or the type of the administered gel could increase it. Furthermore, a great domes dimension was reported in the 3D

reconstruction of the domes in dynamic with peristaltic conditions and bolus-like administration showing an increased surface area (figure 85). The dynamic and complex environment reproduced into the Peristalsis on chip could enhance the physiological efficiency of absorption by the intestinal epithelium mimicking the *in vivo* situation.
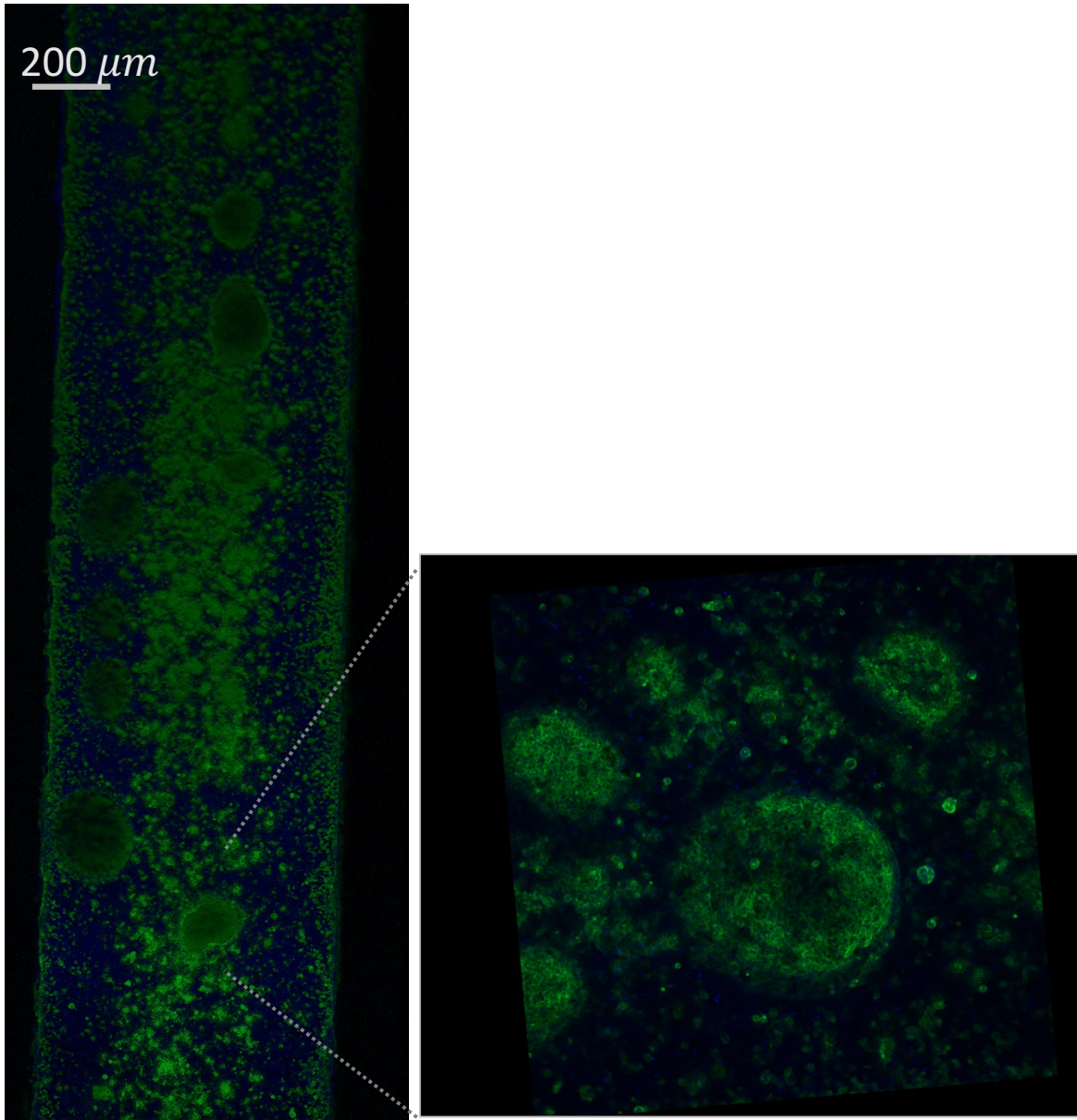
Figure 85. 3D view reconstructed Confocal analysis – (A) Caco-2 intestinal epithelium developed in Peristalsis on chip under dynamic conditions and after 2 hours of peristalsis-like motion and Gelesis passage. Focus on highness of Villi.

6.6.1 Quantitative immunofluorescence analyses

Quantitative characterization in terms of the number of domes, domes diameters and domes height in dynamic conditions was achieved. The data indicated that the presence of gelesis on the luminal side of the Intestine on chip model improved the epithelial polarization with an increase of the number, diameter as well as height of domes structures (Graphic figure 86). As it well known, the human intestinal epithelium in vivo is characterized by macro-villi with a diameter of 85-200 μm and a surface 2 density of 20-40 macro-villi/mm2. According to the in vivo situation, the Caco-2 cells grown in the Peristalsis on chip developed an epithelium with the morphology closest to the intestinal macro-villi. In particular, the 40% of domes, as reported in the histogram in figure, showed the physiological diameter and villi density.
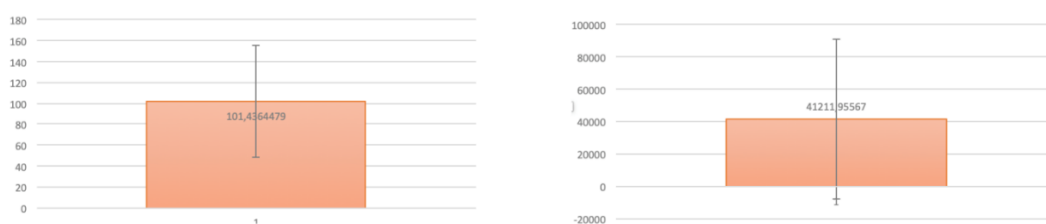
Figure 86. Graphic (on Left) Medium value of Radius Domes and standard deviation. Graphic (on right) Medium value of Area Domes and standard deviation.

6.7 Transepithelilal electrical resistance on Peristalsis on a chip

To monitor Caco-2 cell growth and evaluate cell-cell tight junction integrity, TEER measurements were performed directly into The Peristalsis on a chip. The integration of electrodes within the microfluidic device advantageously reduced signal noise generated by any electrode motion and, above all, allowed continuous non-invasive monitoring of the cells within an incubator without affecting the cell culture environment.

TEER values were acquired after one day from cell seeding and repeated at 0 th 3th 5th 6th and 8th days.

As described before, TEER values were extrapolated from the fitting of the experimental data derived from the measurements with curves obtained from the equivalent model circuit. The results were plotted over time in figure 87.
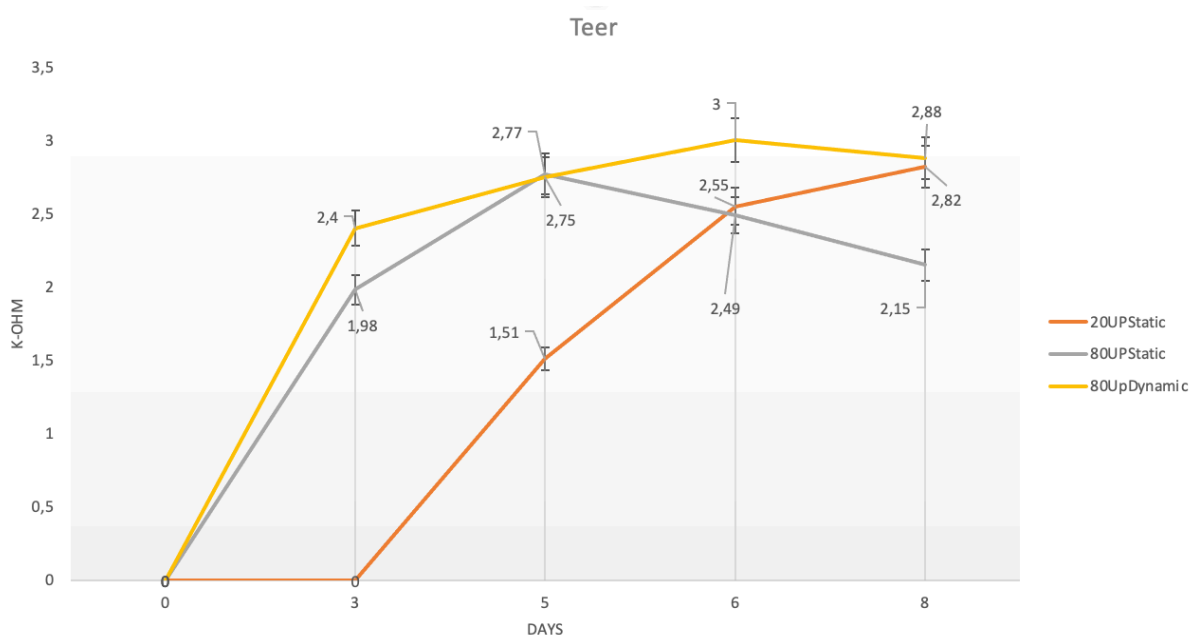
Figure 87. Evaluation of tight junction integrity and differentiation of Caco-2 monolayer cultured in the Peristalsis on chip quantified by measuring TEER.

The TEER value significantly increased with time, displaying a peak on day 6 when the cells reached confluence indicating TJ formation. This point also indicates the beginning of cell differentiation. Caco-2 cells cultured in the Peristalsis on a chip not only differentiated in terms of enterocytes, but also began to produce mucus. Mucin cells intercalated between enterocytesand resulted in a decrease in the TEER value making it closer to the physiological values ofthe small intestine (50-100) [37].

These results confirmed the growth and differentiation of the epithelium as well as its correct and expected barrier functions after eight days of culture in the Peristalsi on a chip under dynamic conditions.

TEER values reached by the Caco-2 epithelium developed in the Peristalsis on chip were higher than values of native tissue: this was expected because of the lack of the stroma in the realized model [38].

6.7.1 Comparison with literature: TEER and absorption

It was very useful to make a comparison between the results obtained in terms of TEER and absorption of molecules through the epithelium grown in the Peristalsis on chip and the literature data. In particular, the realized model was compared with the Ingber et al. model. First, it is important to underline that, although the measurement of TEER and of transepithelial passage of marker molecules determine different experimental parameters, they are both indicators of the integrity of the tight junctions and index of cellular differentiation.
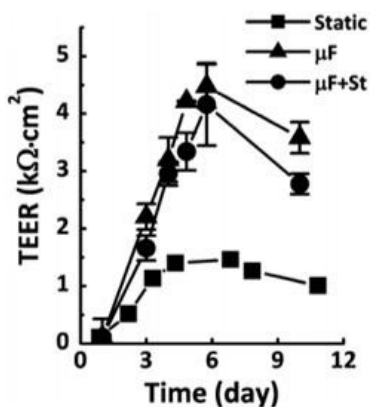
Figure 88. Evaluation of tight junction integrity and differentiation of Caco-2 monolayer cultured in the transwell (Static) or the Ingber Gut-on-Chip in the absence (μF) or presence (μF + St) of cyclic strain – TEER values.

As reported in figure 87, the trend of the TEER values over time is very similar to the Ingber et al. model [20]: it increased over time reaching a peak when the TJs were formed. However, the peak was reached two days earlier, indicating that the differentiation process begun earlier. In addition, all TEER values were lower than the Ingber model ones and this represented an advantage because they were closer to the physiological values of the small intestine. The variation of the TEER value and its slight decrease after the peak demonstrated the cell differentiation (not only in enterocytes, but also mucin cells) and, therefore, the development of an epithelium characterized by villi-like structures. The increase in the surface area was of great importance in the study of the absorption of molecules and compounds.

Ingber et al. measured the amount of dextran particles that cross the epithelium in the unit of time and evinced an increase of steady state flux when peristalsis-like motions were

introduced. They assumed that this was due to some mechanisms such as active transport, ion channels or transcytosis that probably could be activated during peristalsis. Although it was not possible to experimentally determine the steady-state flux of dextran and caffeine in our Peristalsis on chip, it was possible to hypothesize its behaviour.
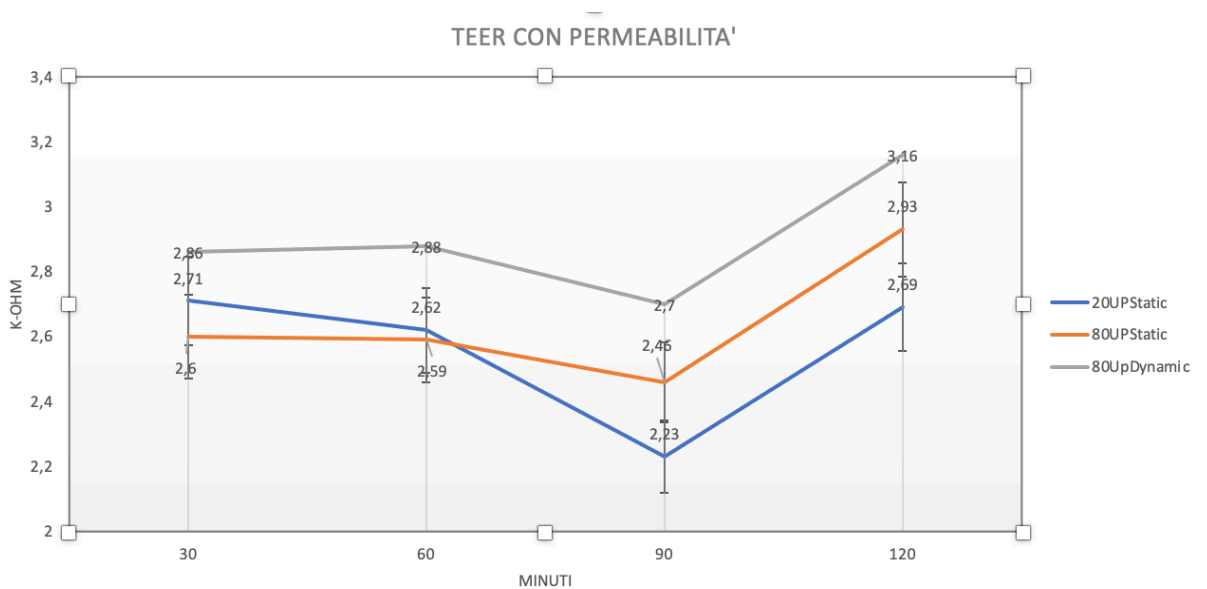
Figure 89. TEER graphic during Permeability test of 2 h on Peristalsis ona chip device. TEER measurement on 30-60-90-120 minutes.

The steady-state flux trend was expected to be similar to that reported by Ingber in his manuscript. As reported, the peristalsis would have increased the absorption of the moleculessince in the presence of mechanical stimuli the epithelium had shown an increase in the surface of the domes and therefore an increase in parameter A. This suggested that the net of the apparent permeability, the behaviour of the stationary flow without and with peristalsiswould be represented by an increasing curve like the one reported in figure 90.
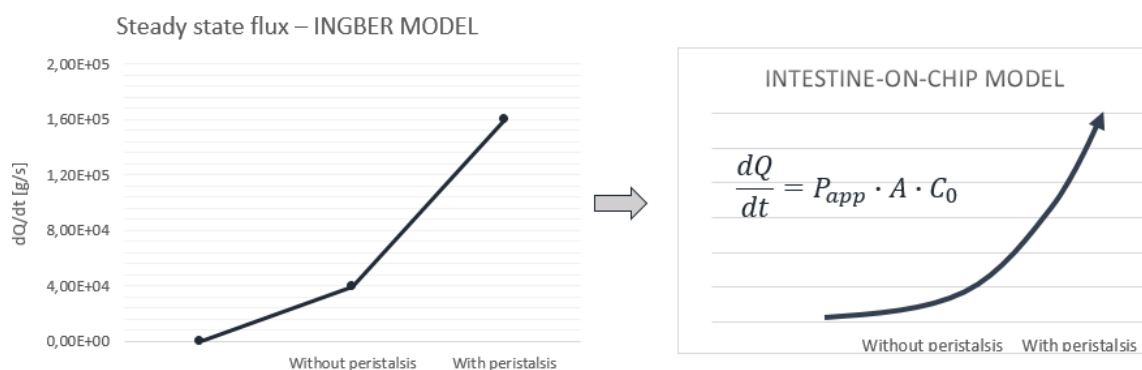
Figure 90. Steady state flux of dextran particles trough epithelium developed in the Peristalsis on chip without and with peristalsis-like motion. The trend was hypothesized based on the Ingber model.

In light of the above, the Peristalsis on chip realized in this work could make a great contribution to drug and food tests. Its capability to develop an equivalent intestinal epithelium with morphological characteristics similar to the native tissue in rather faster times than those reported in the literature is a strength.

6.8 Gelesis Characterization

Once analized the mechanical properties of gelesis, the ultrastructure of the Gelesis were analyzed using scanning electron microscopy (SEM) (Figure 92) and the chemical composition were also analized by using energy dispersive spectroscopy (EDS) (Figure 91).
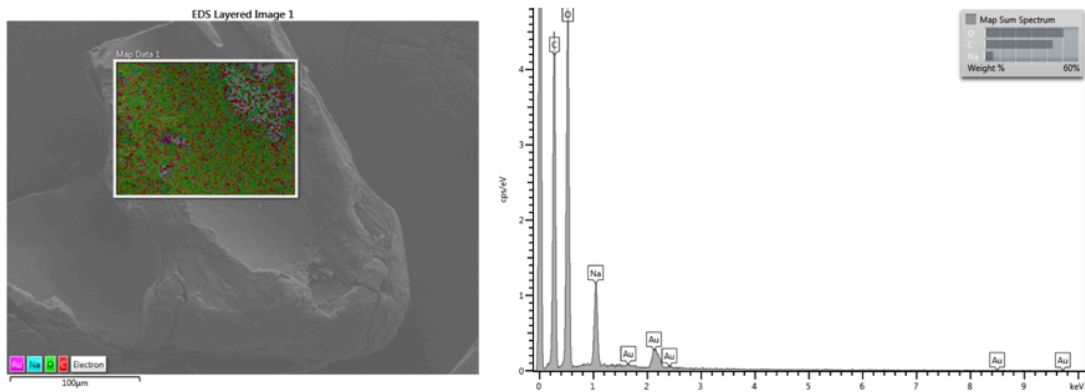
Figure 91. Gelesis characterization, EDS gelesis grain.

Gelesis is presented to ultrastructural analysis in the form of flakes adhered to the stub. The porosity is not evident at high magnifications, probably due to the fact that the granule is completely dehydrated. EDS analysis shows that all Gelesis samples were comprised mainly of Carbon and a smaller amount of Oxygen and Hydrogen.
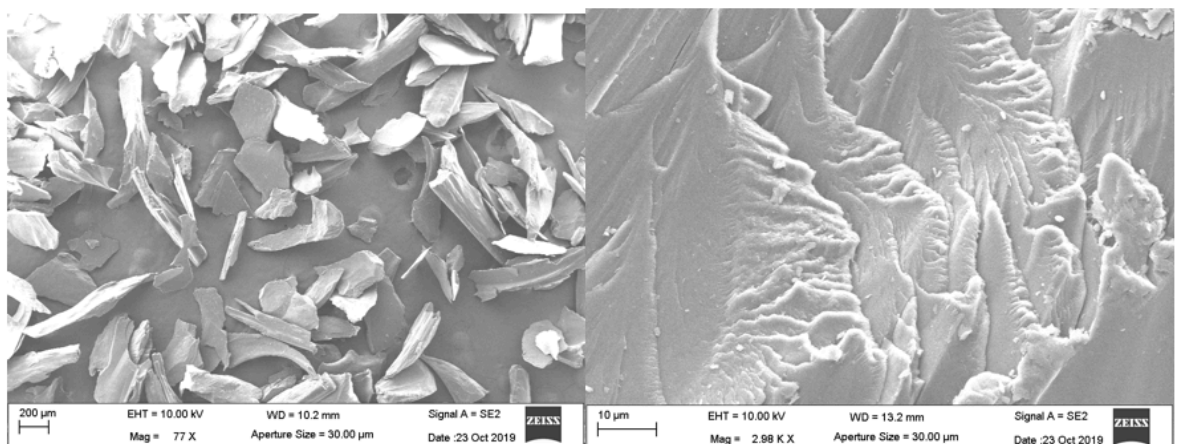
Figure 92. Gelesis characterization, SEM focusing on structure of Grain.

6.9 Evaluation of healthy tau

Our study is designed to obtain the better estimation of the shear stresses that the gel exerts on polarized cells when it flown into the device. In this direction we performed high-resolution measurements of local fluid velocities. To this end, we decide to use the well-known Bingham rheological model that describes the flow curve of a material

with a yield stress τ_0 (the force a fluid must be exposed to in order to start flowing) and a constant viscosity at stresses above the yield stress). The yield stress (τ_0) is the shear stress (τ) at zero shear rate (γ) and the viscosity (η) is the slope of the curve at stresses above the yield stress:

$$\boldsymbol{\tau = \tau_0 + \eta\gamma}$$

- τ_0 **evaluation:**

An initial and rough value for the yield stress has been evaluated by monitoring the minimum value of pressure of compressed air able to overcome the first resistance of the gel. The gel is prepared by mixing hydrogel material with a granulometry comprised between 400÷250 m (Figure 94) and encapsulated fluoresbrite YG polystyrene microspheres (4.5 μm diameter; Polysciences, Warrington, PA) at a final concentration of 1% w/v.Gel was introduced inside the Peristalsis on chip and connected by tubing to air cylinder, after connection, air was pumped inside the microchannel at different pressure, the pressure that overcome first resistence was fixed approximatively equal to 0.1 bar (Figure 93). Furthermore, to calculate in a more precise way this parameter, we are performed additional measurements using stress rheometry.
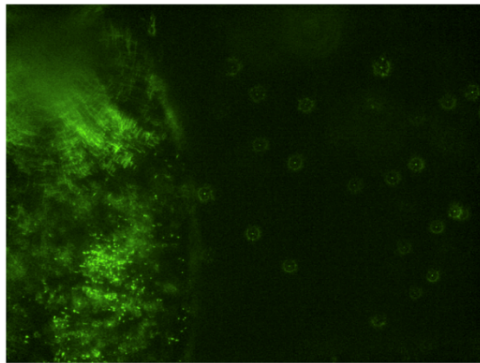
Figure 93. Gelesis with encapsulated fluoresbrite YG polystyrene microspeheres monitored inside Peristalsis on chip..

- **γ evaluation:**

To evaluate the shear stresses exerted by the Gelesis on cells we used the viscosity extrapolated from flow curves at certain values of shear rates.

To determine the wall shear rate at which the gel is sheared during the flow inside the device, we have performed microparticle tracking velocimetry (μ-PTV) experiments. The gel is prepared by mixing hydrogel material with a granulometry comprised between 400÷250 μm (G1 in Figure 94) and encapsulated fluoresbrite YG polystyrene microspheres (4.5 μm diameter; Polysciences, Warrington, PA) at a final concentration of 1% w/v (C1 in Figure 18). The gel has been allowed to pass inside the device and videos of microparticles have been recorded (Figure 93) using a digital camera (Hamamatsu, ORCA-Flash 2.8) attached to a PC and Cam control video capture software mounted on an inverted fluorescence microscope (Olympus IX81) equipped with a fluorescent mercury lamp (Olympus U-LH100L-3) for a total of 1 min at 5 fps (300 frames in total per video).

The microparticle trajectories have been generated by using *Particle Analysis* function available in ImageJ software and velocities have been calculated by dividing the total displacement by the total duration of the video. The shear rates have been calculated in the proximity of the wall by dividing the velocity by the perpendicular distance of the microparticles from the wall and then averaged.

- **(η) evaluation:**

From a dynamic point of view, all the investigated gels present flat dynamic elastic (G') and viscous (G'') moduli curve until 1% strain and 1 Hz.
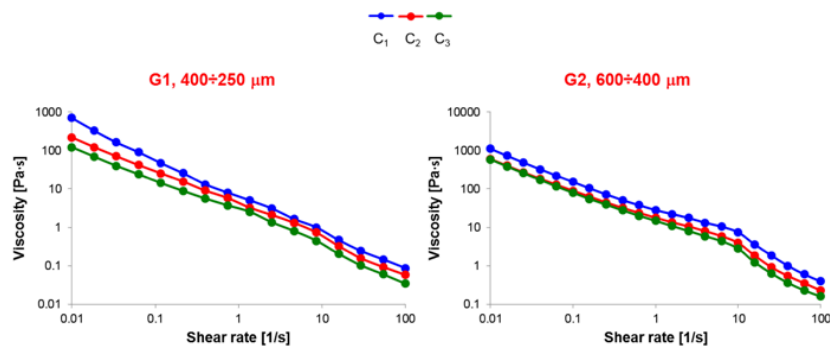
Figure 93. Gelesis G1 e G2 modulus of reological characterization.

Finally we hypotized by graphic .., our first healthy tau, that depends, from peristalsis movement, by also from viscosity of stress.

This results opened to us a lot of possible studies, that we can control from different parameters:

- Peristalsi's velocity of waves
- Viscosity of Gel

These are the most important parameters for testing not only, all type of food and its absorption trough intestinal epithelial layer.

But most important to study the patophysiology of intestine that is regulated by shear of bolus and mechanical transport due to GI gastrointestinal movement like Peristalsis or Segmentation.

General Conclusion

In summary, we have developed first prototype of device called In-Crypts device. An in vitro model of intestinal epithelium suitable for real-time tissue investigations. Precisely, a microfluidic device designed and fabricated with a new "custom made" porous PDMS membrane and successfully integrated in the microfluidic device. The In-Crypts device was designed to mimic and impart the key aspects of the in vivo microenvironment of the human small intestine, including Villus-Crypts axis topography. After brilliantly realizing of this device, we moved, through this, to a next step, to better reproduce the microenvironment and the physiology of the small intestine. With a similar Method, therefore, we have created a second prototype of device: Peristalsis on a chip, which reproduces not only the topography of the microenvironment, but also the mechanics of the intestine itself. The studies on the previous device have allowed us to implement changes and to start from a promising results to implement peristalsis. Therefore, we developed a second prototype device of Peristalsis on chip capable to evaluate the effect of forces transmission across chyme-epithelial layer interface has been realized. The device presents unique feautures, since it allows to recapitulate the complex arrays of mechanical insults occurring on the intestinal tissues due to mechanical consistency of chyme both in physiological and pathological conditions. Furthermore, also the presence of new optically-accessible, "custome made" PDMS Membrane resemble Villi-Crypts axis. Nowadays, there is a high need to get testing platforms as similar to those in vivo to replicate the physiological condition of a human intestinal epithelium and to test functional food and drugs thus avoiding animal models and 2D culture. The realized Peristalsis on chip, optimized in terms of design, materials, mechanic stimuli and microfluidics, was able to reproduce a confluent, well-differentiated epithelium on a PDMS membrane in just 8 days. The replication of the dynamic gut microenvironment as we already reproduce in first, including fluid flow and peristalsislike motion, gave rise an intestinal model with some key features such as well-defined tight junctions and villi-like structures that increase absorption surface area and make the microfluidic device useful for studying absorption and permeability of food, drugs and chemicals. The Peristalsis on chip, in fact, provided convenient and independent access to apical

and basolateral sides and had advantage of controlling the fluid flow in physiologically relevant magnitudes, so regulate the supply of nutrient and drug concentrations. The integration of microelectrodes within these systems allowed continuous monitoring of cells during their various stages of growth and differentiation without disrupting the cell structure.

For future investigation, it should be useful to incorporate four electrodes rather than two, placing them in a strategic way: two electrodes before the first couple of chambers (one in the upper channel and the other in the lower channel) and two immediately after the last one. This arrangement allows to monitor online the correct formation and differentiation of the epithelium along the entire channel where the cells are stimulated by peristalsis. The uniqueness of this device, not only for the presence of the custom made membrane, but above all for the reproduction of perstaltic motility allows us to place it in different fields of application. This is the only device able to reproduce a peristalistal movement like, this allows us to monitor a live physiological tau.

With this device we could be able not only to evaluate the effects of different bolus viscosity on intestine epithelial layer, but also to evaluate the correlation between the physiological tau of small intestine and the condition of well-being of the intestine itself. Once obtained tau behavior in various pathologies, we could even personalized this tau for the individual patient. Focusing on the new frontier of personalized medicine. Another interesting perspective could be integrate our Peristalsis on chip with other functional organ mimetic, such as liver-, lung- and skin-on-chip within a ''human-on-a-chip''. Single organ chips fail to fully reflect the complexity, functional changes, and integrity of organ function. The "multi-organ-on-a-chip", otherwise referred to as the "human-on-a-chip" simultaneously constructs multiple organs attracting obvious research attention. Challenges include reproducing the architectural complexity of the human tissues and organs in vitro in a miniaturised fashion and how to link them in the right format that the interconnected systems also recapitulate the human tissue/organ interactions.

Over the past decade, there has been an exponential growth in organ on chip technology. Real innovation, in my opinion, in the perspective of drug testing and personalized medicine. In addition, organ on chip science can also potentially be

applied in the study of organ physiology and pathology. Furthermore, for drug development they can be a faster identification of effective drugs and drug repurposing. As I said before, all patients could have personalized medicine by testing drugs on patient's own Organ-on-Chip. The hope is that this will eventually lead to more effective treatments, fewer negative side effects, fewer treatment failures, better prediction of disease onset. For industry and production can be better, faster and cheaper health care because of better outcomes of drug treatment and fewer drug failures and reduction or refinement of animal experiments. The overall result could be a better quality of life at lower cost. Organ on chip can be considered the milestone of the beginning of personalized medicine and my expectation is that Organ on Chip will change radically the field of drug testing.

Publication

1. Sara Sibilio ;De Gregorio, Vincenza; Urciuolo, Francesco; Netti, Paolo; Imparato, Giorgia; Effect of peristaltic-like device increases ECM remodelling inducing faster epithelial cell differentiation 2019/09/01; 100027 - 4 - 10.1016/j.mtbio.2019.100027- Materials Today Bio

2. De Gregorio V, Corrado B, Sbrescia S, Sibilio S, Urciuolo F, Netti PA,Imparato G. Intestine-on-chip device increases ECM remodeling inducing faster epithelial cell differentiation. Biotechnol Bioeng. 2020 Feb;117(2):556-566. doi:10.1002/bit.27186. Epub 2019 Nov 27. PubMed PMID: 31598957.

References

1. Wang X, Jiao Q, Zhang S, Ye Z, Zhou Y, Tan WS. Perfusion culture-induced template-assisted assembling of cell-laden microcarriers is a promising route for fabricating macrotissues. Biotechnol J. 2014 Nov;9(11):1425-34. doi:10.1002/biot.201400238.

2. Novel Methodology for Fabrication of Tissue-Engineered Tubular Constructs Using Magnetite Nanoparticles and Magnetic Force Akira Ito, Ph.D.,1 Kousuke Ino, B.Eng.,1 Masao Hayashida, B.Eng.,1 Takeshi Kobayashi, Ph.D.,1,2 Hiroshi Matsunuma, M.D.,3 Hideaki Kagami, D.D.S., Ph.D.,4 Minoru Ueda, D.D.S., Ph.D.,5hiroyuki Honda, Ph.D.1 Tissue Engineering Volume 11, Number 9/10, 2005

3. Imparato G, Urciuolo F, Casale C, Netti PA. The role of microscaffold properties in controlling the collagen assembly in 3D dermis equivalent using modular tissue engineering. Biomaterials. 2013 Oct;34(32):7851-61. doi: 10.1016/j.biomaterials.2013.06.062.

4. Microfluidic organs-on-chips; Sangeeta N Bhatia & Donald E Ingber; Nature Biotechnology; 32,760–772;2014 [13 prev]

5. P. Lundquist *et al.*, "Prediction of In Vivo Rat Biliary Drug Clearance from an In Vitro Hepatocyte Efflux Model," *Drug Metab. Dispos.*, vol. 42, no. 3, pp. 459–468, Feb. 2014

6. "Basic anatomical and physiological data for use in radiological protection: reference values. A report of age- and gender-related differences in the anatomical and physiological characteristics of reference individuals. ICRP Publication 89," *Ann. ICRP*, vol. 32, no. 3–4, pp. 5–265, 2002.

7. Hannah L. Turner & Jerrold R. Turner (2010) Good fences make good neighbors, Gut Microbes, 1:1, 22-29, DOI: 10.4161/gmic.1.1.11427

8. Li N, Wang D, Sui Z, Qi X, Ji L, Wang X, Yang L. Development of an improved three-dimensional in vitro intestinal mucosa model for drug absorption evaluation. Tissue Eng Part C Methods. 2013 Sep;19(9):708-19. doi:10.1089/ten.TEC.2012.0463. PubMed PMID: 23350801.

9. Histological Effects of Aging on Male Albino Rats Duodenum , Maisa M. Al-Qudah Department of Allied Medical Sciences, Zarka University College, Al-Balqa Applied University, Jordan; World Journal of Medical Sciences 10 (2): 174-178, 2014

10. Jun 28, 2016 Vinay Kumar Kapoor, MBBS, MS, FRCS, FAMS; Chief Editor: Thomas R Gest, PhD (Jun 28, 2016) ; Small Intestine Anatomy

11. The Anatomy and Physiology of the Small Bowel; David Gourevitch; Sadler TW. Langman's medical embryology, 9th edition. Philadelphia: Lippincott Williams & Wilkins, 2003.

12. Anatomy and Histology of the Small and Large Intestine; From: http://www.mdconsult.com/das/book/body/1083012334/763548608/1389/683.html#4-u1.0-B1-4160-024 5-6..50098-6_4300

13. Barrett, K. E., & Ganong, W. F. (2012). *Ganong's review of medical physiology*. New York: McGraw-Hill Medical.

14. Gregersen H, Kassab G. Biomechanics of the gastrointestinal tract.Neurogastroenterol Motil. 1996 Dec;8(4):277-97. Review. PubMed PMID: 8959733.

15. Mechanical properties oΓ the humaп gastrointestinal tract* Viacheslav I. Egorov"

16. P. Artursson and R. T. Borchardt, "Intestinal drug absorption and metabolism in cell cultures: Caco-2 and beyond," *Pharm. Res.*, vol. 14, no. 12, pp. 1655–1658, Dec. 1997

17. L. Wang, S. K. Murthy, G. A. Barabino, and R. L. Carrier, "Synergic effects of crypt-like topography and ECM proteins on intestinal cell behavior in collagen based membranes," *Biomaterials*, vol. 31, no. 29, pp. 7586–7598, Oct. 2010.

18. J. H. Sung, J. Yu, D. Luo, M. L. Shuler, and J. C. March, "Microscale 3-D hydrogel scaffold for biomimetic gastrointestinal (GI) tract model," *Lab Chip*, vol. 11, no. 3, pp. 389–392, 2011.

19. J. Yu, S. Peng, D. Luo, and J. C. March, "In vitro 3D human small intestinal villous model for drug permeability determination," *Biotechnol. Bioeng.*, vol. 109, no. 9, pp. 2173–2178, Sep. 2012.

20. he physiological performance of a three-dimensional model that mimics the microenvironment of the small intestine *Biomaterials*, Volume 32, Issue 30, Pages 7469-7478 Jacqueline Pusch, Miriam Votteler, Stella Göhler, Jasmin Engl, Martina Hampel, Heike Walles, Katja Schenke-Layland

21. **D**iMasi, J.A., Grabowski, H.G. & Hansen, R.W. (2014). Innovation in the pharmaceutical industry: new estimates of R&D costs [cited 2017 June 21]

22. Greek R, Menache A. Systematic reviews of animal models: methodology versus epistemology. Int J Med Sci. 2013;10(3):206–221. doi:10.7150/ijms.5529

23. Lancaster, M. A., and Knoblich, J. A. (2014) Organogenesis in a dish: modeling development and disease

using organoid technologies. Science 345, 1247125.

24. S. N. Bhatia and D. E. Ingber, "Microfluidic organs-on-chips," Nature Biotechnology, vol. 32, no. 8. pp. 760–772, 2014, doi: 10.1038/nbt.2989.

25. M. B. Esch *et al.*, "On chip porous polymer membranes for integration of gastrointestinal tract epithelium with microfluidic 'body-on-a-chip' devices," *Biomed. Microdevices*, vol. 14, no. 5, pp. 895–906, Oct. 2012.

26. H. Kimura, T. Yamamoto, H. Sakai, Y. Sakai, and T. Fujii, "An integrated microfluidic system for long-term perfusion culture and on-line monitoring of intestinal tissue models," *Lab. Chip*, vol. 8, no. 5, pp. 741–746, May 2008.

27. H. J. Kim, D. Huh, G. Hamilton, and D. E. Ingber, "Human gut-on-a-chip inhabited by microbial flora that experiences intestinal peristalsis-like motions and flow," *Lab. Chip*, vol. 12, no. 12, pp. 2165–2174, Jun. 2012.

28. Kim HJ, Ingber DE. Gut-on-a-Chip microenvironment induces human intestinal cells to undergo villus differentiation. Integr Biol (Camb). 2013Sep;5(9):1130-40. doi: 10.1039/c3ib40126j. PubMed PMID: 23817533.

29. Henry OYF, Villenave R, Cronce MJ, Leineweber WD, Benz MA, Ingber DE.Organs-on-chips with integrated electrodes for trans-epithelial electrical resistance (TEER) measurements of human epithelial barrier function. Lab Chip.2017 Jun 27;17(13):2264-2271. doi: 10.1039/c7lc00155j.

30. Kasendra M, Tovaglieri A, Sontheimer-Phelps A, Jalili-Firoozinezhad S, Bein A, Chalkiadaki A, Scholl W, Zhang C, Rickner H, Richmond CA, Li H, Breault DT, Ingber DE. Development of a primary human Small Intestine-on-a-Chip using biopsy-derived organoids

31. Sant S, Tao SL, Fisher OZ, Xu Q, Peppas NA, Khademhosseini A. Microfabrication technologies for oral drug delivery. Adv Drug Deliv Rev. 2012 May 1;64(6):496-507. doi: 10.1016/j.addr.2011.11.013. Review. PubMed PMID: 22166590;PubMed Central PMCID: PMC3534972.

32. Liao DH, Zhao JB, Gregersen H. Gastrointestinal tract modelling in health and disease. World J Gastroenterol. 2009 Jan 14;15(2):169-76. Review. PubMed PMID:19132766; PubMed Central PMCID: PMC2653308.

33. De Gregorio V, Corrado B, Sbrescia S, Sibilio S, Urciuolo F, Netti PA,Imparato G. Intestine-on-chip device increases ECM remodeling inducing faster epithelial cell differentiation. Biotechnol Bioeng. 2020 Feb;117(2):556-566. doi:10.1002/bit.27186. Epub 2019 Nov 27. PubMed PMID: 31598957.

34. MECHANOMEDICINE: applications of mechanobiology to medical sciences and next-generation medical technologies

35. Guyton and Hall Textbook of Medical Physiology - 12th-Ed

36. Sara Sibilio;De Gregorio, Vincenza; Urciuolo, Francesco; Netti, Paolo; Imparato, Giorgia; Effect of peristaltic-like device increases ECM remodelling inducing faster epithelial cell differentiation 2019/09/01; 100027 - 4 - 10.1016/j.mtbio.2019.100027- Materials Today Bio

37. Digestion-on-a-chip: a continuous-flow modular microsystem recreating enzymatic digestion in the gastrointestinal tract, Pim de Haan, Margaryta A. Ianovska, Klaus Mathwig, Glenn A. A. van Lieshout, Vassilis Triantis,Hans Bouwmeester and Elisabeth Verpoorte, Lab on a Chip, Issue 9, 2019

38. A complex human gut microbiome cultured in an anaerobic intestine-on-a-chip. Sasan Jalili-Firoozinezhad, Francesca S. Gazzaniga, Elizabeth L. Calamari, Diogo M. Camacho, Cicely W. Fadel, Amir Bein, Ben Swenor, Bret Nestor, Michael J. Cronce, Alessio Tovaglieri, Oren Levy, Katherine E. Gregory, David T. Breault, Joaquim M. S. Cabral, Dennis L. Kasper, Richard Novak & Donald E. Ingber. Nature Biomedical Engineering volume 3, pages520–531(2019)

39. Kim HJ, Huh D, Hamilton G, Ingber DE. Human gut-on-a-chip inhabited by microbial flora that experiences intestinal peristalsis-like motions and flow.Lab Chip. 2012;12(12):2165- 2174.

40. A microfluidics-based in vitro model of the gastrointestinal human–microbe interface. Pranjul Shah, Joëlle V. Fritz, Enrico Glaab, Mahesh S. Desai, Kacy Greenhalgh, Audrey Frachet, Magdalena Niegowska, Matthew Estes, Christian Jäger, Carole Seguin- Devaux, Frederic Zenhausern & Paul Wilmes. Nature Communications volume 7, Article number: 11535 (2016)

41. De Gregorio, V., Telesco, M., Corrado, B., Rosiello, V., Urciuolo, F., Netti, P. A., & Imparato, G. (2020). Intestine-Liver Axis On-Chip Reveals the Intestinal Protective Role on Hepatic Damage by Emulating Ethanol First-Pass Metabolism. *Frontiers in bioengineering and biotechnology*, *8*, 163. https://doi.org/10.3389/fbioe.2020.00163

42. DiMasi, J.A., Grabowski, H.G. & Hansen, R.W. (2014). Innovation in the pharmaceutical industry: new estimates of R&D costs [cited 2017 June 21]

43. Greek R, Menache A. Systematic reviews of animal models: methodology versus epistemology. Int J Med Sci. 2013;10(3):206–221. doi:10.7150/ijms.5529

44. Lancaster, M. A., and Knoblich, J. A. (2014) Organogenesis in a dish: modeling development and disease using organoid technologies. Science 345, 1247125.

45. S. N. Bhatia and D. E. Ingber, "Microfluidic organs-on-chips," Nature Biotechnology, vol. 32, no. 8. pp. 760–772, 2014, doi: 10.1038/nbt.2989.

46. G. J. Tortora and M. T. Nielsen, Principles of human anatomy, Wiley., vol. 257. 1999.

47. VanPutte, C., Regan, J. & Russo, A. (2015). Seeley's Essentials of Anatomy & Physiology, Ninth edition. McGraw-Hill.

48. Feher, J. J. Quantitative Human Physiology: An Introduction. Academic Press: Amsterdam, 2012.

49. Mitic LL, Anderson JM. Molecular architecture of tight junctions. Annu Rev Physiol. 1998;60:121-42. Review. PubMed PMID: 9558457

50. Groschwitz KR, Hogan SP. Intestinal barrier function: molecular regulation and disease pathogenesis. J Allergy Clin Immunol. 2009;124(1):3–22. doi:10.1016/j.jaci.2009.05.038

51. Lee B, Moon KM, Kim CY. Tight Junction in the Intestinal Epithelium: Its Association with Diseases and Regulation by Phytochemicals. J Immunol Res. 2018;2018:2645465. Published 2018 Dec 16. doi:10.1155/2018/2645465

52. Costa J, Ahluwalia A. Advances and Current Challenges in Intestinal in vitro Model Engineering: A Digest. Front Bioeng Biotechnol. 2019;7:144. Published 2019 Jun 18. doi:10.3389/fbioe.2019.00144

53. Powell, D. W., Adegboyega, P. A., Di Mari, J. F., and Mifflin, R. C. (2005). Epithelial cells and their neighbors I. Role of intestinal myofibroblasts in development, repair, and

54. i, N., Wang, D., Sui, Z., Qi, X., Ji, L., Wang, X., et al. (2013). Development of an improved three-dimensional in vitro intestinal mucosa model for drug absorption evaluation. Tissue Eng. Part C 19, 708–719. doi: 10.1089/ten.tec.2012.0463

55. L. Wang, S. K. Murthy, W. H. Fowle, G. A. Barabino, and R. L. Carrier, "Influence of micro-well biomimetic topography on intestinal epithelial Caco-2 cell phenotype," Biomaterials, vol. 30, no. 36, pp. 6825–6834, Dec. 2009.

56. Sung, J. H., Yu, J., Luo, D., Shuler, M. L., and March, J. C. (2011). Microscale 3-D hydrogel scaffold for biomimetic gastrointestinal (GI) tract model. Lab Chip. 11, 389–392. doi: 10.1039/C0LC00273A

57. Yu, J., Peng, S., Luo, D., and March, J. C. (2012). In vitro 3D human small intestinal villous model for drug permeability determination. Biotechnol. Bioeng. 109, 2173–2178. doi: 10.1002/bit.24518

58. Sato, T., Stange, D. E., Ferrante, M., Vries, R. G. J., Van Es, J. H., Van den Brink, S., et al. (2011). Long-term expansion of epithelial organoids from human colon, adenoma, adenocarcinoma, and Barrett's epithelium. Gastroenterology 141, 1762–1772. doi: 10.1053/j.gastro.2011.07.050

59. Sato, T., Vries, R. G., Snippert, H. J., van de Wetering, M., Barker, N., Stange, D. E., et al. (2009). Single Lgr5 stem cells build crypt-villus structures in vitro without a mesenchymal niche. Nature 459, 262–265. doi: 10.1038/nature07935

60. Bein, Amir et al. "Microfluidic Organ-on-a-Chip Models of Human Intestine." Cellular and molecular gastroenterology and hepatology vol. 5,4 659-668. 24 Apr. 2018, doi:10.1016/j.jcmgh.2017.12.010

61. 13 H. J. Kim, D. Huh, G. Hamilton and D. E. Ingber, Lab Chip, 2012, 12, 2165–2174.

62. Hyun Jung Kim, Donald E. Ingber, Gut-on-a-Chip microenvironment induces human intestinal cells to undergo villus differentiation, Integrative Biology, Volume 5, Issue 9,

63. Cremer, J., Segota, I., Yang, C., Arnoldini, M., Sauls, J. T., Zhang, Z., ... Hwa, T. (2016). Effect of flow and peristaltic mixing on bacterial growth in a gut-like channel. Proceedings of the National Academy of Science of the United States of America, 113(41), 11414-11419. [pnas.1601306113].

64. Gao, D., Liu, H., Lin, J., Wang, Y., & Jiang, Y. (2013). Characterization of drug permeability in Caco-2 monolayers by mass spectrometry on a membrane-based microfluidic device. Lab on a chip, 13 5, 978-85.

65. Kornphimol Kulthong et al. (2020). Microfluidic chip for culturing intestinal epithelial cell layers: Characterization and comparison of drug transport between dynamic and static models.

66. Hubatsch, Ina, et al. "Determination of drug permeability and prediction of drug Gale Academic OneFile, Accessed 16 Apr. 2020.

67. Meza, I., Ibarra, G., Sabanero, M., Martinez-Palomo, A. & Cereijido, M. (1980). Occluding junctions and cytoskeletal components in a cultured transporting epithelium. The Journal of Cell Biology, 87(3): 746-754.

68. Rutten, M.J., Hoover, R.L. & Karnovsky, M.J. (1987). Electrical resistance and macromolecular permeability of brain endothelial monolayer cultures. Brain Research, 425(2): 301-310

69. World Precision Instruments (2017). Endohm-12, Endohm for 12 mm Culture Cup (12 wells per plate)

70. NanoAnalytics GmbH (2017). CellZscope [cited 2017 May 18]; Available from: http://www.nanoanalytics.com/en/products/cellzscope.html.

71. Applied BioPhysics (2017). 8W TransFilter Adapter [cited 2017 May 18]; Available from: http://www.biophysics.com/filter_adapter.php.

72. Niraj K Inamdar, Jeffrey T Borenstein - Microfluidic cell culture models for tissue engineering.

73. Microfluidic Organ-on-a-Chip Models of Human Intestine Bein, Amir et al. Cellular and Molecular Gastroenterology and Hepatology, Volume 5, Issue 4, 659 – 668

74. R. G. Lentle and P. W. M. Janssen, J. Comp. Physiol., B, 2008, 178, 673–690.

75. T. Ishikawa, T. Sato, G. Mohit, Y. Imai and T. Yamaguchi, J. Theor. Biol., 2011, 279, 63–73.
76. Mukhopadhyay, Rajendrani. "When PDMS isn't the best." Analytical chemistry 79.9 (2007): 3248-3253.
77. Berthier, Erwin, et al. "Engineers are from PDMS- land, Biologists are from Polystyrenia." Lab on a Chip 12.7 (2012): 1224-1237.
78. Srinivasan B, Kolli AR, Esch MB, Abaci HE, Shuler ML, Hickman JJ. TEER measurement techniques for in vitro barrier model systems. J Lab Autom. 2015;20(2):107- 126. doi:10.1177/2211068214561025 [38]
79. Intestine- on- chip device increases ECM remodeling inducing faster epithelial cell differentiation. V De Gregorio, B Corrado, S Sbrescia, S Sibilio, F Urciuolo, PA Netti. Biotechnology and bioengineering 117 (2), 556-566
80. Marciani, Luca et al. "Gastric response to increased meal viscosity assessed by echo- planar magnetic resonance imaging in humans." The Journal of nutrition (2000).